Stony Brook University

Mantle composition and temperature of western North America revealed from in-situ velocity measurements of KLB-1 peridotite

A Dissertation Presented

by

Xuebing Wang

to

The Graduate School

in Partial Fulfillment of the

Requirements

for the Degree of

Doctor of Philosophy

in

Geosciences

Stony Brook University

August 2016

Stony Brook University

The Graduate School

Xuebing Wang

We, the dissertation committee for the above candidate for the

Doctor of Philosophy degree, hereby recommend

acceptance of this dissertation.

Dr. Baosheng Li– Dissertation Advisor
Research Professor, Mineral physics institute, Stony Brook University

Dr. Robert Liebermann - Chairperson of Defense
Research Professor, Mineral Physics Institute, Stony Brook University

Dr. Lianxing Wen
Professor, Department of Geosciences, Stony Brook University

Dr. William Holt
Professor, Department of Geosciences, Stony Brook University

Dr. David Walker-Outside Member
Professor, Lamont-Doherty Earth Observatory of Columbia University

This dissertation is accepted by the Graduate School

Nancy Goroff

Interim Dean of the Graduate School

Abstract of the Dissertation

Mantle composition and temperature of western North America revealed from in-situ velocity measurements of KLB-1 peridotite

by

Xuebing Wang

Doctor of Philosophy

in

Geosciences

Stony Brook University

2016

The composition and thermal structure of the Earth's mantle, especially the mantle transition zone, still remain controversial due to the lack of direct access to the Earth's interior. An important geophysical approach to constrain the mineralogical composition of the mantle is to compare seismic profiles (e.g., PREM and AK135) with the elasticity of candidate compositional models calculated by averaging schemes based on the phase equilibrium and elasticity data of individual mantle minerals. However, chemical reactions, element partitioning and diffusion cannot be fully taken into account by this approach. In this study, I conducted direct velocity measurements on KLB-1 peridotite which is compositionally close to pyrolite up to the pressure and temperature conditions of the mantle transition zone. The KLB-1 specimens were successfully hot-pressed at mantle conditions followed by X-ray diffraction, optical and scanning electron microscopy (SEM), electron probe micro-analyzer (EPMA) analyses on

specimens for a full characterization before conducting the ultrasonic measurements at high pressure.

For the off-line acoustic measurements, we developed a new method for in-situ pressure determination in multi-anvil, high-pressure apparatus using an acoustic travel time approach within the framework of acoustoelasticity. It not only can be used for continuous in-situ pressure determination at room temperature and high temperatures, during both compression and decompression, but also for simultaneous pressure and temperature determination with a high accuracy (±0.16 GPa in pressure and ±17 ºC in temperature).

Comparison of the P and S wave velocities of a KLB-1 specimen at room temperature with Voigt-Reuss-Hill (VRH) calculations based on literature elasticity data for its constituent minerals indicates that the experimentally measured P and S wave velocities, densities, bulk sound velocities and V_P/V_S ratios fall close to the lower limit of VRH averages within the uncertainties of the mineral elasticity data. Mantle temperatures under western North America have been estimated from a comparison between the velocities of KLB-1 specimens measured at mantle conditions and the TNA2 shear velocity model to be along a 1450 ºC adiabat or along a 1300-1350 ºC adiabat after correction for the effect of inelasticity. The velocity jump at 410 km is 6.6% for P wave and 7.0% for S wave with a volume fraction of 70% for olivine. A Lehmann discontinuity is observed at the pressure of 7.5-7.8 GPa (230-240 km) with the velocity jump of ~1.5% and velocity-pressure slope change for P and S waves, which may be caused by the large mineral compositional change before and after this pressure. Our results also suggest that the temperatures in the mantle of this region are beneath the solidus and the velocity reduction does not require the presence of partial melt beneath this region.

To my family and friends

Make a life, not just a living
O ever Youthful
O ever weeping

Table of Contents

List of Tables

List of Figures

List of Abbreviations

Ol – olivine

Wd – wadsleyite

Rw – ringwoodite

Cpx – clinopyroxene

Opx – orthopyroxene

Gt – garnet

Mj – majorite

Sp – spinel

Pv – perovskite

Mw– magnesiowustite

Fp – ferropericalse

Py – pyrope

Alm – almandine

Grs – grossular

Uv – uvarovite

KBH – Kilbourne Hole

MORB – mid-ocean ridge basalt

WC – tungsten carbide

EOS – equation-of-state

PEO – pulse echo overlap

D-DIA – deformation cubic-anvil apparatus

DAC – diamond anvil cell

SEM – scanning electron microscope

EPMA – electron probe micro-analyzer

PREM – Preliminary Reference Earth Model

TNA – Tectonic North America Model

GCA – Gulf California Model

COMPRES - COnsortium for Materials Properties Research in Earth Sciences

Acknowledgments

First I would like to express my sincere gratitude and special appreciation to my advisor Prof. Baosheng Li for his tremendous help to my reseach, for his encouragement, his patience and continuous support. He encouraged me to work independently but steered me in the right direction, and his office door was always open whenever I had trouble in my research. This work could not have been done without his unselfish guidance and his immense knowledge. I appreciated so much to have him as my Ph.D. advisor and I just cannot thank him enough.

My special gratitude also goes to Dr. Robert Liebermann, who is my academic grandfather, and he has always been an amiable, warm, and knowledgeable elder. He is so kind to any young researcher and proud of our work. I gained a lot of opportunities to talk about my work with famous researchers from all over the world under his help and encouragement.

I would like to thank Dr. David Walker, Dr. Lianxing Wen and Dr. William Holt for spending their valuable time to serve on my defense committee.

I also would like to thank Dr. Claude Herzberg for donating the KLB-1 sample to me. I appreciate the help from him and Dr. Chris Vidito for the probe analyses on KLB-1 specimens. Special appreciation also goes to Dr. Yanbin Wang, Dr. Haiyan Zhang and Dr. Tony Yu for teaching and helping me to do experiments at synchrotron beamlines.

Thanks are also extended to my labmates: Ting Chen and Xintong Qi, for the friendship we built during sleepless nights at beamlines and the High Pressure Lab, during discussions on research projects and the encouragement and support to each other. Also I thank my friends Huanting Hu, Dandan Li and Fang Huang for their support in life and their stimulating discussions with me on other interesting Earth Sciences topics.

Last but not the least, I would like to thank my family: my parents who always support me spiritually throughout my life; my beloved hudsband, Tian Feng, who inspired me and provided constant encouragement during my pursuit of the doctorate degree.

Publications

Zou, Y., Qi, X., **Wang, X.**, Chen, T., Li, X., Welch, D., and Li, B., 2014. High-pressure behavior and thermoelastic properties of niobium studied by in situ x-ray diffraction. Journal of Applied Physics, 116(1), 013516.

Chen, T., Gwanmesia, G. D., **Wang, X.**, Zou, Y., Liebermann, R. C., Michaut, C., and Li, B., 2015. Anomalous elastic properties of coesite at high pressure and implications for the upper mantle X-discontinuity. Earth and Planetary Science Letters, 412, 42-51.

Wang, X., Chen, T., Zou, Y., Liebermann, R. C., and Li, B., 2015. Elastic wave velocities of peridotite KLB-1 at mantle pressures and implications for mantle velocity modeling. Geophysical Research Letters, 42(9), 3289-3297.

Zou, Y., Wang, X., Chen, T., Li, X., Qi, X., Welch, D., Zhu, P., Liu, B., Cui, T. and Li, B., 2015. Hexagonal-structured ε-NbN: ultra-incompressibility, high shear rigidity, and a possible hard superconducting material. Scientific reports, 5.

Wang, X., Chen, T., Qi, X., Zou, Y., Kung, J., Yu, T., Wang, Y., Liebermann, R.C. and Li, B., 2015. Acoustic travel time gauges for in-situ determination of pressure and temperature in multi-anvil apparatus. Journal of Applied Physics, 118(6), p.065901.

Li, Y., Zou, Y., Chen, T., **Wang, X.**, Qi, X., Chen, H., Du, J. and Li, B., 2015. PVT equation of state and high-pressure behavior of CaCO3 aragonite.American Mineralogist, 100(10), pp.2323-2329.

Zou, Y., Qi, X., Zhang, C., Ma, S., Zhang, W., Li, Y., Chen, T., **Wang, X.**, Chen, Z., Welch, D. and Zhu, P., 2016. Discovery of Superconductivity in Hard Hexagonal ε-NbN. Scientific reports, 6.

Chen, T., **Wang, X.**, Qi, X., Ma, M., Xu, Z., and Li, B., 2016. Elasticity and Phase Transformation at High Pressure in Coesite from Experiments and First-Principle Calculations. American Mineralogist, in press.

Qi, X., **Wang, X.**, Chen, T., and Li, B., 2016. Experimental and first-principles studies on the elastic properties of α-hafnium metal under pressure. Journal of applied physics, 119.

Wang, X., Chen, T., Qi, X., Zou, Y., Yu, T., Wang, Y., Liebermann, R.C. and Li, B., 2016. Mantle composition and temperature of western North America revealed from direct P and S wave velocities of KLB-1 peridotite to the conditions of the transition zone. To be submitted.

Chapter 1 Introduction

1.1 Scientific background

One of the most fundamental and long-term standing problems in Earth science is the question of dynamics and the composition of the Earth's interior. In the late 19th century, an Earth model was proposed with a dense metallic core and a less dense rock mantle based on the mass and moment of inertia of the Earth. In the 20th century, a more detailed structure was obtained from seismological studies, which is the most important way to directly obtain the information from deep Earth. The 1-D global models, such as the Preliminary Reference Earth Model (PREM, Dziewonski and Anderson, 1981) and AK135 (Kennett et al., 1995), revealed a more clear Earth's structure with crust, mantle and core. The mantle of the Earth has two parts: (1) the upper mantle from the Mohorovicic discontinuity (Moho) from the base of the crust to 660 km.; including a transition zone ranging from ~410 - ~660 km (Figure 1.1 a), in which the P and S wave velocities have larger gradients than in other regions; (2) the lower mantle with a smoother velocity-depth profile than the upper mantle from the bottom of the transition zone to the core-mantle boundary (Bass and Parise, 2008). However, as of today, the detailed structure and composition of the Earth's mantle still remains controversial due to the lack of direct sampling of rocks from these depths.

The transition zone of the mantle holds the key to understand a number of major geophysical problems (Birch, 1952). However, the depth and the sharpness of the velocity jumps

are not well determined because of the limitations of the sensitivity and the resolutions of long-period data from synthetic seismograms. Birch (1952) proposed that the large gradients in the transition zone might be caused by the structural changes in the constituent minerals of the upper mantle assemblage. Previous studies (Ringwood, 1975; Katsura and Ito, 1989; Akaogi et al., 1989; Akimoto and Fujisawa, 1965, 1968) showed that olivine (Ol, α phase) transforms to its high pressure phase named wadsleyite (Wd, β phase) at the pressure matches well with the seismic discontinuity at 410 km, which may be responsible, at least partially for the velocity jump at 410 km; and further the 520 km discontinuity could be explained by the phase transition from wadsleyite to ringwoodite (Rw, γ phase) (Rigden et al., 1991; Weidner et al., 1984). However, the velocity jumps produced by olivine to wadsleyite at 410 km are much larger than those from seismic models of PREM and AK135 (see Figure 1.1 b). Thus the upper mantle cannot be composed only of olivine. Accompanying olivine in the upper mantle are orthpyroxene (Opx, Ca-poor), clinopyroxene (Cpx, Ca-rich) and garnet (Gt, Al-rich) (Bass and Parise, 2008). Phase equilibrium and transformations for these minerals have been studied by many previous investigators to better understand the composition of the mantle (e.g. Irifune, 1987; Ringwood 1975; Liu 1977; Katsura and Ito, 1989; Ito and Yamada, 1982; Gasparik, 1989; Akaogi et al., 1989; Morishima et al., 1994; Irifune and Ringwood 1993). The pyroxenes also undergo several phase transitions in the upper mantle condition (e.g. Gasparik, 1992). At higher pressures, ringwoodite decomposes to the assemblage of $MgSiO_3$-rich perovskite (Pv) and (Mg, Fe)O periclase at ~24 GPa and pyroxenes transforms to majorite garnet (Mj) at ~16 GPa (Irifune and Ringwood, 1987) (see Figure 1.1 a for the major phases in Earth's interior at their corresponding depths).

Some mineralogical models (e.g. pyrolite and piclogite) have been proposed based on evidence from geochemical and petrological studies. As shown in Table 1.1, pyrolite is more enriched in olivine (57%) with the similar composition as the most fertile olivine-rich mantle xenoliths, while piclogite is predominated by garnet (45%) and pyroxene (33%) (Anderson and Bass, 1984). One of the most commonly used geophysical approaches to distinguish and constrain the composition of the Earth's mantle is to compare velocity and density profiles of mantle mineralogical models with those from seismic studies. In particular, the mineralogical model of the mantle should reproduce both the magnitude and the sharpness of the globally observed seismic discontinuities at 410- and 660-km depths, as well as the velocity gradients in the mantle transition zone. Although some studies show that the pyrolite model (e.g., Weidner, 1985; Ita and Stixrude, 1992; Jackson and Rigden, 1998; Li and Liebermann, 2007) yields seismic velocities more consistent with global seismological models than the piclogite model in the whole mantle, there are also studies arguing that the seismic velocity jump at 410 km can be better reproduced by a piclogitic composition, thereby requiring a layered mantle with a piclogitic transition zone (Bass and Anderson, 1984).

Temperature profiles (geotherms) at the deep mantle are usually constrained by the P T conditions of phase transitions at seismic discontinuities. The principal discontinuities used are inner core boundary, identified with the melting point of an iron alloy, and the 660 km discontinuity with the phase boundary of $MgSiO_3$-perovskite. The geotherms follow an adiabat in the homogeneous regions where the Bullen parameter is close to 1 (e.g., the lower mantle, Poirier, 2000). One of the most important developments in Earth Science in past decades is seismic tomography (Masters et al., 2000; Grand et al., 1997, Romanowicz, 1995, Wen and Anderson, 1995, 1997). It provides the information of the lateral variability in P and S wave

velocities, which is thought to be caused by temperature variation. However, in order to interpret these lateral velocity variations in the mantle, the temperature would be unreasonably high or low in many regions according to mineral physics data (Bass and Parise, 2008). Thus this kind of lateral heterogeneity may be due to the combined effects of chemical composition, temperature and mineralogical phase changes. With an assumed chemical composition, the temperature profile can be inferred from infinitesimal strain approximation for the calculation of seismic velocities (e.g. Goes and Van der Lee, 2002; Cammarano et al., 2003) or a comparison between a directly velocity measurement of mantle phase assemblages and seismic models.

1.2 Mineral physics approach to constrain the composition and temperature of the mantle

Elastic properties of minerals at high pressures and temperatures are the keys to translate seismic information into quantities of composition, minerology and temperatures of the Earth. Elastic properties are directly related to the velocities of seismic waves and the density change of mantle minerals at high pressures through the following relationships:

$$V_p=\sqrt{\frac{K+\left(\frac{4}{3}\right)G}{\rho}} \qquad V_s=\sqrt{\frac{G}{\rho}}$$

Where Vp is the P wave velocity, Vs is the S wave velocity, K is the adiabatic bulk modulus, G is the shear modulus and ρ is the density. K and G of individual mineral are essential properties to infer the velocities of mineral assemblages at high pressures and temperatures.

As the pressures and temperature in the deep Earth are extremely high (up to 360 GPa and 4000-7000 K), various techniques are needed to generate high pressures to investigate the elastic properties of minerals under high P T condition. The diamond anvil cell (DAC) is one of the most commonly used techniques in high pressure research which can reach the pressures of

the Earth's core (Mao et al., 1990). It also can be heated by focusing an infrared laser on the sample to very high temperature (several thousand K, see Meng et al., 2006). By comparison, the multi-anvil apparatus (also called "large volume press") can hold much larger samples (with diameter and length in mm) than the DAC and can reach the pressures up to the top of the lower mantle. With these advanced techniques combined with the ultrasonic methods, light-scattering techniques, inelastic X-ray scattering and other techniques such as the inelastic neutron scattering, the elastic properties of key mantle minerals have been studied under high pressures and temperatures (see Figure 1.1 b), such as olivine and its polymorphs (Duffy et al., 1995; Zha et al., 1996, 1997, 1998; Li et al., 1996,1998, 2004; Li and Liebermann, 2000; Darling et al., 2004; Liu et al., 2005, 2009; Liu et al., 2008; Abramson et al., 1997; Rigden et al., 1993; Li, 2003; Higo et al., 2008; Mao et al., 2008, 2011,2012), pyroxenes (Liebermann and Mayson, 1976; Chai et al., 1997; Angel and Jackson, 2002; Kung et al., 2004, 2005; Li and Neuville, 2010; Sang and Bass, 2014; Collins and Brown, 1998; Zhang et al, 2013; Flesch et al., 1998), garnet (Gwanmesia et al., 2006, 2009, 2014; Irifune et al., 2008; O'Neil et al., 1989; Kono et al., 2010; Zou et al., 2012; Conrad et al., 1999; Lu et al., 2013; Sinogeikin and Bass 2000; Jiang et al., 2004; Wang and Ji, 2001; Chen et al., 1999), perovskite (Sinelnikov et al., 1998; Li and Zhang, 2005, Chantel et al., 2012), ferropericalse (Fp)/magnesiowustite (Mw) (Chen et al., 1998; Li et al., 2006; Jackson and Niesler, 1982; Yoneda, 1990; Kung et al., 2002; Jacobsen et al., 2005). In previous mineral physics approaches, when using elasticity and phase equilibrium data to test compositional models of the mantle, the seismic properties of the mineralogical aggregates were calculated by using averaging schemes such as Hashin-Shtrikman (Hashin and Shtrikman, 1962a, b, 1963) and Voigt-Reuss-Hill (Hill, 1952) based on the proportions and elasticity of each phase (e.g., Ita and Stixrude, 1992; Jackson and Rigden, 1998; Li and

Liebermann, 2007). However, this kind of approach suffers from several disadvantages: (1) these calculated properties only represent the mean values of the upper and lower bounds under assumed [e.g., iso-stress (Reuss) and iso-strain (Voigt) in VRH] conditions which may not be the same as the actual states of the multiphase aggregate (i.e., mantle rocks) under mantle conditions. (2) large variations in the elastic properties, especially for the temperature derivatives of bulk and shear modulus at high pressures for the same mineral from different techniques, make it difficult to obtain accurate velocity profile of these mineralogical models (e.g. Wang et al, 2015); (3) most importantly, chemical interactions and elements partitioning occur among co-existing mantle phases with increasing depths are often ignored, for example, iron partitioning occurs among almost all major mantle minerals at different pressures (i.e. Figure 2, Irifune and Ishiiki, 1998) and garnet can accept many cations with various valence states (Kono et al., 2007).

Núñez-Valdez et al., (2013) summarized the available elasticity data of olivine and wadsleyite and found that iron increases the bulk modulus [K_α = (126.54 + 24x) GPa and K_β = (164.37 + 42.2x) GPa, and decreases the shear modulus, [G_α = (78.17 - 26.2x) GPa and G_β = (107.11 - 47.6x) GPa] for $0 \leq x \leq 0.125$ (x is the mole fraction of Fe). However, there are other minor elements in olivine and other mantle constituent phases other than iron and the composition of these phases changes as the function of pressure and temperature, and there is not an integrated database for all these compositions. According to Irifune and Isshiki (1998), olivine becomes more Mg rich with increasing pressure, from Mg# = 89 at ambient condition to Mg# = 92-93 at 13.5 GPa (410 km). Thus this iron partitioning will affect the velocity jump at 410 km. Irifune and Isshiki (1998) argued that the volume fraction of olivine should be increased by ~4-5% in the estimations from isochemical phase transformation of olivine. For pyroxenes, velocities measurements on a natural orthopyroxene from Kilbourne Hole from Chai et al. (1997)

shows that Al content increases both P and S waves by ~3%. The garnet system is even more complex than olivine and pyroxenes as it has various valence states. For example, the rigidity of grossular is 16% larger than pyrope at ambient condition because the $Ca2^{+}$-$Mg2^{+}$ substitution has a large effect on shear modulus (Jiang et al., 2004).

Recently, Irifune et al., (2008) measured the velocities of a "pyrolite minus olivine" composition to the condition of mantle transition zone and combined with previous velocities of ringwoodite to address the compositions of mantle. The results show that although pyrolite model yields seismic velocities more consistent with global seismic models (e.g. PREM, AK 135) in the upper part of the transition zone than piclogite (except for the large velocity jump at 410 km), neither of these compositional models can reproduce all the features of seismic models and both models have lower shear wave velocities at the lower part of the transition zone. The calculated velocities for these models involve errors as large as 3% owing to uncertainties in the mineral elasticities as stated in their paper. Since chemical reactions and elemental partitioning occur with increasing pressures and temperatures, and it is difficult to take these effects into account. Due to lack of knowledge of detailed chemical composition of mantle minerals and their elastic properties at various PT conditions when modeling the Earth, direct measurements of the elasticities of natural mantle assemblages would be very valuable to constrain the composition and thermal structure of the deep Earth.

With the improved technology to obtain the 3D tomographic images of the deep Earth, recent studies have shown that the Earth's mantle is very heterogeneous especially in the upper mantle (e.g. Masters et al., 2000; Grand et al., 1997, Romanowicz, 1995, Wen and Anderson, 1997). Thus either the chemical composition or the temperature exhibits large lateral variations. Inasmuch as previous mineral physics studies have shown that no single compositional model

can reproduce all of the observed velocity discontinuities and gradients in global seismological models at mantle depths (e.g., Irifune et al., 2008; Xu et. al., 2008), more investigations are needed on regional variations of composition and/or temperature at various tectonic settings with the context of 3D tomographic studies (e.g., Masters et al., 2000; Grand et al., 1997, Romanowicz, 1995) and/or 1D regional velocity models (e.g., Nolet et al., 1994; Van der Lee and Nolet, 1997). This new approach is the focus of this thesis.

In this study, a series of natural rock samples with composition close to pyrolite were hot pressed at mantle solidus temperatures (e.g., Zhang and Herzberg, 1994) along a mantle geotherm and the elastic properties were measured at high pressures and temperatures to the conditions of mantle transition zone; these acoustic measurements were conducted in multi-anvil high-pressure apparatus by combining ultrasonic interferometry with synchrotron X-radiation. The results of these sound velocity measurements and their implications for the composition and thermal structure of the Earth will be described in detail in the following chapters. The techniques for sample hot-pressing, characterization and for acoustic velocity measurements will be presented in Chapter 2. The newly developed techniques for in-situ determination of pressure and temperature by acoustic travel time and the stress and strain determination in the macroscopic scale for multi-anvil apparatus are discussed in Chapter 3. The application for these techniques to the elastic wave velocities measurements of peridotite KLB-1 at mantle pressures and implications for mantle velocity modeling are presented in Chapter 4. In Chapter 5, I will show the result of appling these directly measured P and S wave velocities for KLB-1 peridotite to the conditions of the transition zone (high PT) and the implications for the mantle composition and temperature under western North America.

Table 1. 1 Comparison of composition and properties at ambient conditions between pyrolite and piclogite models (Anderson and Bass, 1984)

	Pyrolite	Piclogite
Ol (wt%)	57	16
Opx (wt%)	17	6
Cpx (wt%)	12	33
Gt (wt%)	14	45
ρ (g/cm3)	3.379	3.497
Vp (km/s)	8.306	8.445
Vs (km/s)	4.801	4.8

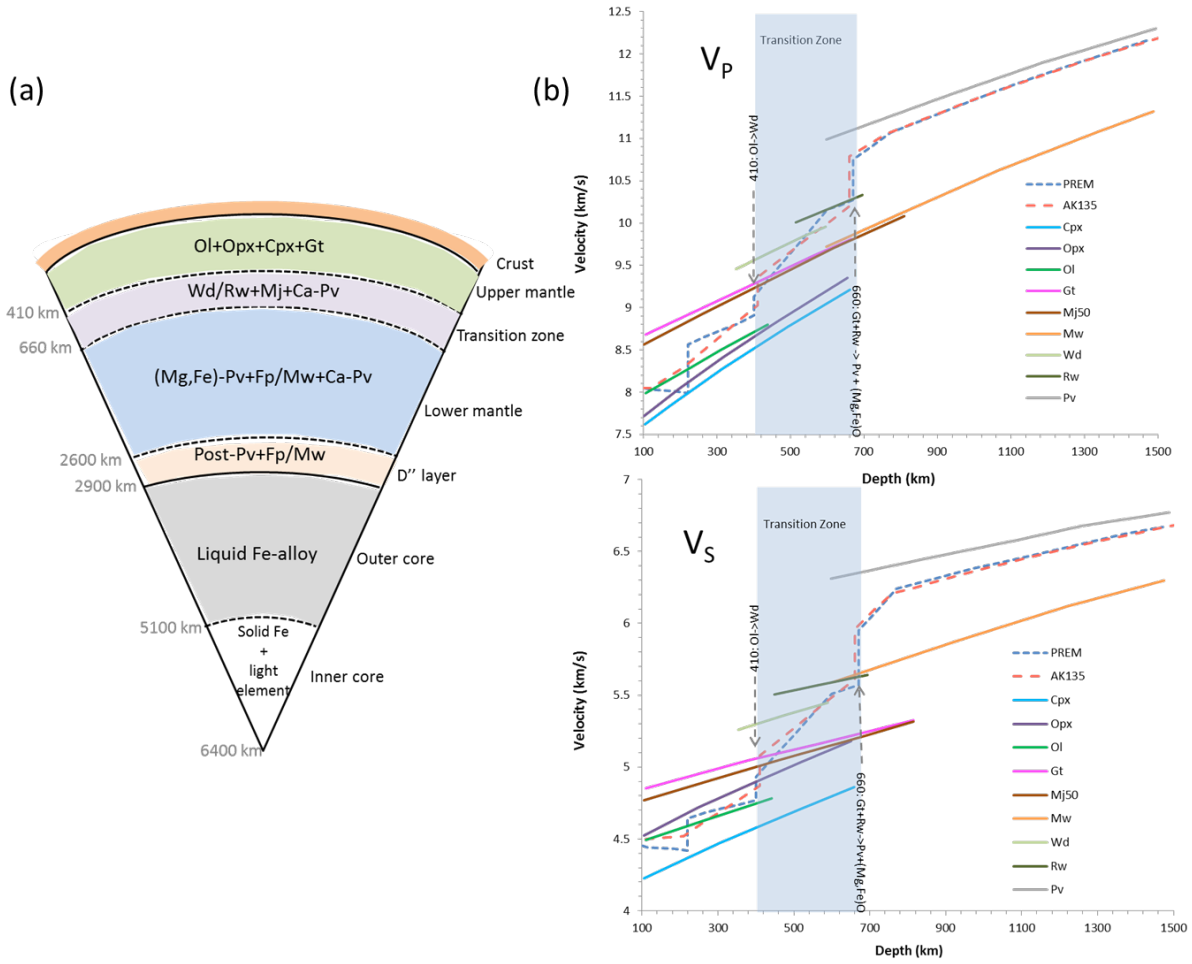

Figure 1. 1 (a) Cross-section of the Earth. The constituent minerals are listed in their corresponding layers. (b) Sound velocities for key mantle minerals as the function of depth along geotherm. Line length for each phase represents the maximum pressure stability. The global average models PREM and AK135 are shown for reference.

Reference

Abramson, E.H., Brown, J.M., Slutsky, L.J. and Zaug, J., 1997. The elastic constants of San Carlos olivine to 17 GPa. Journal of Geophysical Research: Solid Earth, 102(B6), pp.12253-12263.

Akaogi M, Ito E, Navrotsky A. 1989. Olivine-modified spinel-spinel transitions in the system Mg2SiO4- Fe2SiO4: calorimetric measurements, thermochemical calculation, and geophysical application. J. Geophys. Res. 94:15671–85

Akimoto, S.I. and Fujisawa, H., 1968. Olivine-spinel solid solution equilibria in the system Mg2SiO4 - Fe2SiO4. Journal of Geophysical Research, 73(4), pp.1467-1479.

Akimoto, S.I., Fujisawa, H. and Katsura, T., 1965. The olivine-spinel transition in Fe2SiO4 and Ni2SiO4. Journal of Geophysical Research, 70(8), pp.1969-1977.

Anderson, D.L. and Bass, J.D., 1984. Mineralogy and composition of the upper mantle. Geophysical Research Letters, 11(7), pp.637-640.

Angel, R.J. and Jackson, J.M., 2002. Elasticity and equation of state of orthoenstatite, MgSiO3. American Mineralogist, 87(4), pp.558-561.

Bass, J.D. and Anderson, D.L., 1984. Composition of the upper mantle: Geophysical tests of two petrological models. Geophysical Research Letters, 11(3), pp.229-232.

Bass, J.D. and Parise, J.B., 2008. Deep Earth and recent developments in mineral physics. Elements, 4(3), pp.157-163.

Birch, F., 1952. Elasticity and constitution of the Earth's interior. Journal of Geophysical Research, 57(2), pp.227-286.

Cammarano, F., Goes, S., Vacher, P. and Giardini, D., 2003. Inferring upper-mantle temperatures from seismic velocities. Physics of the Earth and Planetary Interiors, 138(3), pp.197-222.

Chai, M., Brown, J.M. and Slutsky, L.J., 1997. The elastic constants of an aluminous orthopyroxene to 12.5 GPa. Journal of Geophysical Research: Solid Earth, 102(B7), pp.14779-14785.

Chantel, J., Frost, D.J., McCammon, C.A., Jing, Z. and Wang, Y., 2012. Acoustic velocities of pure and iron-bearing magnesium silicate perovskite measured to 25 GPa and 1200 K. Geophysical Research Letters, 39(19).

Chen, G., Cooke, J.A., Gwanmesia, G.D. and Liebermann, R.C., 1999. Elastic wave velocities of Mg3Al2Si3O12-pyrope garnet to 10 GPa. American Mineralogist, 84(3), pp.384-388.

Chen, G., Liebermann, R.C. and Weidner, D.J., 1998. Elasticity of single-crystal MgO to 8 gigapascals and 1600 kelvin. Science, 280(5371), pp.1913-1916.

Collins, M.D. and Brown, J.M., 1998. Elasticity of an upper mantle clinopyroxene. Physics and chemistry of minerals, 26(1), pp.7-13.

Conrad, P.G., Zha, C.S., Mao, H.K. and Hemley, R.J., 1999. The high-pressure, single-crystal elasticity of pyrope, grossular, and andradite. American Mineralogist, 84(3), pp.374-383.

Darling, K.L., Gwanmesia, G.D., Kung, J., Li, B. and Liebermann, R.C., 2004. Ultrasonic measurements of the sound velocities in polycrystalline San Carlos olivine in multi-anvil, high-pressure apparatus. Physics of the Earth and Planetary Interiors, 143, pp.19-31.

Duffy, T.S., Zha, C.S., Downs, R.T., Mao, H.K. and Hemley, R.J., 1995. Elasticity of forsterite to 16 GPa and the composition of the upper mantle. Nature, 378(6553), pp.170-173.

Dziewonski, A.M. and Anderson, D.L., 1981. Preliminary reference Earth model. Physics of the earth and planetary interiors, 25(4), pp.297-356.

Flesch, L.M., Li, B. and Liebermann, R.C., 1998. Sound velocities of polycrystalline MgSiO3-orthopyroxene to 10 GPa at room temperature. American Mineralogist, 83(5), pp.444-450.

Gasparik, T., 1989. Transformation of enstatite-diopside-jadeite pyroxenes to garnet. Contributions to Mineralogy and Petrology, 102(4), pp.389-405.

Gasparik, T., 1992. Enstatite-jadeite join and its role in the Earth's mantle. Contributions to Mineralogy and Petrology, 111(3), pp.283-298.

Goes, S. and van der Lee, S., 2002. Thermal structure of the North American uppermost mantle inferred from seismic tomography. Journal of Geophysical Research: Solid Earth, 107(B3).

Grand, S.P., van der Hilst, R.D. and Widiyantoro, S., 1997. High resolution global tomography: a snapshot of convection in the Earth. Geological Society of America Today, 7(4).

Gwanmesia, G.D., Wang, L., Heady, A. and Liebermann, R.C., 2014. Elasticity and sound velocities of polycrystalline grossular garnet ($Ca_3Al_2Si_3O_{12}$) at simultaneous high pressures and high temperatures. Physics of the Earth and Planetary Interiors, 228, pp.80-87.

Gwanmesia, G.D., Wang, L., Triplett, R. and Liebermann, R.C., 2009. Pressure and temperature dependence of the elasticity of pyrope–majorite [Py60Mj40 and Py50Mj50] garnets solid solution measured by ultrasonic interferometry technique. Physics of the Earth and Planetary Interiors, 174(1), pp.105-112.

Gwanmesia, G.D., Zhang, J., Darling, K., Kung, J., Li, B., Wang, L., Neuville, D. and Liebermann, R.C., 2006. Elasticity of polycrystalline pyrope ($Mg_3Al_2Si_3O_{12}$) to 9 GPa and 1000 ºC. Physics of the Earth and Planetary Interiors, 155(3), pp.179-190.

Hashin, Z. and Shtrikman, S., 1962a. A variational approach to the theory of the effective magnetic permeability of multiphase materials. Journal of applied Physics, 33(10), pp.3125-3131.

Hashin, Z. and Shtrikman, S., 1962b. On some variational principles in anisotropic and nonhomogeneous elasticity. Journal of the Mechanics and Physics of Solids, 10(4), pp.335-342.

Hashin, Z. and Shtrikman, S., 1963. A variational approach to the theory of the elastic behaviour of multiphase materials. Journal of the Mechanics and Physics of Solids, 11(2), pp.127-140.

Higo, Y., Inoue, T., Irifune, T., Funakoshi, K.I. and Li, B., 2008. Elastic wave velocities of (Mg $_{0.91}$ Fe $_{0.09}$) $_2$ SiO $_4$ ringwoodite under P–T conditions of the mantle transition region. Physics of the Earth and Planetary Interiors, 166(3), pp.167-174.

Hill, R., 1952. The elastic behaviour of a crystalline aggregate. Proceedings of the Physical Society. Section A, 65(5), p.349.

Irifune, T. and Isshiki, M., 1998. Iron partitioning in a pyrolite mantle and the nature of the 410-km seismic discontinuity. Nature, 392(6677), pp.702-705.

Irifune, T. and Ringwood, A.E., 1987. Phase transformations in a harzburgite composition to 26 GPa: implications for dynamical behaviour of the subducting slab. Earth and Planetary Science Letters, 86(2), pp.365-376.

Irifune, T. and Ringwood, A.E., 1993. Phase transformations in subducted oceanic crust and buoyancy relationships at depths of 600–800 km in the mantle. Earth and Planetary Science Letters, 117(1-2), pp.101-110.

Irifune, T., 1987. An experimental investigation of the pyroxene-garnet transformation in a pyrolite composition and its bearing on the constitution of the mantle. Physics of the Earth and Planetary Interiors, 45(4), pp.324-336.

Irifune, T., Higo, Y., Inoue, T., Kono, Y., Ohfuji, H. and Funakoshi, K., 2008. Sound velocities of majorite garnet and the composition of the mantle transition region. Nature, 451(7180), pp.814-817.

Ita, J. and Stixrude, L., 1992. Petrology, elasticity, and composition of the mantle transition zone. Journal of Geophysical Research: Solid Earth, 97(B5), pp.6849-6866.

Ito, E. and Yamada, H., 1982. Stability relations of silicate spinels, ilmenites, and perovskites. High-pressure research in geophysics, pp.405-419.

Jackson, I. and Niesler, H., 1982. The elasticity of periclase to 3 GPa and some geophysical implications. High pressure research in geophysics, 12, pp.93-113.

Jackson, I., and Rigden, S. M., 1998. In the Earth's Mantle: Composition, Structure, and Evolution, ed. Jackson I (Cambridge U. Press, Cambridge, UK), 405–460.

Jacobsen, S.J., Reichmann, H.J., Kantor A., Spetzler, H.A., 2005. A gigahertz ultrasonic interferometry for the diamond anvil cell and high-presure elasticity of some iron-oxide materials. In: Advances in High-Pressure Technology for Geophysical Applications, Chen, J. Wang, Y. Duffy, T.S. Shen, G. Dobrzhinetskaya, L.F. Elsevier, pp. 25–48

Jiang, F., Speziale, S. and Duffy, T.S., 2004. Single-crystal elasticity of grossular-and almandine-rich garnets to 11 GPa by Brillouin scattering. Journal of Geophysical Research: Solid Earth, 109(B10).

Katsura, T. and Ito, E., 1989. The system Mg_2SiO_4-Fe_2SiO_4 at high pressures and temperatures: Precise determination of stabilities of olivine, modified spinel, and spinel. Journal of Geophysical Research: Solid Earth, 94(B11), pp.15663-15670.

Kennett, B.L.N., Engdahl, E.R. and Buland, R., 1995. Constraints on seismic velocities in the Earth from traveltimes. Geophysical Journal International, 122(1), pp.108-124.

Kono, Y., Gréaux, S., Higo, Y., Ohfuji, H. and Irifune, T., 2010. Pressure and temperature dependences of elastic properties of grossular garnet up to 17 GPa and 1 650 K. Journal of Earth Science, 21(5), pp.782-791.

Kono, Y., Higo, Y., Ohfuji, H., Inoue, T. and Irifune, T., 2007. Elastic wave velocities of garnetite with a MORB composition up to 14 GPa. Geophysical Research Letters, 34(14).

Kung, J., Li, B., Uchida, T. and Wang, Y., 2005. In-situ elasticity measurement for the unquenchable high-pressure clinopyroxene phase: Implication for the upper mantle. Geophysical research letters, 32(1).

Kung, J., Li, B., Uchida, T., Wang, Y., Neuville, D. and Liebermann, R.C., 2004. In situ measurements of sound velocities and densities across the orthopyroxene→ high-pressure clinopyroxene transition in MgSiO 3 at high pressure. Physics of the Earth and Planetary Interiors, 147(1), pp.27-44.

Kung, J., Li, B., Weidner, D.J., Zhang, J. and Liebermann, R.C., 2002. Elasticity of ($Mg_{0.83}$, $Fe_{0.17}$) O ferropericlase at high pressure: ultrasonic measurements in conjunction with X-radiation techniques. Earth and Planetary Science Letters, 203(1), pp.557-566.

Li, B. and Liebermann, R.C., 2000. Sound velocities of wadsleyite b-$(Mg_{0.88}Fe_{0.12})_2SiO_4$ to 10 GPa. American Mineralogist, 85(2-3), pp.292-295.

Li, B. and Liebermann, R.C., 2007. Indoor seismology by probing the Earth's interior by using sound velocity measurements at high pressures and temperatures. Proceedings of the National Academy of Sciences, 104(22), pp.9145-9150.

Li, B. and Neuville, D.R., 2010. Elasticity of diopside to 8GPa and 1073K and implications for the upper mantle. Physics of the Earth and Planetary interiors, 183(3), pp.398-403.

Li, B. and Zhang, J., 2005. Pressure and temperature dependence of elastic wave velocity of MgSiO 3 perovskite and the composition of the lower mantle. Physics of the Earth and Planetary Interiors, 151(1), pp.143-154.

Li, B., 2003. Compressional and shear wave velocities of ringwoodite γ-Mg_2SiO_4 to 12 GPa. American Mineralogist, 88(8-9), pp.1312-1317.

Li, B., Gwanmesia, G.D. and Liebermann, R.C., 1996. Sound velocities of olivine and beta polymorphs of Mg_2SiO_4 at Earth's transition zone pressures. Geophysical Research Letters, 23(17), pp.2259-2262.

Li, B., Kung, J. and Liebermann, R.C., 2004. Modern techniques in measuring elasticity of Earth materials at high pressure and high temperature using ultrasonic interferometry in conjunction

with synchrotron X-radiation in multi-anvil apparatus. Physics of the Earth and Planetary Interiors, 143, pp.559-574.

Li, B., Liebermann, R.C. and Weidner, D.J., 1998. Elastic moduli of wadsleyite (β-Mg_2SiO_4) to 7 Gigapascals and 873 Kelvin. Science, 281(5377), pp.675-677.

Li, B., Woody, K. and Kung, J., 2006. Elasticity of MgO to 11 GPa with an independent absolute pressure scale: Implications for pressure calibration. Journal of Geophysical Research: Solid Earth, 111(B11).

Liebermann, R.C. and Mayson, D.J., 1976. Elastic properties of polycrystalline diopside ($CaMgSi_2O_6$). Physics of the Earth and Planetary Interiors, 11(3), pp.P1-P4.

Liu, L.G., 1977. The system enstatite-pyrope at high pressures and temperatures and the mineralogy of the earth's mantle. Earth and Planetary Science Letters, 36(1), pp.237-245.

Liu, Q., Liu, W., Whitaker, M.L., Wang, L. and Li, B., 2008. Compressional and shear wave velocities of Fe2SiO4 spinel at high pressure and high temperature. High Pressure Research, 28(3), pp.405-413.

Liu, W., Kung, J. and Li, B., 2005. Elasticity of San Carlos olivine to 8 GPa and 1073 K. Geophysical Research Letters, 32(16).

Liu, W., Kung, J., Li, B., Nishiyama, N. and Wang, Y., 2009. Elasticity of $(Mg_{0.87}Fe_{0.13})_2SiO_4$ wadsleyite to 12GPa and 1073K. Physics of the Earth and Planetary Interiors, 174(1), pp.98-104.

Lu, C., Mao, Z., Lin, J.F., Zhuravlev, K.K., Tkachev, S.N. and Prakapenka, V.B., 2013. Elasticity of single-crystal iron-bearing pyrope up to 20GPa and 750K. Earth and Planetary Science Letters, 361, pp.134-142.

Mao, H.K., Wu, Y., Chen, L.C., Shu, J.F. and Jephcoat, A.P., 1990. Static compression of iron to 300 GPa and $Fe_{0.8}Ni_{0.2}$ alloy to 260 GPa: Implications for composition of the core. Journal of Geophysical Research: Solid Earth, 95(B13), pp.21737-21742.

Mao, Z., Jacobsen, S.D., Frost, D.J., McCammon, C.A., Hauri, E.H. and Duffy, T.S., 2011. Effect of hydration on the single-crystal elasticity of Fe-bearing wadsleyite to 12 GPa. American Mineralogist, 96(10), pp.1606-1612.

Mao, Z., Jacobsen, S.D., Jiang, F., Smyth, J.R., Holl, C.M. and Duffy, T.S., 2008. Elasticity of hydrous wadsleyite to 12 GPa: implications for Earth's transition zone. Geophysical Research Letters, 35(21).

Mao, Z., Lin, J.F., Jacobsen, S.D., Duffy, T.S., Chang, Y.Y., Smyth, J.R., Frost, D.J., Hauri, E.H. and Prakapenka, V.B., 2012. Sound velocities of hydrous ringwoodite to 16GPa and 673K. Earth and Planetary Science Letters, 331, pp.112-119.

Masters, G., Laske, G., Bolton, H. and Dziewonski, A., 2000. The relative behavior of shear velocity, bulk sound speed, and compressional velocity in the mantle: implications for chemical

and thermal structure. Earth's deep interior: mineral physics and tomography from the atomic to the global scale, pp.63-87.

Meng, Y., Shen, G. and Mao, H.K., 2006. Double-sided laser heating system at HPCAT for in situ x-ray diffraction at high pressures and high temperatures. Journal of Physics: Condensed Matter, 18(25), p.S1097.

Morishima, H., Kato, T., Suto, M., Ohtani, E., Urakawa, S., Utsumi, W., Shimomura, O. and Kikegawa, T., 1994. The phase boundary between α-and β-Mg_2SiO_4 determined by in situ X-ray observation. Science, 265(5176), pp.1202-1203.

Nolet, G., Grand, S.P. and Kennett, B.L.N., 1994. Seismic heterogeneity in the upper mantle. Journal of Geophysical Research: Solid Earth, 99(B12), pp.23753-23766.

Núñez‐Valdez, M., Wu, Z., Yu, Y.G. and Wentzcovitch, R.M., 2013. Thermal elasticity of $(Fex, Mg1-x)_2SiO_4$ olivine and wadsleyite. Geophysical Research Letters, 40(2), pp.290-294.

O'Neill, B., Bass, J.D., Smyth, J.R. and Vaughan, M.T., 1989. Elasticity of a grossular-pyrope-almandine garnet. Journal of Geophysical Research: Solid Earth, 94(B12), pp.17819-17824.

Poirier, J.P., 2000. Introduction to the Physics of the Earth's Interior. Cambridge University Press.

Rigden, S.M. and Jackson, I., 1991. Elasticity of germanate and silicate spinels at high pressure. Journal of Geophysical Research: Solid Earth, 96(B6), pp.9999-10006.

Rigden, S.M., Gwanmesia, G.D., Jackson, I. and Liebermann, R.C., 1993. Progress in High-Pressure Ultrasonic Interferometry, the Pressure Dependence of Elasticity of Mg_2SiO_4 Polymorphs and Constraints on the Composition of the Transition Zone of the Earth's Mantle. High-pressure research: application to earth and planetary sciences, pp.167-182.

Ringwood, A. E., 1975. Composition and petrology of the earth's mantle, McGraw-Hill, New York, pp. 618.

Romanowicz, B., 1995. A global tomographic model of shear attenuation in the upper mantle. Journal of Geophysical Research: Solid Earth, 100(B7), pp.12375-12394.

Sang, L. and Bass, J.D., 2014. Single-crystal elasticity of diopside to 14GPa by Brillouin scattering. Physics of the Earth and Planetary Interiors, 228, pp.75-79.

Sinelnikov, Y.D., Chen, G., Neuville, D.R., Vaughan, M.T. and Liebermann, R.C., 1998. Ultrasonic shear wave velocities of MgSiO3 perovskite at 8 GPa and 800 K and lower mantle composition. Science, 281(5377), pp.677-679.

Sinogeikin, S.V. and Bass, J.D., 2000. Single-crystal elasticity of pyrope and MgO to 20 GPa by Brillouin scattering in the diamond cell. Physics of the Earth and Planetary Interiors, 120(1), pp.43-62.

Van der Lee, S., and Nolet, G., 1997. Upper mantle S velocity structure of North America. Journal of Geophysical Research: Solid Earth 102, no. B10: 22815-22838.

Wang, X., Chen, T., Zou, Y., Liebermann, R.C. and Li, B., 2015. Elastic wave velocities of peridotite KLB-1 at mantle pressures and implications for mantle velocity modeling. Geophysical Research Letters, 42(9), pp.3289-3297.

Wang, Z. and Ji, S., 2001. Elasticity of six polycrystalline silicate garnets at pressure up to 3.0 GPa. American Mineralogist, 86(10), pp.1209-1218.

Weidner, D.J., 1985. A mineral physics test of a pyrolite mantle. Geophysical Research Letters, 12(7), pp.417-420.

Weidner, D.J., Sawamoto, H., Sasaki, S. and Kumazawa, M., 1984. Single-crystal elastic properties of the spinel phase of Mg_2SiO_4. Journal of Geophysical Research: Solid Earth, 89(B9), pp.7852-7860.

Wen, L. and Anderson, D.L., 1995. The fate of slabs inferred from seismic tomography and 130 million years of subduction. Earth and Planetary Science Letters, 133(1), pp.185-198.

Wen, L. and Anderson, D.L., 1997. Slabs, hotspots, cratons and mantle convection revealed from residual seismic tomography in the upper mantle. Physics of the Earth and Planetary Interiors, 99(1), pp.131-143.

Yoneda, A., 1990. Pressure derivatives of elastic constants of single crystal MgO and $MgAl_2O_4$. Journal of Physics of the Earth, 38(1), pp.19-55.

Zha, C.S., Duffy, T.S., Downs, R.T., Mao, H.K. and Hemley, R.J., 1996. Sound velocity and elasticity of single-crystal forsterite to 16 GPa. Journal of Geophysical Research: Solid Earth, 101(B8), pp.17535-17545.

Zha, C.S., Duffy, T.S., Downs, R.T., Mao, H.K. and Hemley, R.J., 1998. Brillouin scattering and X-ray diffraction of San Carlos olivine: direct pressure determination to 32 GPa. Earth and Planetary Science Letters, 159(1), pp.25-33.

Zha, C.S., Duffy, T.S., Mao, H.K., Downs, R.T., Hemley, R.J. and Weidner, D.J., 1997. Single-crystal elasticity of β-Mg_2SiO_4 to the pressure of the 410 km seismic discontinuity in the Earth's mantle. Earth and Planetary Science Letters, 147(1), pp.E9-E15.

Zhang, D., Jackson, J.M., Chen, B., Sturhahn, W., Zhao, J., Yan, J. and Caracas, R., 2013. Elasticity and lattice dynamics of enstatite at high pressure. Journal of Geophysical Research: Solid Earth, 118(8), pp.4071-4082.

Zhang, J. and Herzberg, C., 1994. Melting experiments on anhydrous peridotite KLB-1 from 5.0 to 22.5 GPa. Journal of Geophysical Research: Solid Earth, 99(B9), pp.17729-17742.

Zou, Y., Gréaux, S., Irifune, T., Whitaker, M.L., Shinmei, T. and Higo, Y., 2012. Thermal equation of state of $Mg_3Al_2Si_3O_{12}$ pyrope garnet up to 19 GPa and 1,700 K. Physics and Chemistry of Minerals, 39(7), pp.589-598.

Chapter 2 Experimental techniques and data processing

2.1 Sample hot-pressing techniques

2.1.1 Introduction

KLB-1 peridotite is a spinel lherzolite xenolith from the Kilbourne Hole, New Mexico (Takahashi, 1986; Zhang and Herzberg, 1994). Since the chemical composition of KLB-1 closely matches that of pyrolite, many authors have conducted research on its melting temperature at high pressures as well as the compositions of the melts and the residual phases upon partial melting to investigate the petrogenesis of mid-ocean ridge basalts (MORB) and the evolution of the continental lithosphere (e.g., Takahashi, 1986; Zhang and Herzberg, 1994). When equilibrated at various pressures along the geotherm, KLB-1 produces a synthetic "rock" whose mineralogy closely resembles that of pyrolitic mantle; thus, acoustic velocities measurement on these synthetic rocks can yield elasticity data that account for the physical (pressure, temperature) and chemical conditions (phase fractions, elemental partitioning among co-existing phases, and the effect of minor and trace elements on elasticity) at relevant mantle depths.

The starting material for the acoustic samples is KLB-1 peridotite rocks donated by Dr. Claude Herzberg. Its bulk composition has been determined in several previous studies (e.g. Herzberg et al., 1990; Takahashi, 1986); in which are summarized Table 2.1 and compared with pyrolite and CI carbonaceous chondrite. In this section, the sample hot-pressing methods and conditions will be summarized. We will also show the results for the sample characterization

including electron microprobe results for determination of the mineral composition, SEM images before/after acoustic experiments and X-ray diffraction to determine the crystal structure.

2.1.2 Hot pressing of KLB-1 specimens

One of the key points for accurately determining the velocity-depth profile of the KLB-1 mantle is to fabricate specimens of high quality KLB-1 aggregates at equilibrium P and T conditions which are suitable for high-frequency ultrasonic interferometric measurements of P and S wave velocities at high P-T conditions. In synthesis experiments, the starting material is KLB-1 peridotite powder, whose bulk composition is identical to those of Herzberg et al. (1990). Previous studies have shown that powdered samples of KLB-1 equilibrate quickly during hot pressing, while the sintered samples re-equilibrate more slowly at different PT conditions (Sojda and Wang, 2002). Thus, it is essential to hot press multiple specimens at conditions up to the mantle transition zone with an increment of 2-3 GPa in pressure at temperatures closely following the mantle geotherm.

The high-pressure apparatus used for hot pressing and sound velocity measurements is a two stage multi-anvil press capable of synthesizing large volume samples (mm sized) at mantle conditions. The first stage of this 2000-ton uniaxial split-sphere apparatus (USSA-2000) (Gwanmesia and Liebermann, 1992; Gwanmesia et al., 1993 and Liebermann and Wang, 1992) consists of a six-piece tool steel sphere glued to the upper and lower guide blocks. The second stage consists of eight tungsten carbide (WC) cubes with truncated corners, which form an octahedral cavity containing the cell assembly. Pyrophllite gaskets placed along the lengths of the truncated edges separate the WC cubes. The cell assemblies used in this study are 14/8 G2 cell, 14/8 High T cell and 10/5 cell obtained from Kurt Leinenweber at Arizona State University

through the COMPRES (COnsortium for Materials Properties Research in Earth Sciences) Multi-Anvil Cell Assembly Initiative. These dimensions (generally designed as 14/8, 10/5 and 8/3) allow a wide range of pressures and temperatures to be achieved for high pressure experiments. 14/8 means the MgO octahedron has a 14 mm edge length and the truncated edges of the WC cubes are 8 mm. 14/8 G2 cell uses graphite as heater and the 14/8 High T cell and 10/5 cell use Re as heater for higher temperatures. The differences between the 14/8 G2 cell and the 14/8 High T cell are shown in Figure 2.1. 10/5 cell is similar to the 14/8 High T cell with a straight Re furnace while the 14/8 G2 cell has a box furnace made of graphite (see detailed descriptions in Leinenweber et al., 2012).

The hot pressing cell assembly, procedures and PT path are shown in Figure 2.1 and Figure 2.2. Briefly, in the cross section of the MgO octahedron in Figure 2.1, a powder sample is enclosed in an iron/rhenium capsule; heating to the sample is provided through resistivity heater of graphite/rhenium. The duration is 1 hour for the sample under 8 GPa and 11 hours for the sample hot pressed above 10 GPa. The longer duration for the sample hot pressed at the condition of the transition zone is to ensure the olivine is fully transformed to wadsleyite and the long term diffusion and partitioning are completed. During decompression, a special PT path was used by firstly decreasing the temperature until it reached ~300ºC. Then the temperature was maintained during decompression (~20 bars/hr) until oil pressure decreased to 50 bars. The purpose of the path is to anneal intergranular stress to avoid shattering (e.g., Gwanmesia et al., 1993). All of the hot pressing experiments are summarized in Table 2.2. KLB-1 specimens were successfully synthesized and hot-pressed at 3 GPa 1400 °C, 3 GPa 1200 °C, 5 GPa 1200 °C, 6 GPa 1200 °C and 8GPa 1300 °C and 15 GPa 1200 °C using 14/8 and 10/5 cell assemblies in 1000-ton/2000-ton uniaxial split-cylinder apparatus, following the procedures described in

Gwanmesia et al. (1993) (see also Figure 2.2). Previous attempts to synthesize KLB-1 specimens at pressures between 9 GPa and 14 GPa at various temperatures have all failed. The recovered samples are all still powder. A suggested cause for this is that the phase transition from orthopyroxene to high pressure clinopyroxene at ~8 GPa is not reversible. The high pressure clinopyroxene would transform to a low pressure clinopyroxene which has a larger unit cell volume during decompression.

2.2 Characterization of KLB-1 specimens

An ideal sample for in-situ velocity measurements should be uniform, full dense and of small grain size to be used in high-frequency ultrasonic measurements to avoid scattering. The recovered samples are in cylindrical shape, with diameter in the range of 2-3 mm and length of 1.5-2.5 mm. Density measurement on these KLB-1 specimens hot pressed at 3-8 GPa using the Archimedes' method yielded the bulk density of 3.34-3.36 g/cm^3. The specimens for acoustic measurements, are examined and characterized by scanning electron microscope (SEM) and Electron probe micro-analyzer (EPMA) analyses by polishing with 1-μm diamond paste. SEM analysis reveals that the specimens used for acoustic measurements (e.g., K657, K973, and K1000) are well-sintered, of average grain size ~ 10 micron, and free of visible micro-cracks (see Figure 2.3, 2.4). The melted specimens have special features as shown in Figure 2.5. The sample has become olivine rich and has metallic spots inside the sample.

2.2.1 Electron Microprobe Analysis

EPMA analyses have the capability to acquire precise, quantitative analyses with the beam size as small as 1-2 microns. Combining the secondary and back-scattered electrons to

create detailed images of the sample surface, it is the most commonly used method to obtain the chemical composition of geological materials like KLB-1 peridotite.

In this study, we examined most of the sintered samples to check their composition. The chemical compositions of the constituent mineral phases were obtained by averaging at least 4-5 electron microprobe analyses of KLB-1 specimens (see Table 2.3). The olivine (Ol) has a Mg # [Mg / (Mg+Fe)] of 89-90, which is similar to that observed for fertile xenoliths (e.g. Lee, 2003). Only trace amounts of Ca, Al, and Mn are detected in olivine grains. The compositions of orthopyroxene (Opx, Mg#~89-90) and clinopyroxene (Cpx, Mg#~89-90), in the current KLB-1 aggregate show a good agreement with those reported by Chai et al. (1997) and Collins and Brown (1998) for natural Kilbourne Hole orthopyroxenes (KBH Opx) and clinopyroxenes (KBH Cpx). With the averaged composition of each mineral, the modal composition of each specimen can be obtained using mass balance based on the bulk composition of KLB-1 from previous studies (e.g., Herzberg et al., 1990; Davis et al., 2009). The composition of each specimen is summarized in Table 2.3. As shown in Table 2.3, five phases have been identified from microprobe analysis: Ol, Opx, Cpx, Gt and spinel (Sp). Mineral modes were calculated based on the bulk composition reported in Herzberg et al., (1990). We note that when spinel was included in the products, an unrealistic (negative) value is resulted; we therefore calculated the modes with an estimated amount of spinel (<< 1%) as shown in Table 2.3. The modes agree with previous studies on natural peridotites which indicate that the formation of garnet involves the consumption of orthopyroxene and spinel through 2Opx + Sp = Gt + Ol (O'Neill, 1981; Perkins and Anthony, 2011) and/or Cpx + Sp = Gt + Ol (Perkins and Anthony 2011).

The mineral composition and their fractions of specimens hot pressed at 3-8 GPa are very close as shown in Figure 2.6 and Table 2.3. These results are similar with the composition of

pyrolite samples as the function of pressure by Irifune and Isshiki, (1998). After 8 GPa (~230 km), all the opx are dissolved into garnet, and the mineral compositions changed also. The Mg # slightly increased after that depth.

Tests with previously established clinopyroxene geothermobarometers (Nimis and Taylor, 2000) yield an equilibrium pressure of ~ 3.4 GPa for specimens hot pressed at 3 GPa which is consistent with experimental synthesis pressure (~3 GPa) within mutual uncertainties. Applying the partitioning of Na between Opx and Cpx thermometer given by Brey and Köhler (1990) yields an equilibrium temperature of 1164 ºC, which also shows a good agreement with the experimental temperature of 1200 ºC for specimen K973. However, these thermometers and barometers yield very unreasonable results for specimens hot pressed after 3 GPa.

2.2.2 Powder X-ray diffraction Analysis

X-ray diffraction was also used to identify the phases and obtain the mineral structure information. It is a widely used technique in physics, material sciences and Earth sciences to study the crystal structures by using X-ray on powder/bulk samples, in which the atoms of the crystal will cause the X-ray beam to diffract into specific directions according to the Bragg's Law ($2d\sin\theta = n\lambda$).

To verify if the X-ray diffraction method can provide reasonable results on phase fractions, we did a test by mixing the olivine and pyroxene powders in the weight percentage of 78% and 22% respectively, and collected the X-ray diffraction data using a Scintag powder diffractometer with a Cu target and analyzed the data by GSAS. Rietveld refinement yielded the weight fraction of olivine and pyroxene of 80% and 20%. Thus the powder X-ray diffraction can also be used to obtain phase fractions on multiphase polycrystalline samples. We did two powder

X-ray diffraction experiments on specimen K973 and S4253. For sample S4253, olivine completed the phase transition and all became wadsleyite and was hot pressed at the same condition as S4255. There are small variations between the X-ray results and the probe analyses. The weight fractions results for all three specimens are summarized in Table 2.4.

The main purpose of the X-ray diffraction is to obtain the theoretical density of the specimen and compare it with the measured density by Archimedes' method. Rietveld refinement for specimen K973 yielded a density of 3.344(3) g/cm3, 3.295(3) g/cm3, 3.325(3) g/cm3, and 3.674(5) g/cm3 for olivine, orthopyroxene, clinopyroxene, and garnet, respectively; this results in a theoretical density of 3.353(4) g/cm3 for K973 which is indistinguishable from the measured bulk density (3.357(18) g/cm3), suggesting a maximum porosity of 0.5 % in the specimen. All other specimens used in the acoustic measurements have the same quality as K973 to guarantee high quality ultrasonic signals and reliable velocity results.

2.3 Elastic wave velocity measurements in a multi-anvil apparatus using ultrasonic interferometry

2.3.1 Introduction

In the last half century, several methods were used to obtain the elasticities of mantle rock samples and the key mantle minerals, such as the resonant ultrasound spectroscopy method (e.g., Anderson and Liebermann 1968; Anderson and Isaak, 1995; Yoneda, et al., 2012), ultrasonic methods including pulse-transmission techniques (Hughes and Jones, 1950; Birch, 1960, 1961) and ultrasonic interferometric methods (McSkimin, 1950; Thurston and Brugger, 1964), laser scattering techniques [e.g. Brillouin scattering method (Weidner et a., 1975) and

impulsive stimulated scattering (Abramson et al., 1999)], inelastic scattering (Burkel, 2000) and other techniques.

Among all these methods, ultrasonic interferometric methods have been widely used in obtaining the elastic properties of rocks (e.g., Wang et al., 2015), minerals (e.g., Liu et al., 2005; Kung et al, 2004; Chen et al., 2015; Li and Liebermann, 2000) and glass (e.g., Liu et al., 2011) at high pressures and temperatures in last five decades. These techniques have also been utilized in measurements of sound velocities and attenuation of melts (e.g., Katahara et al., 1981; Rai et al., 1981). The high resolution of ultrasonic interferometry enables the high precision travel time measurements for both P and S wave velocities of interested materials (see McSkimin, 1950, 1961; Wang et al., 2015b).

In this section, I will demonstrate the experimental techniques used in velocity measurements on KLB-1 specimens including the high pressure generation and cell assembly, ultrasonic interferometry used for obtaining travel times, velocity measurements at simultaneous high PT conditions, and the data processing methods.

2.3.2 High pressure generation and cell assembly

Acoustic measurements were conducted in a 1000-ton uniaxial split-cylinder apparatus (USCA-1000) with a Walker-type split cylinder multi-anvil module (Walker et al., 1990) in the Stony Brook High Pressure Lab and a 1000-ton Kawai type large volume apparatus (T-25) at synchrotron X-ray beamline 13-ID-D of Advanced Photon Source, Argonne National Laboratory. The module (Figure 2.7) consists of six removable split cylinder anvils. These first stage tool steel anvils enclose a cubic cavity, in which the eight tungsten carbide cubes form the second stage for compressing the cell. The cubes used in this study have 25 cm edge and eight truncated

corners with a triangular face. The size of the cubes and their truncations vary depending on the desired pressure and sample volume of the experiment.The truncated corners with an edge length of 8 mm are used in all acoustic velocity measurements in this study. The cubes are separated by pyrophyllite gaskets and balsa wood spacers. A semi-sintered MgO octahedron is placed in the cavity formed at the center of the eight tungsten carbide cubes and served as pressure transmitting medium. The pressure determination methods will be described in detail in Chapter 3.

Figure 2.8 shows the cross section of the octahedral cell assembly used at room temperature velocity measurements at the High Pressure Lab at Stony Brook University (Figure 2.8 a) and the high temperature measurements at Beamline 13-ID-D of Argonne National Lab (Figure 2.8 b). For both assemblies, a dual-mode $LiNbO_3$ transducer (10ºY-cut) mounted on the back of one WC cube is used for simultaneously generating and receiving P and S wave signals. The WC cube serves as an external buffer rod to transmit the acoustic signals to and from the cell. The standard materials such as Al_2O_3 and W placed next to the sample are used as internal buffer rod with suitable acoustic impedance relative to the sample and the WC anvil. The backing piece is a soft material like NaCl and leads to a pseudohydrostatic pressure environment for the sample. In high-temperature experiments at synchrotron beamline (Figure 2.8 b), the sample is surrounded by a mixture of NaCl plus BN (10:1 by weight) to serve as the pressure standard (see Chapter 3 for details). A graphite heater is used for the high-temperature measurements. The temperature is measured using W3%Re-W25%Re thermocouples placed against the MgO cap next to the NaCl backing piece.

2.3.3 Ultrasonic interferometry

Figure 2.9 shows the principle of travel time measurements using interferometric method. The input signal is transmitted from the transducer via the buffer rod into the sample. The propagating wave is partially reflected back at the interface of the buffer rod and sample (buffer rod echo) and the remaining acoustic energy transmitted into the specimen is reflected at the back of the sample (sample echo). These echoes are recorded by the transducer with a delay time of Δt corresponding to the waves traveling round trip inside the sample. The dual-mode LiNbO3 transducers enable measurements of P and S wave velocities simultaneously. The transfer function method was developed (Li et al., 2002) by using a wideband input signal containing all the frequency components centered at the resonance frequency of the transducer. It can reduce the data collection time from more than 30 min using individual frequencies to a few seconds (Li et al., 2002, 2004). The pulse echo overlap (PEO) method is used for the determination of travel times by directly moving the sample echo to overlap with the buffer rod echo in time axis (Papadakis, 1968).

2.3.4 Velocity measurements at simultaneous high PT conditions

2.3.4.1 Introduction

Using synchrotron radiation in conjunction with the recent state-of-the-art of ultrasonics and X-ray diffraction techniques enables sound velocity measurements of the elastic/mechanical properties for both single-crystal and polycrystalline materials at simultaneous high-pressure and high-temperature conditions . In particular, the more recent implementation of X-radiography to the existing setup enables us to measure sample lengths directly at high P-T conditions in large-

volume apparatus on beamline X17B2 at Brookhaven National Laboratory and 13-ID-D at Argonne National Laboratory.

With the application of these state-of-the-art techniques, synchrotron experiments show many advantages, as compared with the conventional ex-situ (quench) experiments. The traditional ex-situ experiments for determining pressure (i.e., a calibration curve fitted by some fixed points calibrated by using well-known phase transitions) are not precise enough to obtain the pressure and temperature dependences of the elastic modulus and cannot readily be applied at high temperatures. Moreover, the estimation of the sample length (needed for converting travel times to velocities at high pressures and temperatures) using previous equation-of-state (EOS) data is not reliable, especially when the sample environment deviates from hydrostatic conditions and plastic deformation occurs at high temperatures.

Therefore, with the application of the synchrotron radiation, we can obtain high-quality in-situ X-ray diffraction patterns of the pressure marker and specimen as well as its X-radiography images, which enable us to precisely determine the stability and elastic properties of KLB-1 at high pressure and high temperature combined with simultaneous X-ray diffraction and ultrasonic measurement techniques in multi-anvil apparatus.

2.3.4.2 Experimental setup

Figure 2.10 shows the schematic diagram of the experimental configuration for simultaneous ultrasonic, X-ray diffraction, and X-ray imaging measurements using the 1000-ton Kawai type large volume apparatus (T-25) installed at synchrotron X-ray beamline 13-ID-D of Advanced Photon Source, Argonne National Laboratory.

The experimental setup includes the multi-anvil press, the ultrasonic measurement system, the solid-state detector and the X-ray imaging system. Data collected in my experiments using this setup mainly includes the X-ray diffraction from the sample and the pressure standard, the ultrasonic waveforms using transfer function method and the X-ray radiographic image of the sample. During the experiment, X-ray diffraction patterns from both the sample and the pressure standard surrounding the sample (e.g., NaCl) are collected using energy dispersive X-radiation source at a certain diffracting angle to detect the structure change of the sample and the cell pressure. The X-ray imaging system for capturing the image of the sample during the high-pressure experiment contains of an aluminum garnet YAG scintillator and a charge-coupled device CCD camera (Li et al., 2004, 2005). The brightness contrast between the sample and its neighboring materials results from the difference in the X-ray absorption coefficients of the various materials in the high-pressure cell assembly (Figure 2.10 c) Gold foils with high x-ray absorption are placed on the front and the back of the sample (Figure 2.8 b) in case the sample have similar absorption coefficients with buffer rod or the backing piece. In high-pressure ultrasonic measurements, such 2 μm thick gold foils are used at the sample/buffer rod interface to enhance the mechanical coupling between the buffer rod and sample as shown in Figure 2.8 a and Figure 2.8 b (e.g., Wang et al., 2015a). The sample length is obtained from the pixel numbers between two gold foils combining with the length per pixel defined by the total pixel number of the sample region in the last image collect at ambient condition to be the metric length of the recovered sample measured by a precise micrometer (Li et al., 2004).

The set up at beamline X-17B2 at the Brookhaven National Laboratory is very similar to the setup discussed above with a one stage Deformation-DIA (D-DIA) type multi-anvil apparatus (SAM 85) (see details in Li et al., 2004).

2.3.5 Data analysis method

Since V=2l/t (V is the velocity, l is the length of the sample and t is the round trip travel time for the sample), with high-precision P and S wave travel times obtained from PEO method, the sample length is needed for calculating velocities. In experiments conducted at synchrotron beamlines, the sample length is obtained from the X-ray image of the sample from the number of pixels of the sample region as discussed in the section above. For off-line high pressure experiments at room temperature, with the measurements of both P and S wave travel times, the length change at high pressures can be obtained by Cook's method (Cook, 1957): $\frac{l_0}{l}=1+\frac{1+\alpha\gamma T}{12\rho_0 l_0^2}\int_0^p \frac{dp}{\frac{1}{t_p^2}-\frac{4}{3t_s^2}}$, where t_p and t_s are the P and S wave travel times with specimen length l, subscript ''0'' represents values at ambient condition. The term $(1 + \boldsymbol{\alpha\gamma T})$ accounts for the conversion from adiabatic to isothermal values for the bulk modulus $K_S = K_T (1 + \boldsymbol{\alpha\gamma T})$, $\boldsymbol{\alpha}$ is the thermal expansion coefficient, $\boldsymbol{\gamma}$ is the Grüneisen parameter, and T is temperature. $\boldsymbol{\alpha\gamma T}$ =~0.01 at room temperature for most mantle minerals. With the lengths from Cook's method and the measured travel times, the P and S wave velocities can be calculated at all pressures. As the density changes following the equation $\rho/\rho_0 = (l_0/l)^3$ under hydrostatic compression, the bulk (K) and shear moduli (G) can be obtained from $K_S = \rho (V_P^2 - 4/3V_S^2)$ and $G = \rho V_S^2$ at high pressures Alternatively, a finite strain approach can be used to calculate velocities and moduli using the following finite strain equations (e.g. Davies and Dziewonski, 1975):

$$\rho Vp^2 = (1-2\varepsilon)^{5/2}(L_1+L_2\varepsilon) \quad (1)$$

$$\rho Vs^2 = (1-2\varepsilon)^{5/2}(M_1+M_2\varepsilon) \quad (2)$$

$$P = -3K_{0T}((1-2\varepsilon)^{5/2}(1-3(4-K'_{0T})\varepsilon/2)\varepsilon \quad (3)$$

in which $\mathfrak{E} = 1-(V_0/V)^{2/3}/2$, $G_0 = M_1$, $K_{0S} = L_1-4/3\ G_0$, $G_0' = 1/3(5M_1-M_2)/K_{0S}$, $K_{0S}' = 1/3(5L_1-L_2)/K_{0S} -4/3G_0'$.

With a set of estimated values for K_{0S}, G_0, K_{0S}', G_0' and ρ at each high pressure, V_P and V_S and P can be calculated using Eqs. (1) – (3). Then the final values for K_{0S}, G_0, K_{0S}', G_0' and ρ can be obtained by a nonlinear least-square minimization of the difference between the calculated V_P, V_S and P and those measured in the experiment. By comparison, the finite strain method has the advantage of maintaining a self-consistency within the finite strain framework by searching for a set of densities that satisfies all three equations of the finite strain theory (Li and Liebermann, 2014). As stated in Li and Liebermann, 2014, these two methods are almost identical with a difference of < 0.01% at all pressures.

Table 2. 1 Comparison of the composition of KLB-1 peridotites with pyrolite and CI carbonaceous models.

	Pyrolite (McDonough and Sun, 1995)	CI model (Taylor and McLennan, 1985)	KLB-1 (Takahashi, 1986)	KLB-1 (Herzberg et al., 1990)
SiO_2	45	49.9	44.48	44.3
TiO_2	0.201	0.16	0.16	0.12
Al_2O_3	4.45	3.65	3.59	3.54
Cr_2O_3	0.384	0.44	0.31	--
MnO	0.135	0.13	0.12	0.14
FeO	8.05	8	8.1	8.59
NiO	0.25	0.25	0.25	--
MgO	37.8	35.15	39.9	39.5
CaO	3.55	2.9	3.44	3.03
Na_2O	0.36	0.34	0.3	0.3
K_2O	0.029	0.022	0.01	0.01
P_2O_5	0.021	--	--	--

Table 2. 2 Summary of the hot-pressing experiments of KLB-1 specimens.

Run#	Condition	Cell assembly	Quality
K657	3GPa 1400 ºC 1h	14/8 G2 cell	good
K968	3GPa 1400 ºC 1h	14/8 G2 cell	sample melted
K973	3GPa 1200 ºC 1h	14/8 G2 cell	good
K984	6 GPa	14/8 G2 cell	failed, heater broke, sample melted
K986	6 GPa 1200 ºC 1h	14/8 G2 cell	good
K998	3GPa 1200 ºC 1h	14/8 G2 cell	good
K1000	8GPa 1250 ºC 1h	14/8 G2 cell	good
K1001	8GPa 1200 ºC 1h	14/8 G2 cell	good
k1030	10 GPa	14/8 G2 cell	Failed, sample melted
K1031	8GPa	14/8 G2 cell	heater lost control after 20 min
K1032	8GPa 1300 ºC 1h	14/8 G2 cell	good
K1033	8GPa 1300 ºC 1h	14/8 G2 cell	good
S4238	15GPa 1500 ºC 1h	10/5 cell	layered, not homogeneous
S4239	15GPa 1500 ºC 1h	10/5 cell	layered, not homogeneous
S4240	15GPa 1500 ºC 2h	10/5 cell	not well sintered
S4241	15GPa 1500 ºC 4h	10/5 cell	layered, not homogeneous
S4242	15 GPa	10/5 cell	blowout during heating
S4247	15GPa 1500 ºC	10/5 cell	heater broke at 1500 ºC
S4249		10/5 cell	blowout at 280 bar
S4250	15 GPa 1500 ºC	14/8 high T cell	Fe capsule melted current drop to 0 at 1500 ºC
S4251	15GPa 1400 ºC 12h	14/8 high T cell	Fe capsule melted
S4252	15GPa 1300 ºC 3h	14/8 high T cell	use Re capsule sample not homogeneous has color difference on the edge
S4253	15GPa 1200 ºC 11h	14/8 high T cell	same cell as 4252. Sample is homogeneous but slightly crumble
S4255	15GPa 1200 ºC 11h	14/8 high T cell	same cell as 4252. Sample is homogeneous

Table 2. 3 Summary of mineral chemical compositions and the weight fractions of each mineral.

K657	**SiO_2**	**Al_2O_3**	**FeO**	**MgO**	**Na_2O**	**TiO_2**	**Cr_2O_3**	**CaO**	**MnO**	**Sum**	**wt%**
cpx avrg	53.36	5.14	3.89	18.16	1.38	0.34	0.40	17.34	0.00	100.00	**13.32**
grt avrg	41.80	23.09	6.76	21.46	0.00	0.23	1.24	5.42	0.00	100.00	**9.24**
ol avrg	40.70	0.05	10.24	48.83	0.00	0.00	0.04	0.14	0.00	100.00	**62.51**
opx agrg	54.67	4.86	6.57	32.35	0.18	0.12	0.19	1.06	0.00	100.00	**14.82**
spn avrg	0.00	62.26	10.18	21.10	0.06	0.01	0.12	6.27	0.00	100.00	**0.00**
K973	**SiO_2**	**Al_2O_3**	**FeO**	**MgO**	**Na_2O**	**TiO_2**	**Cr_2O_3**	**CaO**	**MnO**	**Sum**	**wt%**
cpx avrg	51.88	7.71	3.29	15.19	1.73	0.55	0.33	19.22	0.10	100.00	**12.88**
grt avrg	42.19	23.51	6.63	21.05	0.02	0.28	0.91	5.19	0.22	100.00	**6.81**
ol avrg	40.45	0.06	10.11	49.02	0.03	0.02	0.02	0.13	0.16	100.00	**62.48**
opx agrg	54.35	5.40	6.53	32.26	0.16	0.14	0.17	0.85	0.13	100.00	**17.82**
spn avrg	0.14	62.09	10.07	20.61	0.00	0.14	6.80	0.05	0.09	100.00	**0.00**
K998	**SiO_2**	**Al_2O_3**	**FeO**	**MgO**	**Na_2O**	**TiO_2**	**Cr_2O_3**	**CaO**	**MnO**	**Sum**	**wt%**
cpx avrg	51.75	7.42	3.17	15.40	1.90	0.56	0.38	19.33	0.09	100.00	**12.62**
grt avrg	42.27	22.89	7.04	20.72	0.06	0.25	1.27	5.18	0.32	100.00	**7.34**
ol avrg	40.62	0.05	10.25	48.78	0.02	0.01	0.01	0.11	0.15	100.00	**62.90**
opx agrg	54.18	5.33	6.64	32.35	0.12	0.15	0.15	0.93	0.15	100.00	**17.21**
spn avrg	0.13	62.01	9.90	20.67	0.04	0.16	6.92	0.05	0.12	100.00	**0.00**
K986	**SiO_2**	**Al_2O_3**	**FeO**	**MgO**	**Na_2O**	**TiO_2**	**Cr_2O_3**	**CaO**	**MnO**	**Sum**	**wt%**
cpx avrg	51.55	7.85	3.36	15.04	1.89	0.53	0.41	19.27	0.09	100.00	**12.73**
grt avrg	42.53	22.11	6.90	21.75	0.04	0.31	1.65	4.43	0.27	100.00	**7.05**
ol avrg	40.68	0.10	10.40	48.41	0.03	0.01	0.04	0.16	0.15	100.00	**64.01**
opx agrg	54.64	5.34	6.61	32.02	0.13	0.13	0.17	0.83	0.14	100.00	**16.25**
spn avrg	0.06	62.32	10.27	20.00	0.03	0.13	7.06	0.05	0.08	100.00	**0.00**
K1000	**SiO_2**	**Al_2O_3**	**FeO**	**MgO**	**Na_2O**	**TiO_2**	**Cr_2O_3**	**CaO**	**MnO**	**Sum**	**wt%**
cpx avrg	51.77	7.75	3.20	15.09	1.81	0.55	0.40	19.36	0.09	100.00	**13.13**
grt avrg	42.23	22.15	7.57	21.34	0.03	0.33	1.72	4.29	0.34	100.00	**7.41**
ol avrg	40.73	0.04	10.00	48.98	0.03	0.01	0.02	0.06	0.13	100.00	**63.23**
opx agrg	54.33	5.49	6.56	32.08	0.19	0.15	0.17	0.86	0.15	100.00	**16.23**
spn avrg	0.10	62.10	10.49	20.27	0.01	0.14	6.76	0.03	0.09	100.00	**0.00**
K1001	**SiO_2**	**Al_2O_3**	**FeO**	**MgO**	**Na_2O**	**TiO_2**	**Cr_2O_3**	**CaO**	**MnO**	**Sum**	**wt%**
cpx avrg	51.35	7.80	3.24	15.04	1.94	0.59	0.42	19.52	0.09	100.00	**12.98**
grt avrg	42.40	22.17	8.41	20.71	0.06	0.35	1.24	4.29	0.38	100.00	**7.70**
ol avrg	40.82	0.01	9.89	48.98	0.06	0.04	0.02	0.05	0.15	100.00	**63.29**
opx agrg	54.35	5.36	6.58	32.29	0.15	0.16	0.17	0.80	0.15	100.00	**16.06**
spn avrg	0.16	61.99	10.64	20.21	0.02	0.11	6.75	0.02	0.10	100.00	**0.00**
K1032	**SiO_2**	**Al_2O_3**	**FeO**	**MgO**	**Na_2O**	**TiO_2**	**Cr_2O_3**	**CaO**	**MnO**	**Sum**	**wt%**
cpx avrg	52.74	6.13	3.29	16.06	1.65	0.36	0.71	18.96	0.10	100.00	**17.12**
grt avrg	42.88	21.55	6.45	22.59	0.04	0.23	1.84	4.21	0.21	100.00	**12.78**
ol avrg	41.07	0.14	9.32	49.13	0.05	0.01	0.10	0.22	0.11	100.00	**69.89**
S4255	**SiO_2**	**Al_2O_3**	**FeO**	**MgO**	**Na_2O**	**TiO_2**	**Cr_2O_3**	**CaO**	**MnO**	**Sum**	**wt%**
cpx avrg	52.41	7.01	2.85	15.04	1.97	0.34	0.73	19.55	0.11	100.00	**15.80**
grt avrg	42.83	21.07	5.82	21.47	0.15	0.11	2.51	5.68	0.35	100.00	**12.73**
ol avrg	41.07	0.14	9.32	49.13	0.05	0.01	0.10	0.22	0.11	100.00	**71.06**

Table 2. 4 Mineral fractions of KLB-1 specimens from powder X-ray diffraction analyses and EPMA.

	X-ray (K973)	EPMA(K973)	X-ray (S4253)	EPMA(S4255)
cpx (wt%)	13	13	10	16
grt (wt%)	8	7	19	13
ol (wt%)	56	62	71	71
opx (wt%)	24	18	0	0

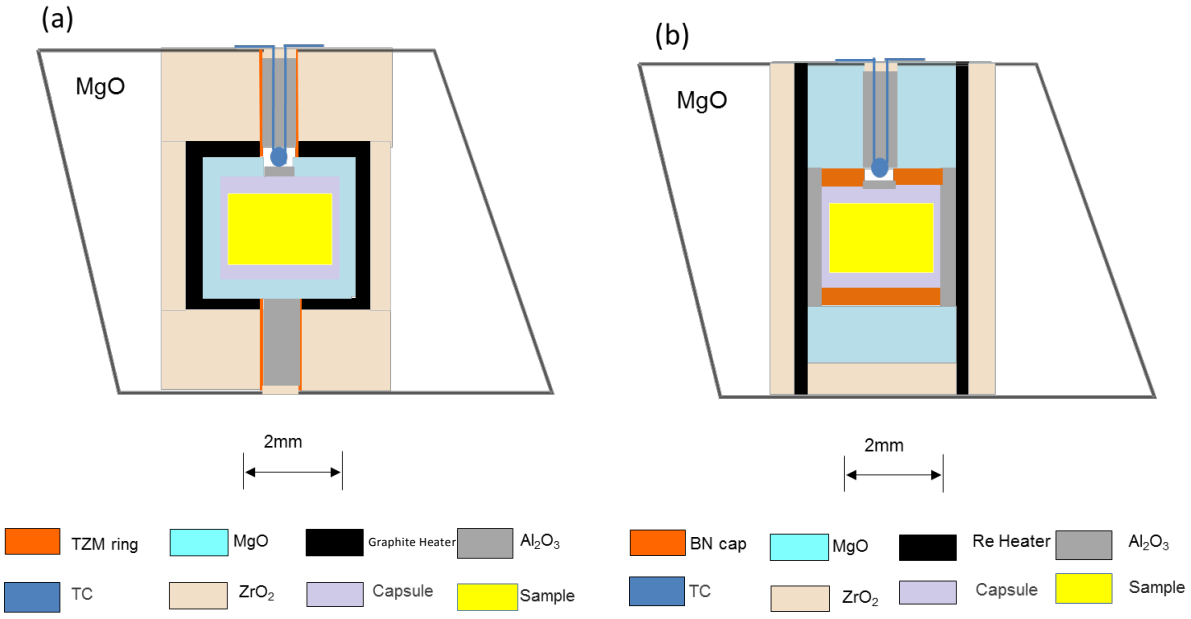

Figure 2. 1 Cross sections of cell assemblies used for hot pressing KLB-1 specimens. (a) 14/8 G2 cell (b) 14/8 high T cell.

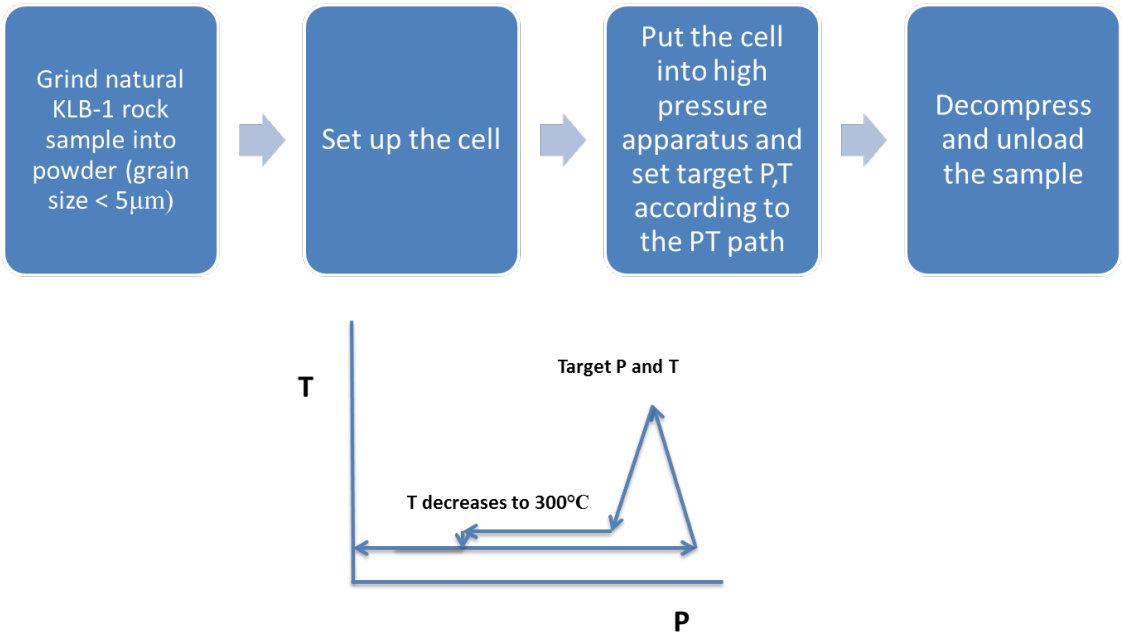

Figure 2. 2 Hot-pressing procedures and the PT path.

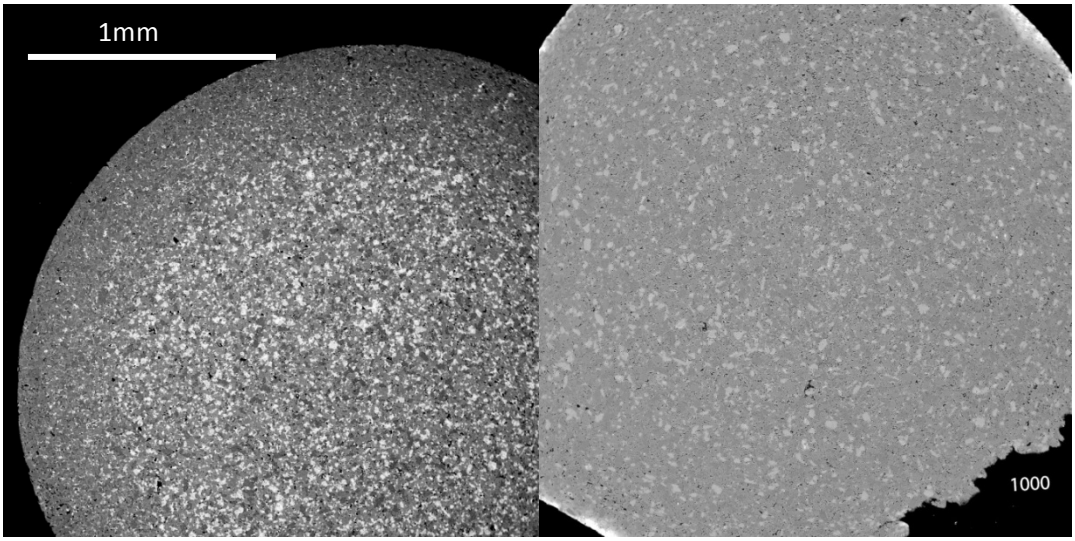

Figure 2. 3 SEM images of KLB-1 specimens in the large scale. Sample diameter: ~2.5 mm. Left: SEM image of KLB-1 specimen (K657) hot pressed at 3 GPa and 1400 °C Right: SEM image of KLB-1 specimen (K1000) hot pressed at 8 GPa and 1250 °C. Dark parts are a combination of voids left by lost grains during polishing and a small amount of porosity.

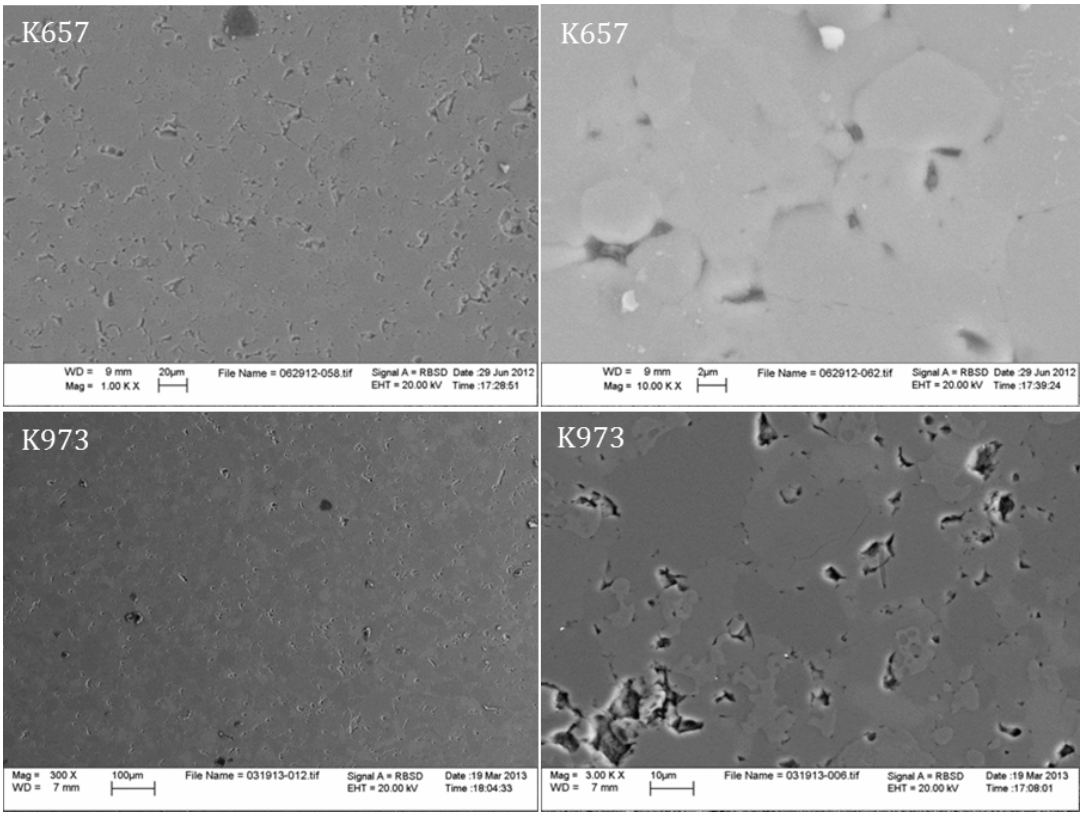

Figure 2. 4 SEM images of KLB-1 specimens in the small scale. SEM image of KLB-1 specimen hot pressed at 3 GPa and 1200 °C (K973) and 3 GPa and 1400 °C (K973). Dark parts are a combination of voids left by lost grains during polishing and a small amount of porosity.

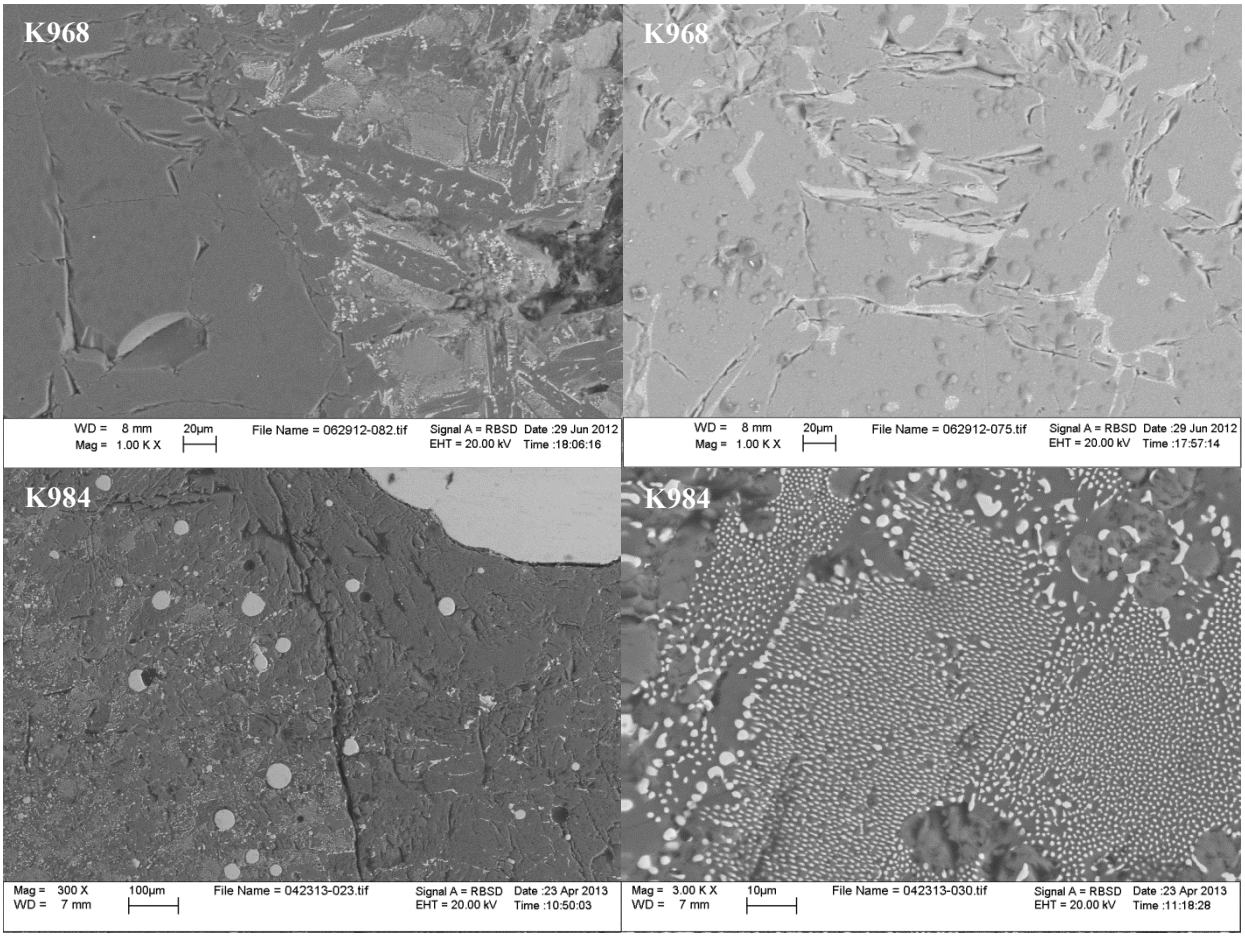

Figure 2. 5 Melting feature of specimen K968 and K984. For K968, the entire sample is Mg-rich olivine. No other minerals remain. Light regions in the sample center are Ca-rich melts. White dots in the specimen K984 are Fe.

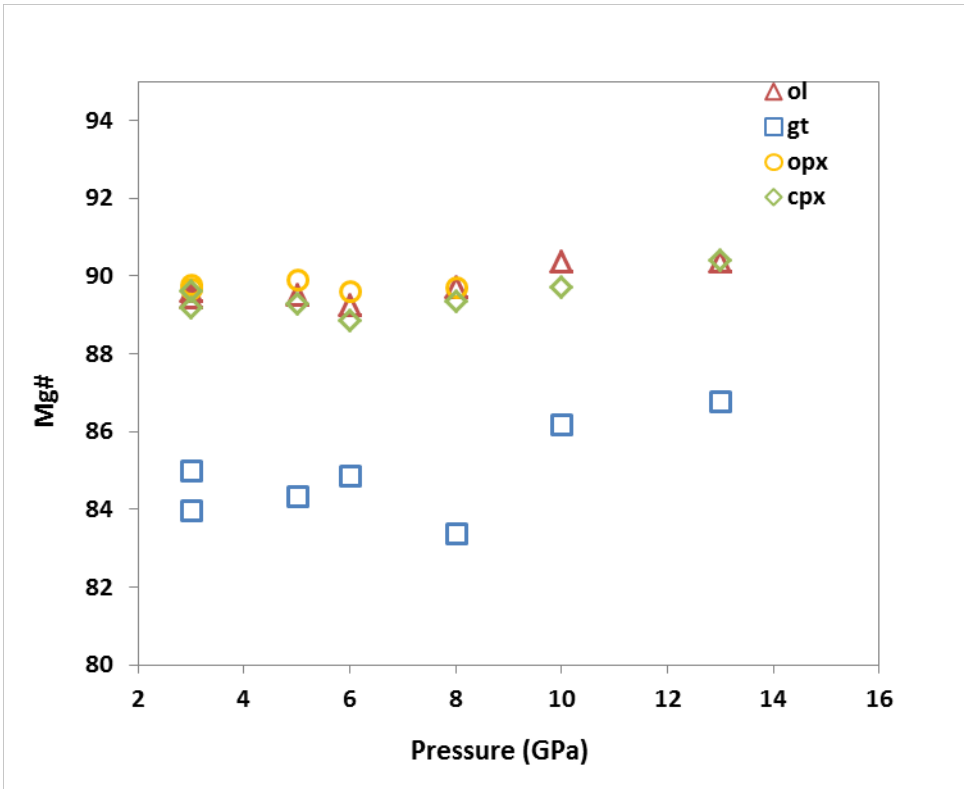

Figure 2. 6 Variations of Mg# with pressure in coexisting phases of KLB-1 peridotite.

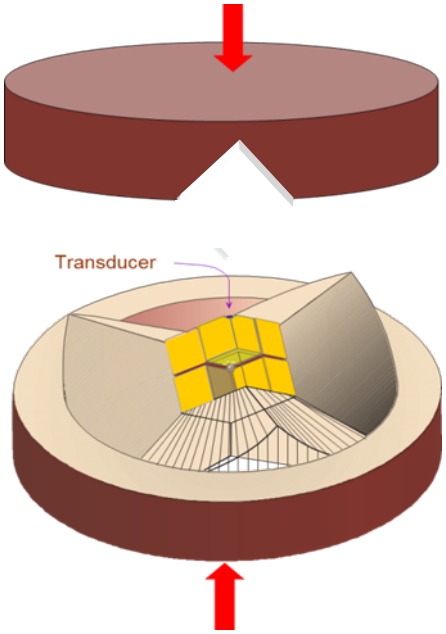

Figure 2. 7 Exploded view of the multi-anvil apparatus adapted for ultrasonic measurements. The eight inner cubes are WC anvils that compress an octahedron-shaped sample assembly. Dual mode $LiNbO_3$ transducer (50 MHz for P wave and 30 MHz for S wave) are mounted on the back of the WC anvil.

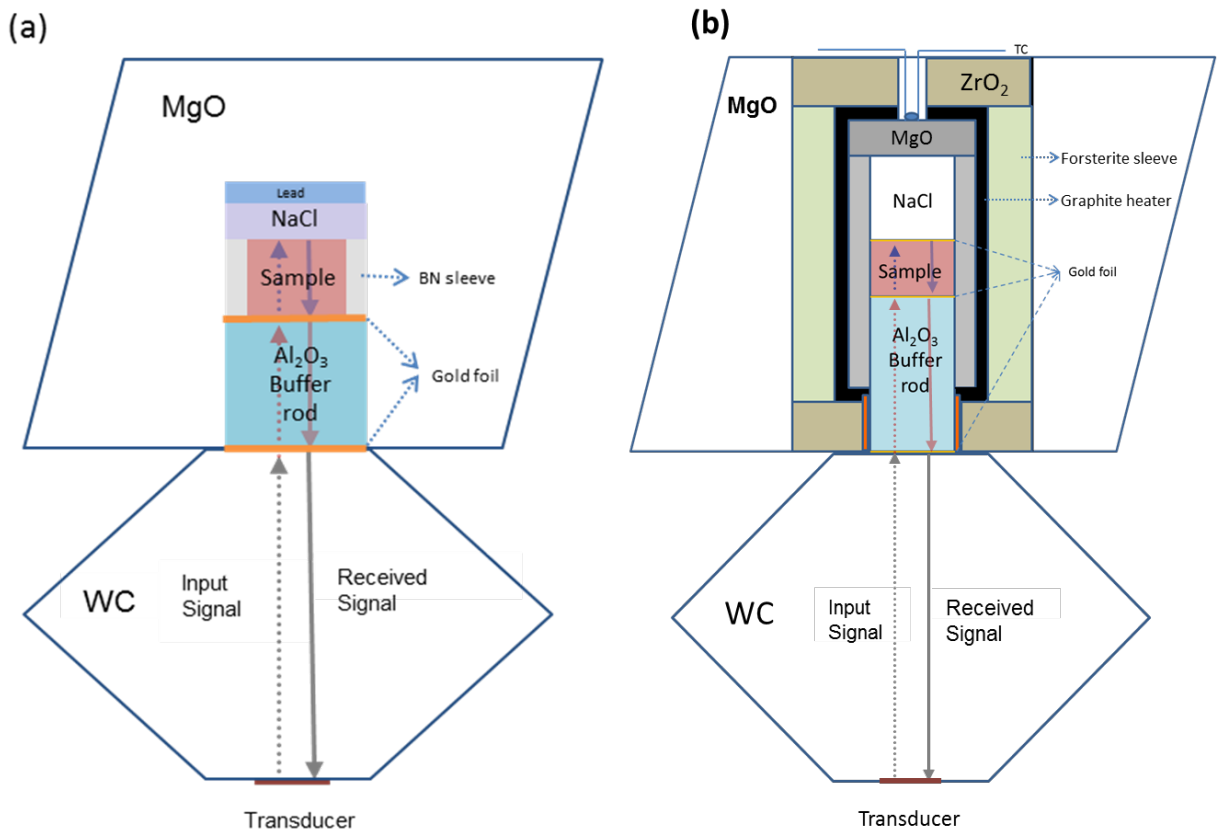

Figure 2. 8 A cross section of the WC anvil and the MgO octahedral cell assembly for the room temperature acoustic measurement (a) and high-temperature measurement at beamline (b).

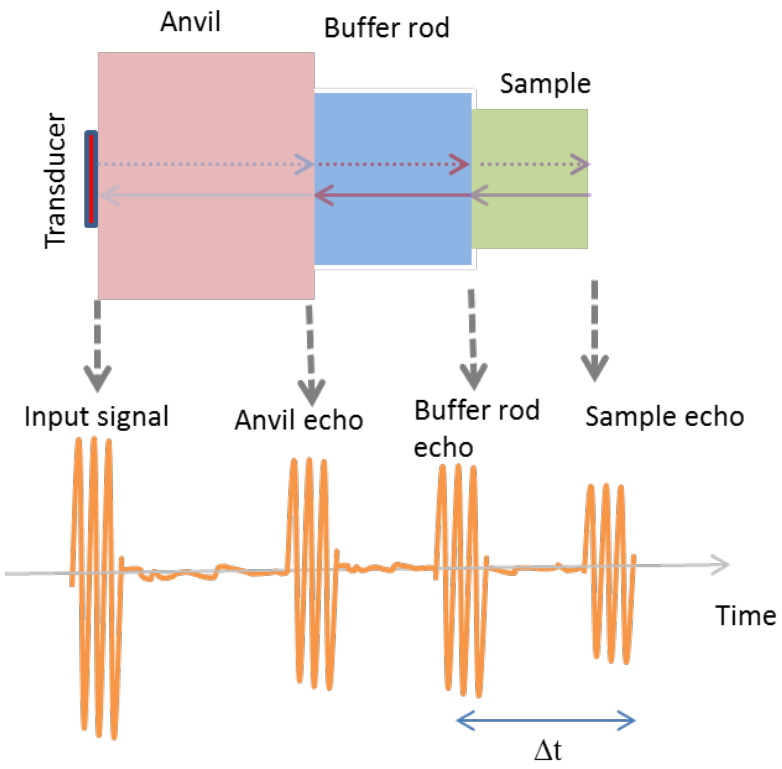

Figure 2. 9 Schematic diagram for ultrasonic interferometry method for travel time measurements.

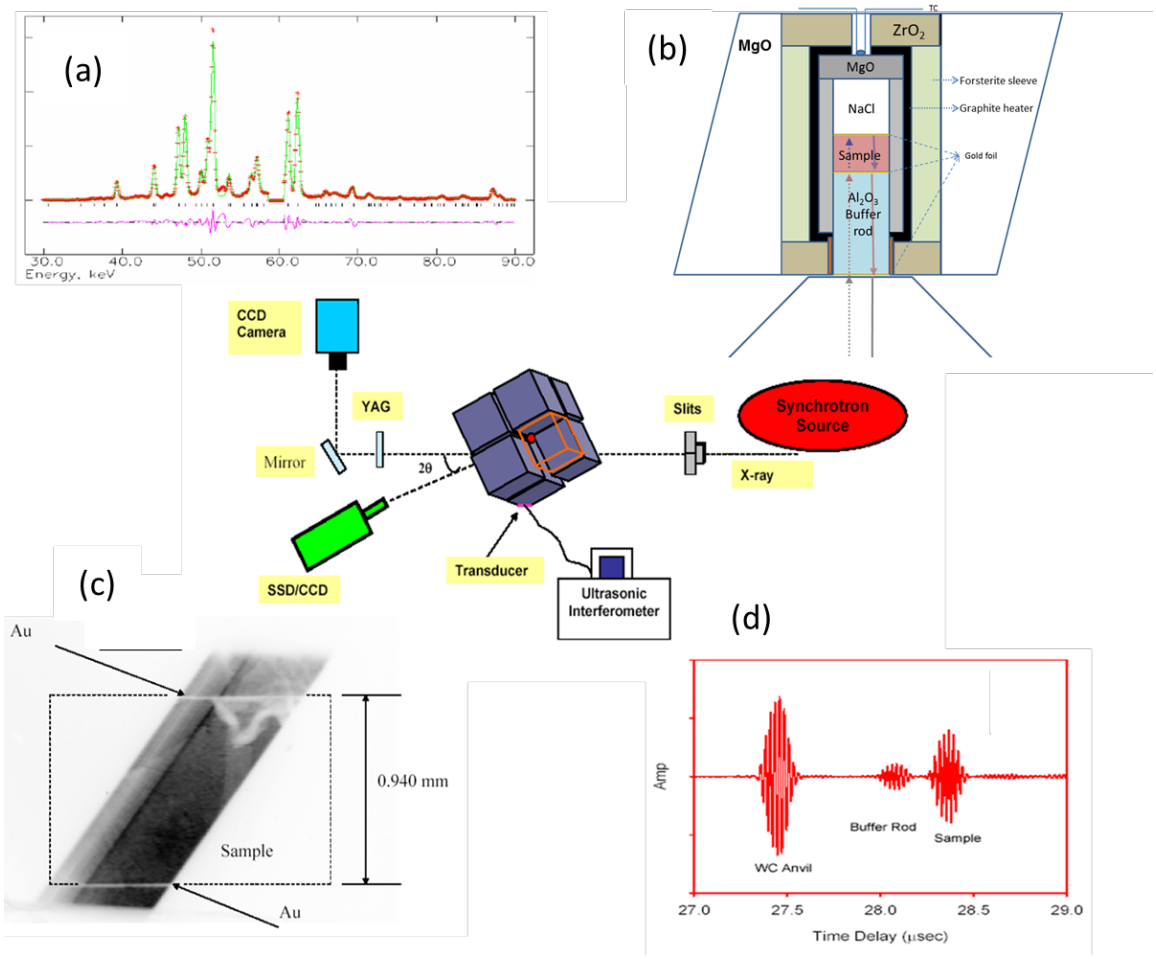

Figure 2. 10 Schematic diagram of the experimental configuration for simultaneous ultrasonic, X-ray diffraction, and X-ray imaging measurements using the 1000-ton Kawai type large volume apparatus (T-25) installed at synchrotron X-ray beamline 13-ID-D of Advanced Photon Source, Argonne National Laboratory. (a) Example of the X-ray diffraction peaks of the sample. (b) Cross section of the cell assembly. (c) Length measurement using X-ray imaging. (d) Example of reflections from rear surfaces of WC anvil, buffer rod, and sample.

Reference

Abramson, E.H., Brown, J.M. and Slutsky, L.J., 1999. Applications of impulsive stimulated scattering in the earth and planetary sciences. Annual review of physical chemistry, 50(1), pp.279-313.

Anderson, O.L. and Isaak, D.G., 1995. Elastic constants of mantle minerals at high temperature. Mineral Physics & Crystallography: A Handbook of Physical Constants, pp.64-97.

Anderson, O.L., Schreiber, E., Liebermann, R.C. and Soga, N., 1968. Some elastic constant data on minerals relevant to geophysics. Reviews of Geophysics, 6(4), pp.491-524.

Birch, F., 1960. The velocity of compressional waves in rocks to 10 kilobars: 1. Journal of Geophysical Research, 65(4), pp.1083-1102.

Birch, F., 1961. The velocity of compressional waves in rocks to 10 kilobars: 2. Journal of Geophysical Research, 66(7), pp.2199-2224.

Brey, G.P. and Köhler, T., 1990. Geothermobarometry in four-phase lherzolites II. New thermobarometers, and practical assessment of existing thermobarometers. Journal of Petrology, 31(6), pp.1353-1378.

Burkel, E., 2000. Phonon spectroscopy by inelastic x-ray scattering. Reports on Progress in Physics, 63(2), p.171.

Chai, M., Brown, J.M. and Slutsky, L.J., 1997. The elastic constants of an aluminous orthopyroxene to 12.5 GPa. Journal of Geophysical Research: Solid Earth, 102(B7), pp.14779-14785.

Chen, T., Gwanmesia, G.D., Wang, X., Zou, Y., Liebermann, R.C., Michaut, C. and Li, B., 2015. Anomalous elastic properties of coesite at high pressure and implications for the upper mantle X-discontinuity. Earth and Planetary Science Letters, 412, pp.42-51.

Collins, M.D. and Brown, J.M., 1998. Elasticity of an upper mantle clinopyroxene. Physics and chemistry of minerals, 26(1), pp.7-13.

Cook, R.K., 1957. Variation of elastic constants and static strains with hydrostatic pressure: a method for calculation from ultrasonic measurements. The Journal of the Acoustical Society of America, 29(4), pp.445-449.

Davies, G.F. and Dziewonski, A.M., 1975. Homogeneity and constitution of the Earth's lower mantle and outer core. Physics of the Earth and Planetary Interiors, 10(4), pp.336-343.

Davis, F.A., Tangeman, J.A., Tenner, T.J. and Hirschmann, M.M., 2009. The composition of KLB-1 peridotite. American Mineralogist, 94(1), pp.176-180.

Gwanmesia, G. D., and Liebermann, R. C., 1992. Polycrystals of high-pressure phases of mantle minerals: Hot-pressing and characterization of physical properties. In High Pressure Research: Application to Earth and Planetary Sciences (eds. Syono, Y. and Manghnani, M.) (Terra

Scientific Publishing Co., and American Geophysical Union, Tokyo and Washington, D.C.) pp. 117-135.

Gwanmesia, G.D., Li, B. and Liebermann, R.C., 1993. Hot-pressing of polycrystals of high pressure phases of mantle minerals in multi-anvil apparatus, PAGEOPH, Schreiber Volume, (eds. R.C. Liebermann and C. H. Sondergeld) pp. 467-484.

Herzberg, C., Gasparik, T. and Sawamoto, H., 1990. Origin of mantle peridotite: constraints from melting experiments to 16.5 GPa. Journal of Geophysical Research: Solid Earth, 95(B10), pp.15779-15803.

Hughes, D.S. and Jones, H.J., 1950. Variation of elastic moduli of igneous rocks with pressure and temperature. Geological Society of America Bulletin, 61(8), pp.843-856.

Katahara, K.W., Rai, C.S., Manghnani, M.H. and Balogh, J., 1981. An interferometric technique for measuring velocity and attenuation in molten rocks. Journal of Geophysical Research: Solid Earth, 86(B12), pp.11779-11786.

Kung, J., Li, B., Uchida, T., Wang, Y., Neuville, D. and Liebermann, R.C., 2004. In situ measurements of sound velocities and densities across the orthopyroxene→ high-pressure clinopyroxene transition in MgSiO 3 at high pressure. Physics of the Earth and Planetary Interiors, 147(1), pp.27-44.

Lee, C.T.A., 2003. Compositional variation of density and seismic velocities in natural peridotites at STP conditions: Implications for seismic imaging of compositional heterogeneities in the upper mantle. Journal of Geophysical Research: Solid Earth, 108(B9).

Leinenweber, K.D., Tyburczy, J.A., Sharp, T.G., Soignard, E., Diedrich, T., Petuskey, W.B., Wang, Y. and Mosenfelder, J.L., 2012. Cell assemblies for reproducible multi-anvil experiments (the COMPRES assemblies). American Mineralogist, 97(2-3), pp.353-368.

Li, B. and Liebermann, R.C., 2000. Sound velocities of wadsleyite b-$(Mg_{0.88}Fe_{0.12})_2SiO_4$ to 10 GPa. American Mineralogist, 85(2-3), pp.292-295.

Li, B. and Liebermann, R.C., 2014. Study of the Earth's interior using measurements of sound velocities in minerals by ultrasonic interferometry. Physics of the Earth and Planetary Interiors, 233, pp.135-153.

Li, B., Chen, K., Kung, J., Liebermann, R.C. and Weidner, D.J., 2002. Sound velocity measurement using transfer function method. Journal of Physics: Condensed Matter, 14(44), p.11337.

Li, B., Kung, J. and Liebermann, R.C., 2004. Modern techniques in measuring elasticity of Earth materials at high pressure and high temperature using ultrasonic interferometry in conjunction with synchrotron X-radiation in multi-anvil apparatus. Physics of the Earth and Planetary Interiors, 143, pp.559-574.

Li, B., Kung, J., Uchida, T. and Wang, Y., 2005. Pressure calibration to 20GPa by simultaneous use of ultrasonic and x-ray techniques. Journal of applied physics, 98(1), p.013521.

Liebermann, R. C., and Wang, Y., 1992. Characterization of sample environment in a uniaxial split-sphere apparatus. In High Pressure Research: Application to Earth and Planetary Sciences (eds. Syono, Y., and Manghnani, M.) (Terra Scientific Publishing Co., and American Geophysical Union, Tokyo and Washington, D.C.) pp. 19-31.

Liu, W., Kung, J. and Li, B., 2005. Elasticity of San Carlos olivine to 8 GPa and 1073 K. Geophysical Research Letters, 32(16).

Liu, W., Zeng, Q., Jiang, Q., Wang, L. and Li, B., 2011. Density and elasticity of Zr 46 Cu 37.6 Ag 8.4 Al 8 bulk metallic glass at high pressure. Scripta Materialia, 65(6), pp.497-500.

McDonough, W.F. and Sun, S.S., 1995. The composition of the Earth. Chemical geology, 120(3), pp.223-253.

McSkimin, H.J., 1950. Ultrasonic measurement techniques applicable to small solid specimens. The Journal of the Acoustical Society of America, 22(4), pp.413-418.

McSkimin, H.J., 1961. Pulse superposition method for measuring ultrasonic wave velocities in solids. The Journal of the acoustical society of America, 33(1), pp.12-16.

Nimis, P. and Taylor, W.R., 2000. Single clinopyroxene thermobarometry for garnet peridotites. Part I. Calibration and testing of a Cr-in-Cpx barometer and an enstatite-in-Cpx thermometer. Contributions to Mineralogy and Petrology, 139(5), pp.541-554.

O'Neill, H.S.C., 1981. The transition between spinel lherzolite and garnet lherzolite, and its use as a geobarometer. Contributions to Mineralogy and Petrology, 77(2), pp.185-194.

Papadakis, E.P., 1976. Ultrasonic velocity and attenuation: Measurement methods with scientific and industrial applications. Physical acoustics, 12, pp.277-374.

Perkins, D. and Anthony, E.Y., 2011. The evolution of spinel lherzolite xenoliths and the nature of the mantle at Kilbourne Hole, New Mexico. Contributions to Mineralogy and Petrology, 162(6), pp.1139-1157.

Rai, C.S., Manghnani, M.H. and Katahara, K.W., 1981. Ultrasonic studies on a basalt melt. Geophysical Research Letters, 8(12), pp.1215-1218.

Sojda, S.M. and Wang, L., 2002, December. Kinetics of the Pyroxene-Garnet Transformation: Preliminary Results. In AGU Fall Meeting Abstracts (Vol. 1, p. 1085).

Takahashi, E., 1986. Melting of a dry peridotite KLB-1 up to 14 GPa: Implications on the origin of peridotitic upper mantle. Journal of Geophysical Research: Solid Earth, 91(B9), pp.9367-9382.

Taylor. S.R. and McLennan. S.M., 1985. The continental crust: Its composition and evolution. Blackwcll. Oxford, pp.312.

Thurston, R.N. and Brugger, K., 1964. Third-order elastic constants and the velocity of small amplitude elastic waves in homogeneously stressed media. Physical Review, 133(6A), p.A1604.

Walker, D., Carpenter, M.A. and Hitch, C.M., 1990. Some simplifications to multianvil devices for high pressure experiments. American Mineralogist, 75(9-10), pp.1020-1028.

Walter, M.J., 1998. Melting of garnet peridotite and the origin of komatiite and depleted lithosphere. Journal of Petrology, 39(1), pp.29-60.

Wang, X., Chen, T., Qi, X., Zou, Y., Kung, J., Yu, T., Wang, Y., Liebermann, R.C. and Li, B., 2015b. Acoustic travel time gauges for in-situ determination of pressure and temperature in multi-anvil apparatus. Journal of Applied Physics, 118(6), p.065901.

Wang, X., Chen, T., Zou, Y., Liebermann, R.C. and Li, B., 2015a. Elastic wave velocities of peridotite KLB-1 at mantle pressures and implications for mantle velocity modeling. Geophysical Research Letters, 42(9), pp.3289-3297.

Weidner, D.J., Swyler, K. and Carleton, H.R., 1975. Elasticity of microcrystals. Geophysical Research Letters, 2(5), pp.189-192.

Yoneda, A., Cooray, T. and Shatskiy, A., 2012. Single-crystal elasticity of stishovite: New experimental data obtained using high-frequency resonant ultrasound spectroscopy and a Gingham check structure model. Physics of the Earth and Planetary Interiors, 190, pp.80-86.

Zhang, J. and Herzberg, C., 1994. Melting experiments on anhydrous peridotite KLB-1 from 5.0 to 22.5 GPa. Journal of Geophysical Research: Solid Earth, 99(B9), pp.17729-17742.

Chapter 3 Acoustic travel time gauges for in-situ determination of pressure and temperature in multi-anvil apparatus

3.1 Introduction

The behavior of materials in response to extreme conditions is of great interest to scientists in many disciplines, such as condensed matter physics, solid-state chemistry, materials sciences and Earth and planetary sciences. Currently, the diamond anvil cell (DAC) and multi-anvil large volume presses are the two most commonly utilized techniques to generate static pressures for laboratory studies of structural, physical and chemical properties of condensed matter under compression (e.g., Hemley and Ashcroft, 1998; McMillan, 2010), synthesis and discovery of new materials with desired functionality (e.g., McMillan, 2002), and an improved understanding about the composition, dynamics and history of the Earth and other planets (e.g., Bassett, 2009; Liebermann, 2011; Li and Liebermann 2007, 2014). In these experimental studies, accurate determination of pressure is needed in order to compare with and validate predictions from atomistic simulations (e.g., Li et al., 2014), perform thermodynamic calculations for systematic and predictive modeling in material design (Moriarty et al, 2002; McMillan, 2002), and relate the experimentally observed material behavior and physiochemical properties to the corresponding depths in the interior of the Earth (e.g., Irifune et al., 1998; Jackson and Rigden, 1998; Liebermann, 2000; Li and Liebermann, 2014; and references therein).

Many techniques have been developed for pressure measurements under static loading (see review in Decker et al., 1972). These can be classified into two broadly defined approaches.

The first approach uses fixed-point pressure calibration, which relies on monitoring changes in a characteristic physical property (e.g., electrical, optical, elastic, etc.) at some known transition pressures which have been determined previously. Electrical resistance is one of the most widely used methods (e.g., Matityahu et al., 2015, references therein). Phase transitions in many materials have been established as discrete fixed-points (e.g., Bi I-II at 2.55GPa, III-V at 7.7 GPa; ZnTe: 9.6 GPa and 12.2 GPa; see Bridgman, (1948) for phase transitions in various metals). A second approach is to establish a general relationship between pressure and certain experimentally measurable properties of a given material. Theories of material under compression allow such pressure scales to be described as continuous analytical or empirical functions, which can be used to determine pressure. Good examples of such scales are diffraction-based equations of state pressure scales using NaCl (Decker, 1971), Au (Anderson, et al., 1989; Jamieson et al., 1982; Tsuchiya 2003; Hirose, et al., 2008; Dorfman et al., 2012; Fei et al., 2007), MgO (Wu, et al., 2008; Speziale et al., 2001), and peak shifts in fluorescence (Ruby, SmB_4O_7) and Raman spectra (diamond, cBN) (see Dorogopets and Oganov, 2007). Compared to the discrete fix-point calibrations, which are often presented as calibrated ram load versus cell pressure at limited P-T positions and can only be used during compression, the continuous pressure scales have the advantages of providing continuous pressure determination and being used for both compression and decompression. On the other hand, reconciling the internal consistency among different pressure gauges remains a challenging task. The status of different scales at high pressure and temperature can be found in recent studies for equation of state based (e.g., Dorfman et al., 2012; Fei et al., 2007, Dorogopets and Oganov, 2007) and optical property based scales (e.g., Syassen, 2008).

Previously, acoustic measurements have been primarily used to detect phase transition pressures for fixed-point calibration (e.g., Wang et al., 2012), a pressure scale based on acoustic velocity/travel time, especially at high temperatures, has never been explored in the past. In the last 2 decades, sound velocity measurements have been extended to above 20 GPa in pressure and 1500 °C in temperature in Kawai-type multi-anvil apparatus and have been successfully applied to many materials (see review in Li and Liebermann, 2007, 2014; Irifune et al., 2008), yielding a large amount of velocity data at simultaneous high pressures and high temperatures. In principle, all these velocity data can be used for continuous pressure determination, provided that both the high quality acoustic pressure marker and the sample can be placed under hydrostatic pressures and accurate velocity measurements can be performed. In practice, however, the sophisticated procedures as well as the stringent requirements for experimental implementation have made it less appealing than the X-ray diffraction based approach. Recently, ultrasonic experiments have been regularly performed in conjunction with synchrotron X-radiation to allow for simultaneous ultrasonic interferometry and X-ray diffraction measurements, this opens new opportunities to obtain pressure without using any pressure standard (a.k.a, absolute pressure; see Ruoff et al., 1973; Li et al., 2005; Mueller et al., 2003) and to establish velocity / travel time based new pressure scales for offline use.

In this Chapter, I will present a new travel time pressure gauge up to 15 GPa and 900 ºC, which was obtained by calibrating the travel times of the polycrystalline Al_2O_3 against the unit cell volumes of NaCl using the Decker pressure scale (Decker, 1965). Separate pressure scales are derived for in-situ pressure determination at room temperature, high temperature, as well as for simultaneous pressure and temperature determination. The new pressure scale at room temperature was applied to an offline experiment for the study of coesite (Chen et al., 2015), in

which the pressures on compression determined using the new Al_2O_3 travel time scale were found to be in excellent agreement with the existing fixed-point pressure calibration curve; this experiment also provides additional information about the well-known pressure hysteresis on decompression in multi-anvil apparatus. Moreover, the densities of coesite as a function of pressure from this offline experiment are in complete agreement with those from previous single crystal compression studies under hydrostatic pressures, indicating that these acoustic pressure scales can be conveniently and reliably used for laboratory high-pressure measurements.

3.2 Experiment method

Figure 3.1 shows the standard 14/8 cell assembly used for high pressure and high temperature acoustic velocity measurement experiments (see also Li et al., 2004; Kung et al., 2004; Bass et al., 2008). The acoustic signals are generated by a dual-mode $LiNbO_3$ (10º rotated Y-cut) transducer (central frequencies 50 MHz for P wave and 30 MHz for S wave) mounted on the back corner of one of the eight WC cubes and serving as both a transmitter and a receiver. A commercial grade (Coors 998), double-side polished polycrystalline Al_2O_3 was used as the buffer rod to propagate high-frequency acoustic waves into the sample, which was surrounded and backed by NaCl to provide quasi-hydrostatic environment and serves as an in-situ pressure calibrant based on the equation of state of Decker (1965). High quality (pure composition, high density, small grain size) polycrystalline Al_2O_3 is an excellent material to use as buffer rod as it provides suitable acoustic impedance and ensures good coupling of the buffer rod with both the sample and the WC anvil. Details of Coors 998 alumina: composition: 99.8% Al_2O_3, density: 3.914(2) g/cm^3 [98.2% of theoretical X-ray density of 3.986 g/cm^3 (Smyth and McCormick, 1995)], average grain size: 6 microns, diameter: 3.18 mm, length: 3.65-3.85 mm.

To establish a travel-time pressure gauge, the materials contacting the top and/or the bottom surface of the sample could both be considered as candidates (e.g., Al_2O_3 buffer rod and NaCl backing in Figure 3.1(a)). However, our previous experience suggests that it is not practical to use the NaCl backing as an acoustic calibrant, primarily due to its low yield strength (hence large deformation) as well as the difficulty of distinguishing reliably its acoustic signal at high pressures and high temperatures. Thus, without further complicating and perturbing the standard cell assembly, the travel time from the Al_2O_3 buffer rod is the most practical and convenient choice for the construction of an acoustic pressure scale. Note that the Al_2O_3 buffer rod in the current high pressure cell assemblies extends from the top surface of the sample to the edge of the octahedron pressure medium where it is in contact with the WC anvil (see Figure 3.1(a)) so that the buffer rod is expected to experience deviatoric stresses as well as pressure and temperature gradients; thus, the velocities (or travel times) of the Al_2O_3 buffer rod are expected to be different from those for Al_2O_3 under hydrostatic/quasi-hydrostatic conditions (see Figure 3.2). A key point for obtaining a reliable pressure scale is to measure the Al_2O_3 travel times under the stress conditions similar to the current buffer rod/sample/NaCl configuration (see Figure 3.1(a)) and correlate them with the cell pressures determined by X-ray diffraction from the NaCl adjacent to the sample.

Acoustic measurements were conducted up to 10 GPa at 25 ºC and 15 GPa, 900 ºC in the 1000-ton Kawai type large volume apparatus (T-25) installed at synchrotron X-ray beamline 13-ID-D of Advanced Photon Source, Argonne National Laboratory, with KLB-1 peridotite (Wang et al., 2014) and enstatite (Kung et al., 2004) as samples, respectively. In the high temperature experiment, the temperature was measured using W3%Re-W25%Re thermocouples placed next to the sample and NaCl interface. After reaching peak pressure and temperature conditions, five

heating/cooling cycles up to 900 ºC were performed during decompression from 13 to 6 GPa. At each data point, ultrasonic interferometry measurements and X-ray diffraction data acquisition were performed simultaneously to ensure a high degree of synchronization and consistency between the two data sets. Additional details can be found in Wang et al. (2014) and Kung et al. (2004).

For ultrasonic measurements, the transfer function method of Li et al. (2002) was used to acquire acoustic response in the frequency range of 25-70 MHz followed by a pulse echo overlap (PEO) analysis at monochromatic frequencies to obtain the travel times (see Papadakis, 1976). As shown by the acoustic signals at ~5 GPa in Figure 3.1(b), the high signal to noise ratio ensured a clear identification of the acoustic reflections from the interfaces encountered along the wave propagation path. P and S wave travel times inside the Al_2O_3 buffer rod were obtained by overlapping the echoes reflected from the anvil and the buffer rod with a precision better than 0.2 % (see also Li et al., 2002).

3.3 Results and discussion

3.3.1 Pressure scale at room temperature

The pressure scale at ambient temperature is parameterized via the normalized travel time of S wave t_S/t_{S0}, where t_S is the measured round-trip travel time at high pressure and t_{S0} is at zero pressure. In theory, either P or S wave travel time can be used to derive a pressure scale at ambient temperature; compared to S wave, the travel time for P wave has a slightly higher rate of change with pressure ($\Delta t/\Delta P$, hence higher sensitivity) but with smaller absolute values for t and Δt. Thus, if we consider the sampling step size (0.2 ns) in the recorded waveform (limited by the sampling rate of the current oscilloscope, 5 GS/s) as the system uncertainty of the measured

travel time, the S wave travel time has a slight advantage due to its relatively smaller uncertainty. Since the overall error in the derived pressure scale is larger than their respective sensitivities (see later sections), both P and S waves are expected to work equally well within the reported uncertainty. Another practical point is that S wave echoes from buffer rod and sample are separated much farther along the time axis such that the buffer rod echo is less likely to be contaminated by the echo from the sample in the case of a very short buffer rod. Thus, in the current study, the room temperature pressure scale is derived only based on S wave travel time.

Theoretical support for the current Al_2O_3 travel time pressure scale can be sought within the framework of acoustoelasticity by considering the stress field on the Al_2O_3 buffer rod to consist of a hydrostatic pressure (P) that equals to that at the center of the high pressure cell and a mean uniaxial stress σ. The normalized travel time in the Al_2O_3 buffer rod can be described by $t_S/t_{S0} = (L/L_0)\times(V_{S0}/V_S)$, where L_0 and V_{S0} are the length and S wave velocity at ambient conditions; L and V_S are the length and S wave velocity under nonhydrostatic experimental condition. Based on acoustoelasticity, the S wave velocity in the Al_2O_3 buffer rod propagating along the stress direction is approximated by $V_S = \sqrt{\frac{G+1/2\sigma}{\rho}}$, with the $1/2\sigma$ term accounting for the effect of stress (e.g., Dey et al., 1984). The normalized Al_2O_3 buffer rod length (L/L_0) consists of a hydrostatic pressure component $L(P)/L_0$ and an uniaxial stress (σ) component $\Delta L(\sigma)/L_0$, resulting in a total length change $L/L_0 = [L(P) + \Delta L(\sigma)]/L_0$. From the definition of bulk modulus, we obtain the normalized volume $V/V_0 = \rho(P)/\rho_0 = [L(P)/L_0]^3 = (1 + P/K_0)^{-1}$ under hydrostatic pressures. A rearrangement of the L/L_0 results in $L/L_0 = [L(P) + \Delta L(\sigma)]/ L_0 = (1+ \sigma/E) \times (1 + P/K_0)^{-1/3}$, in which $E = \sigma/[\Delta L(\sigma)/L(P)]$ is the Young's modulus at high pressure. Similarly, the V_{S0}/V_S can be evaluated by $V_{S0}/V_S = \sqrt{\frac{G_0}{\rho_0}}/\sqrt{\frac{G+1/2\sigma}{\rho}} = \{[G + 1/(2\sigma)]/G_0\}^{-1/2} \times (\rho/\rho_0)^{1/2}$. By

assuming $G = G_0 + G'P$, V_{S0}/V_S can be approximated by $[1 + \sigma/(2G_0) + G'P/G_0]^{-1/2} \times (L/L_0)^{-3/2}$ $=[(2G_0 + \sigma)/(2G_0) + G'P/G_0]^{-1/2} \times (1 + P/K_0)^{1/2} \times (1 + \sigma/E)^{-2/3}$. Taking into account both the length and velocity changes, the final expression for the normalized S wave travel time in terms of hydrostatic pressure and stress can be derived as the following:

$t_S/t_{S0} = (L/L_0) \times (V_{S0}/V_S) = [(2G_0 + \sigma)/(2G_0) + G'P/G_0]^{-1/2} \times (1+P/K_0)^{1/6} \times (1+\sigma/E)^{-1/2}$.

By using a Taylor expansion to only the second order of pressure, we obtain

$t_S/t_{S0} = A+BP+CP^2$

with $A = [(2G_0 + \sigma)/(2G_0) \times (1 + \sigma/E)]^{-1/2}$

$B = \{1/(6K_0) \times [(2G_0 + \sigma)/(2G_0)]^{-1/2} - G'/(2G_0) \times [(2G_0 + \sigma)/(2G_0)]^{-3/2}\} \times (1+\sigma/E)^{-1/2}$

$C = \{-5/(72K_0^2) \times [(2G_0 + \sigma)/(2G_0)]^{-1/2} - G'/(12K_0G_0) \times [(2G_0+\sigma)/(2G_0)]^{-3/2} + 3G'^2/(8G_0^2) \times [(2G_0 + \sigma)/(2G_0)]^{-5/2}\} \times (1 + \sigma/E)^{-1/2}$

Thus, by fitting the experimentally observed t_S/t_{S0} to the measured hydrostatic pressure from the equation of state of NaCl, the coefficients for the travel time pressure scale can be derived. With the elastic properties of Al_2O_3 and a wide range of guessed values for the axial stress, the second order term contributes to well less than 1% within current pressure range. Note that, although the mean stress is dependent on pressure, this dependence is implicitly included in the fitted coefficients. A more rigorous treatment of the acoustoelastic effect will be present in a separate paper (Wang and Li, in preparation).

Figure 3.2 shows the normalized S wave travel time of Al_2O_3 buffer rods as a function of pressure from Run#1 and Run #2 during compression as well as those obtained during decompression from Run #2. It can be seen that the data from these two runs are highly consistent, even though in Run#2 the sample underwent a first order phase transition between 12-14 GPa (e.g., Kung et al., 2004; Li et al., 2014). The normalized travel time of S wave

appears to decrease linearly as a function of pressure within the current experimental pressure range, in spite of the nonhydrostatic stress field and/or pressure gradient experienced by the buffer rod, which is consistent with the theoretical approximation based on acoustoeleasticity. A linear fit was therefore performed to obtain the relation between the normalized travel time and pressure, yielding the following expression for the travel time pressure scale at room temperature:

$$P\ (GPa) = 249.7(7) \times (1-t_S/t_{S0}) \quad (1)$$

The error associated with this linear least squares fit is calculated using $\sigma_P = \sqrt{\frac{\sum_{i=1}^{n}(P_i-\bar{P})^2}{n-1}}$ $= \sqrt{\frac{\sum_{i=1}^{n}(\Delta P_i)^2}{n-1}}$, where P_i is the calculated pressure, $\bar{P}$ is the pressure measured using NaCl, n is the number of data points and σ_P is the standard error. With all the 48 data points in Figure 3.2 from compression and decompression that are used to derive the pressure scale, the standard error is ±0.18 GPa. It should be noted that since the Decker NaCl pressure scale has a reported uncertainty ~3% within the current pressure range which is much larger than the uncertainty introduced by the fitting (~0.6%) and travel time measurement (~0.02%), the uncertainty for the current travel time scale is thus predominately determined by the accuracy of the NaCl scale; this is similar to the establishment of ruby florescence scale that was calibrated against NaCl in previous studies (e.g., Yamaoka et al., 2012). In future experiment, this scale can be derived by calibrating the travel times against the absolute pressures obtained using MgO or NaCl as the sample (e.g., Li et al., 2005; Zha et al., 2000; Mueller, et al., 2003; Matsui et al., 2009).

For comparison, the travel times of Al_2O_3 based on previous ultrasonic experiments under hydrostatic conditions (Gieske and Barsh, 1968) and quasi-hydrostatic conditions (Li et al., 1996) are also included in Figure 3.2, which can be well described by a linear relation P =

217(3)×(1-t_S/t_{S0}) within uncertainties (e.g., Li and Liebermann, 2014). This indicates that, at a measured travel time t/t_0 for the buffer rod, if the literature results from hydrostatic/quasi-hydrostatic conditions are used as reference values (e.g., Sinelnikov et al., 2004) without accounting for the stress effect, the pressure will be underestimated by as much as ~13%. This difference mainly reflects the effect of stresses and pressure gradients across the buffer rod (e.g., Mazaki et al., 1973) due to the fact that the measured travel time represents an average from the center to the edge inside the pressure medium. However, for the purpose of establishing a pressure gauge, the linear pressure dependence displayed by the current travel time data as well as the pressure distribution inside the pressure medium (e.g., Mazaki, 1973) suggests that a pressure scale can be reliably established by correlating the measured travel time with the independently measured pressure in the center of the pressure medium; effectively, it may be viewed as if it were derived from its hydrostatic equation of state with a correction for the effects of stress/pressure gradient ($P=217 \times (1-t_S/t_{S0}) + 32.7 \times (1-t_S/t_{S0})$) or from the equation of state using an effective K' and G' of Al_2O_3. We note that the lengths of the Al_2O_3 buffer rod differ by ~5% in Run#1 and Run #2 which used MgO (55wt%)-$MgAl_2O_4$ (45wt%) and MgO (99%) as pressure medium, respectively; the normalized travel times from the two runs, however, are completely indistinguishable (see Figure 3.2). In addition, a previous study on two different types of polycrystalline alumina (Lucalox with a bulk density of 3.972(2) g/cm^3 and Coors 998 with a bulk density of 3.914(2) g/cm^3, ~1.5% difference) shows that even though the S wave velocities have ~2-3% difference between them (P wave velocities are almost identical), their normalized travel times as the function of pressure are almost identical (see Table 2.3, Table 2.4, Figure 2.12 and Figure 2.13 of Li, 1996). These important attributes allow the current travel time

pressure scale to be safely used in high pressure cell assemblies with slightly different buffer rod dimensions, densities and/or surrounding materials without introducing appreciable uncertainties.

Another important feature to note in Figure 3.2 is that the normalized S wave travel time of Al_2O_3 buffer rod along decompression displays a good agreement with those obtained along compression, implying that the same pressure scale can be used for pressure determination along decompression without being affected by the complication of hysteresis in the apparatus and, consequently, the pressure hysteresis along decompression can be fully characterized from the travel time pressure gauge.

3.3.2 Pressure scale at high temperature

High temperature measurements were conducted up to 13 GPa and 900 ºC in run #2, and the results of travel time of the Al_2O_3 buffer rod as a function of pressure and temperature are shown in Figure 3.3. Similar to the strategy utilized for the pressure scale at room temperature, the pressure at high temperature is expressed by linear terms of normalized travel time and temperature, $P = P_0 + a \times (1- t_S/t_{S0}) + b \times (T-T_0)$, where T is the experimental temperature measured by thermocouple, and P_0 and T_0 are the pressure and temperature at the reference condition (P_0 = 0 GPa and T_0 = 25 ºC in this study). A multi-variable linear regression is applied which treats the normalized S wave travel time and temperature as independent variables and pressure as the dependent variable, yielding the following expression with P in GPa and T in ºC:

$$P\ (GPa) = 242.5(9) \times (1-t_S/t_{S0}) + 0.01099(5) \times (T-T_0) \quad (2)$$

Figure 3.3 shows the comparison between the experimentally measured pressure from the NaCl scale and those from the least squares fit. The fitting has a standard error ~0.13 GPa for the entire pressure and temperature range, which is comparable to that for the pressure scale at room temperature. With this scale, we believe that the cell pressure at high temperatures in offline

experiments can be determined with an uncertainty comparable to that of NaCl scale measured by X-ray diffraction in synchrotron-based experiments.

One practical note is that if the value of t_0 at zero pressure after experiment is different from the one before experiment, the value after the experiment should be used in order to make it consistent with the travel time data at high temperatures. This is because the current pressure scale is parameterized through t/t_0 and requires that the buffer rod length is fully recovered after high temperature. In some cases, the buffer rod may experience plastic deformation if the stress exceeds the yield strength of polycrystalline Al_2O_3 during heating to the peak pressure and temperature conditions of the experiment in the first heating cycle. However, as seen in previous experiments, as long as the subsequent heating along decompression is not above the peak temperature, the cell assembly (buffer rod, sample, pressure medium) is expected to experience only elastic deformation and recovery, thus a single t_0 value can be preserved for all the data at high pressure and high temperature along decompression.

3.3.3 Simultaneous pressure and temperature scale

To date, simultaneous pressure and temperature determination using pressure scale approach remains a challenge. Previously, a double X-ray diffraction pressure standard approach has been investigated and its practical use is still under investigation due to the stringent precision and accuracy requirements in the measurement of unit cell volume and the associated equation of states (e.g., Utsumi et al., 1996). Since both P and S waves are simultaneously measured in the current study, the same approach used above offers a unique opportunity to construct a travel time scale for simultaneous determination of temperature and pressure. The intrinsic difference between P and S waves in their respective pressure and temperature dependences warrants a unique solution for P and T. For polycrystalline Al_2O_3 used in the

current study, t_0 for S wave is ~ 1100 ns and its sensitivity to pressure is ~ 4 ns/GPa (Figure 3.2); theoretically, under the resolution of the current travel time measurement (0.2 ns), the maximum pressure change can be resolved is ~0.05 GPa; by analogy, the S wave travel time displays a temperature sensitivity of ~ 0.04 ns/ºC (Figure 3.3), implying that the maximum resolving power for temperature change would be limited to 5 °C. As seen above in the derived pressure scales, the resultant standard error is on the order of three times the maximum resolvable changes.

For the simultaneous P-T scale, the pressure and temperature are both expressed as a linear function of P and S wave travel times, $P = P_0 + a \times (1- t_S/t_{S0}) + b \times (1- t_P/t_{P0})$ and $T = T_0 + c \times (1- t_S/t_{S0}) + d \times (1- t_P/t_{P0})$, in which "0" denotes the reference condition (in this study, $P_0 = 0$ GPa, $T_0 = 25$ °C), and a, b, c, and d are the coefficients. A least squares fit of all the P and S wave travel time data to the observed P (from NaCl) and T (from thermocouple reading) yielded the following expressions,

$$P\ (GPa) = - 245.4\ (\pm 3.4) \times (1- t_S/t_{S0}) + 402.7\ (\pm 2.1) \times (1- t_P/t_{P0}) \quad (3)$$

$$T\ (ºC) = T_0 - 44278.2(\pm 353.6) \times (1- t_S/t_{S0}) + 36496.5(\pm 224.6) \times (1- t_P/t_{P0}) \quad (4)$$

Figure 3.4 shows the comparison between the experimental results and fitting results. The fit results in a standard error of 0.16 GPa in pressure and ~17 °C in temperature. Note that the standard error in pressure appears to be preserved regardless whether the temperature is measured using thermocouple or to be determined using the travel time scale. A closer examination of the error distribution did not reveal any correlation with pressure which might result from the pressure effect on the EMF reading of the thermocouple. Note that, although the standard error in temperature is about 12 °C higher than the lowest temperature change resolvable by the current precision of travel time measurement, it is smaller than the temperature gradient (25 °C/mm) measured from the center to the edge across the sample region (Gwanmesia

et al., 1993) in a similar cell assembly. In addition, the easy access and the accuracies attainable of the current travel time scale make it superior to the double X-ray diffraction standard approach for simultaneous pressure and temperature determination in multi-anvil apparatus.

3.4 Application of the scale for offline experiment at room temperature

The new travel time pressure scale has been utilized in an ultrasonic measurement of coesite under high pressure in the 1000-ton double-stage multi-anvil apparatus installed in the High Pressure Lab of Stony Brook University (also see Chen et al., 2015). The cell assembly used is similar to the one in Figure 3.1(a) but without the graphite heater. Previously, the cell pressure versus ram load at room temperature for this apparatus has been calibrated using the fixed-point method to 12 GPa (e.g., Gasparik, 1989). As compared in Figure 3.5(a), the pressures derived from this new travel time method (equation 1) are in excellent agreements with those from the fixed-point method. Additionally, Figure 3.5(a) also includes the pressures obtained in the current study along decompression, which clearly shows the pressure hysteresis versus those along compression. Note that, at the first stage of decompression, the cell pressure only changed slightly (<1GPa) when the oil pressure decreased from 600 bar to 300 bar compared to that along compression (~ 4GPa), followed by a rapid drop in the lower oil pressure range (< 200 bar). This pressure dependent hysteresis prevents the fixed-point method from being reliably used during decompression for in-situ pressure determination.

To further evaluate the current travel time pressure scale, we derived the equation of state for coesite based on the measured P and S wave velocities and calculated the densities at high pressures (see also Chen et al., 2015). Figure 3.5 (b) shows the comparison of the density as a function of pressure from the current experiment with those of Angel et al. (2001) which were obtained from X-ray diffraction study on single crystal coesite in a diamond anvil cell with

hydrostatic pressure medium (4:1 mixture of methanol and ethanol) and a quartz crystal as internal pressure standard. The excellent agreement between the current data and those from previous single crystal study provides convincing evidence that this pressure determination method is very reliable. Needless to say, this development will greatly extend the capability of the multi-anvil apparatus for offline laboratory investigations of acoustic velocities, electrical resistivity/ conductivities, equation of state as well as other physical and chemical properties of condensed matter under high pressure.

3.5 Exploratory application for stress and strain measurements on the macroscopic scale

Based on acoustoelastic theory, we developed a new stress and strain determination method on the macroscopic scale using synchrotron X-radiation image technique in conjunction with ultrasonic technique at GSECARS beamline 13-ID-D of the Advanced Photon Source. The cell assembly is similar as shown in Figure 2.8 b with smaller amount of NaCl. Polycrystalline San Carlos olivine is used as sample, which was compressed to 15 GPa at room temperature with a higher pressurizing rate. As shown in Figure 3.6, the unit cell volume of San Carlos olivine sample at each pressure from our experiment is smaller than that from the hydrostatic compression by Abramson et al., (1997), which indicates that our sample is under differential stress.

As in conventional deformation experiments, the macroscopic stress field in the sample is divided into two terms at the center of the sample:

$$\sigma ij = \begin{pmatrix} \sigma 1 & 0 & 0 \\ 0 & \sigma 1 & 0 \\ 0 & 0 & \sigma 3 \end{pmatrix} = \begin{pmatrix} \sigma_P & 0 & 0 \\ 0 & \sigma_P & 0 \\ 0 & 0 & \sigma_P \end{pmatrix} + \begin{pmatrix} 2t/3 & 0 & 0 \\ 0 & -t/3 & 0 \\ 0 & 0 & -t/3 \end{pmatrix}$$

Where σ_1 and σ_3 represent the maximum and minimum principal stress, representatively; $\sigma_P = (\sigma_1+2\ \sigma_3)/3$, is the hydrostatic pressure; $t= \sigma_1-\sigma_3$, is the differential stress.

Based on acoustoelasticity, the S-wave velocity in the olivine specimen propagating along the stress direction is approximated by $V_S = \sqrt{\frac{G+1/2t}{\rho}}$, with the 1/2t term accounting for the effect of stress (e.g., Dey et al., 1984). Thus with the directly measured S wave velocities and shear modulus of San Carlos olivine under the hydrostatic condition from previous studies (e.g. Abramson et al., 1997; Zha et al., 1998) the differential stress t ($\sigma_1-\sigma_3$) can be obtained by $t=2(G-G_{hydro})$. Here we use the elasticities of San Carlos olivine from Abramson et al., (1997) to calculate the shear modulus as the function of pressure under hydrostatic conditions as their pressure range is close to that of our experiment. Figure 3.7a shows the differential stress of the sample as the function of pressure. The differential stress increases until ~13 GPa and starts to decrease after this pressure under the configuration of our experimental setup and conditions. Further analysis of this stress-strain curve is needed to determine if this is the yield point.

Deviatoric Strain is defined as follows:

$\varepsilon_1= (L-L_{hydro})/L_{hydro}$, where L_{hydro} is the sample length under hydrostatic conditions.

$\varepsilon_2= \varepsilon_3 =(D-D_{hydro})/D_{hydro}$, where D_{hydro} is the sample diameter under hydrostatic conditions.

L_{hydro} at each experimental pressure can be obtained by the equation $L/L_0 = (V/V_0)^{1/3}$ based on the equation of state of San Carlos olivine from previous studies (e.g., Abramson et al., 1997). Lengths of the sample from the experiment are from the radiographic images as discussed in Chapter 2. For sample diameter, $\rho_{hydro}\times V_{hydro}= \rho_{exp}\times V_{exp}$ since the density is the same, so the volume is also conserved. i.e., at the same P, $D_{hydro}^2\times L_{hydro} = D^2\times L$. Thus $\varepsilon_2= \varepsilon_3 =$ (D-

$D_{hydro})/D_{hydro}$ =D/D_{hydro}-1 can be calculated from the hydrostatic length and experimental length above (see results in Figure 3.7 b)

Figure 3.8 shows the plot of differential stress (σ_1-σ_3) as the function of differential strain (ε_1- ε_3). Thus we confirmed that the olivine sample yield at ~13 GPa under the configuration of our experiment and the yield strength is ~4.5 GPa.

This newly-established method has the advantage of in-situ measurement of the shear modulus under high pressures over previous methods like the lattice strain approach. The differential stress and strain and the yield strength are determined in the macroscopic scale. However, as this is an exploratory study, more work is needed to verify the results, especially about locating the yielding point (Wang and Li, in preparation).

3.6 Conclusions and concluding Remarks

Within the framework of acoustoelasticity accounting for the effects of hydrostatic and nonhydrostatic pressures, we have established a travel time pressure gauge using polycrystalline Al_2O_3 which was calibrated against NaCl by performing simultaneous synchrotron X-ray diffraction and ultrasonic interferometry measurements up to 15 GPa and 900°C. The scales for room temperature and high temperature pressure determination are given by equations (1) and (2), respectively.

The standard errors associated with these scales are less than 0.2 GPa. As demonstrated in the offline experiment for the study of coesite coupled with a pressure determination method using the current Al_2O_3 buffer rod travel time pressure scale, the equation of state of coesite from our study completely reproduced the results from previous single crystal hydrostatic compression data at room temperature, indicating that the travel time pressure scales offer reliable

measurements with a comparable accuracy to other in-situ primary pressure scales. A great advantage of these scales is that it allows for precise and continuous pressure determination not only during compression but also during decompression.

Compared to previous pressure scales, the current travel time pressure gauge bears a novel feature that allows for simultaneous determination of pressure and temperature due to the simultaneous measurements of compressional and shears waves. The corresponding pressure and temperature scales are expressed as a linear combination of P and S wave travel times (equations 3 and 4).

Within the resolution of the current experimental apparatus, the standard errors associated with the determined pressures and temperatures are 0.16 GPa and 17 ^{o}C, respectively. Giving its reliability, easy access, as well as the accuracy, this travel time approach can be a superior and practical choice for simultaneous pressure and temperature determination in both offline and online multi-anvil apparatus. Before direct data are available, we expect that, with the approximation of a linear pressure distribution in the pressure medium as supported by previous experimental study of Mazaki et al. (1973), the current pressure scale may also be applied to other cell assemblies (e.g., for 10/5, 8/3) by normalizing the observed pressure difference in Figure 3.2 to the initial Al_2O_3 buffer rod length and re-scaling to the desired buffer rod length.

Our final remarks are that the polycrystalline Al_2O_3 is probably the most preferable buffer rod material for acoustic pressure scale development because of its wide pressure and temperature stability fields, high strength, and chemical resistance; more importantly, its moderately high acoustic impedances make it an excellent matching material between high acoustic impedance WC anvil and most condensed matter under study (e.g., medals and alloys, oxides, and silicates). Together with previous equation of state results under hydrostatic pressure

conditions, the Al_2O_3 travel time scales can now be utilized for in-situ pressure and temperature determination in offline multi-anvil experiments under both hydrostatic and non-hydrostatic cell configurations. These developments are expected to enable new opportunities for laboratory studies of materials under high pressure and high temperature in multi-anvil apparatus, ranging from ultrasonic velocities, equation of state, phase equilibrium, new material synthesize, and thermal and electrical conductivity, with a precise and continuous pressure scale. And the newly developed method for stress and strain determination also enables new opportunities for the study of deformation, rheology of a wide range of materials under high pressure and high temperature in multi-anvil apparatus.

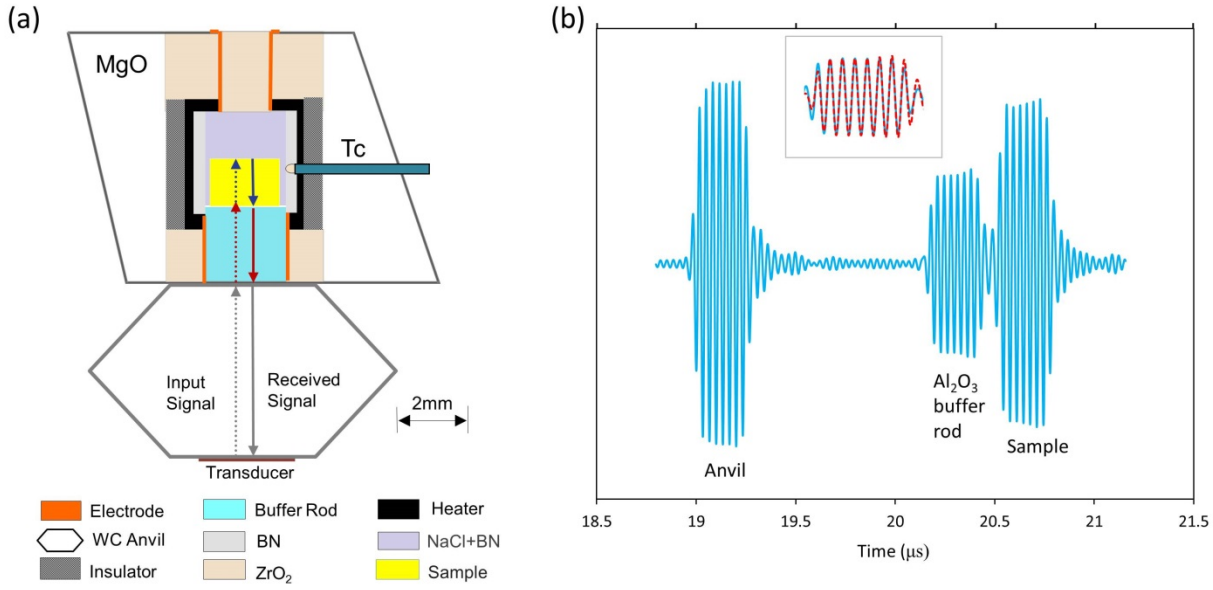

Figure 3. 1 (a) Cross section of the 14/8 cell assembly for high pressure ultrasonic measurements in the 1000-ton uniaxial split-cylinder apparatus (WC anvil is not in scale). (b) Observed 30 MHz shear wave signal at 5 GPa (run #1) showing the reflections from the anvil, buffer rod and sample, respectively. The inset shows the overlap of anvil and buffer rod echoes.

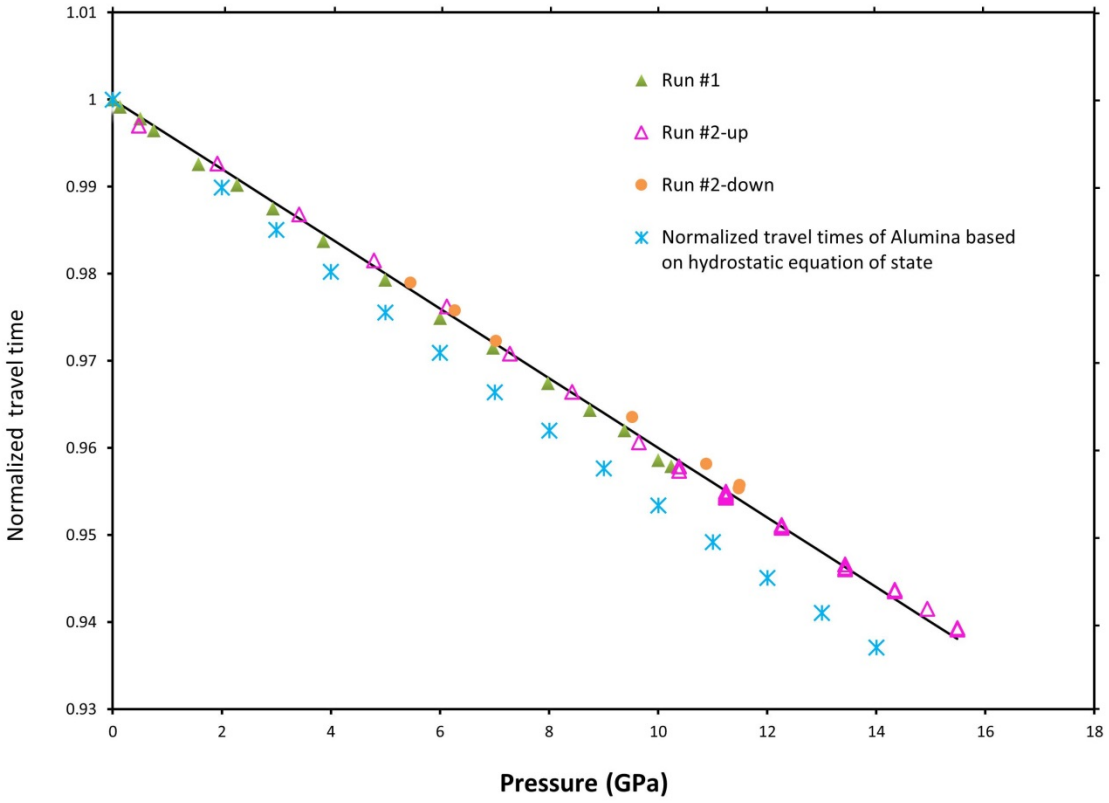

Figure 3. 2 Normalized S wave travel time of alumina buffer rod as a function of pressure from Run #1 (Wang et al., 2014) and Run #2 (Kung et al., 2004). The green triangles are data from Run #1 during compression; the pink open triangles and the orange dots are from Run #2 during compression and decompression, respectively. The black line is the linear least square fitting results to all data along compression. Blue stars are calculated S wave travel times based on data for single crystal Al_2O_3 under hydrostatic (Gieske and Barsch, 1968) and polycrystalline sample under quasi-hydrostatic pressures (e.g., Li et al., 1996).

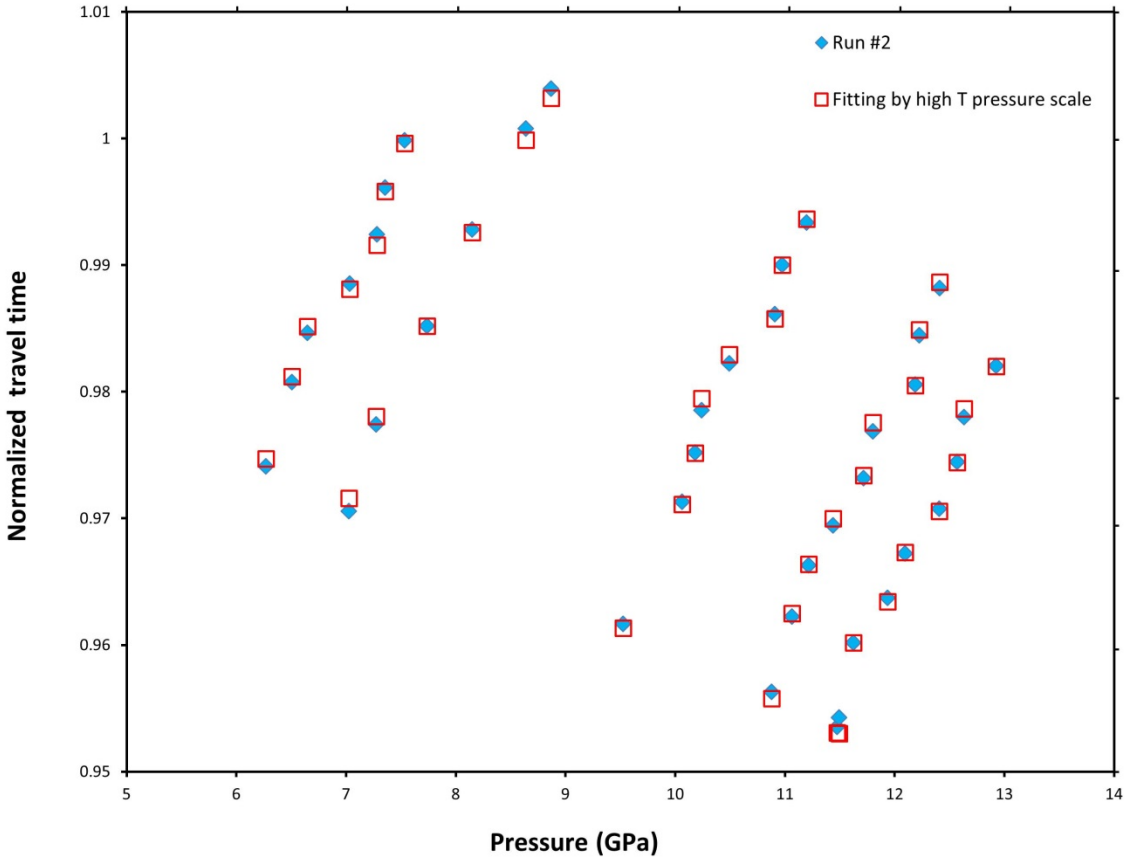

Figure 3. 3 Comparison between the experimentally measured pressures (blue diamonds) from the NaCl scale and those from the least squares fit (empty red squares) as the function of normalized S wave travel times of Run #2 at high temperatures.

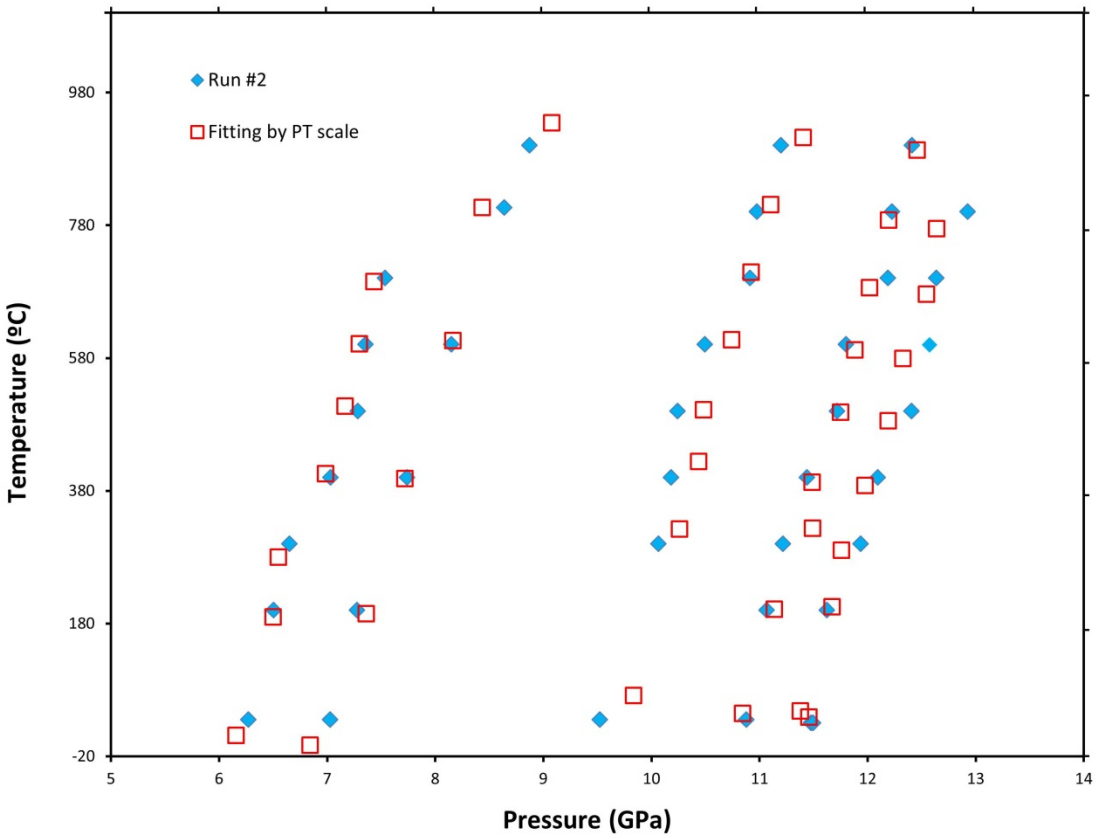

Figure 3. 4 Comparison between the experimentally measured pressures and temperatures (blue diamonds) and those from the least squares fit (empty red squares) of Run #2.

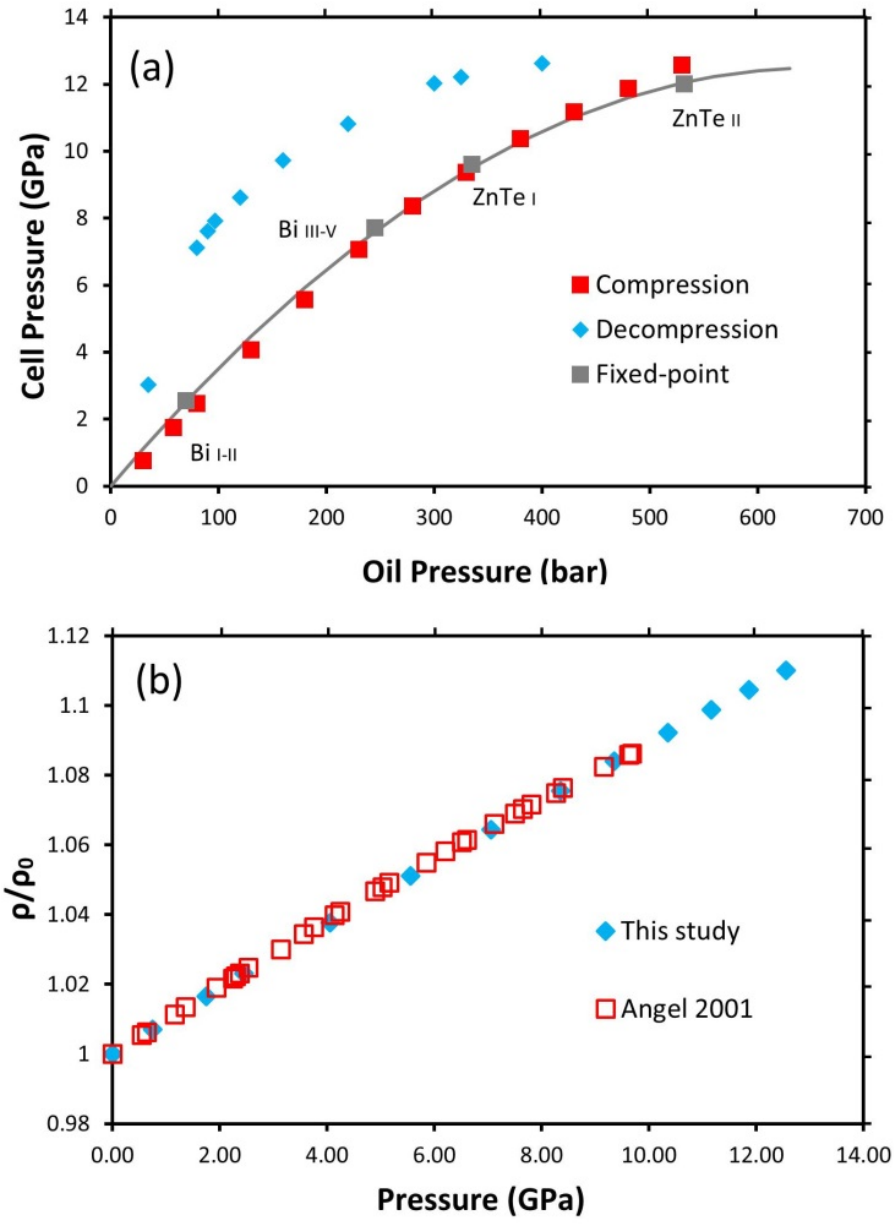

Figure 3. 5 (a) Comparison of pressure determined using buffer rod as in-situ pressure marker with previous calibration from fixed-point method; (b) Densities of coesite from the current study with pressure determined using the travel time pressure scale and comparison with single crystal data of Angel et al. (2001) obtained under hydrostatic conditions.

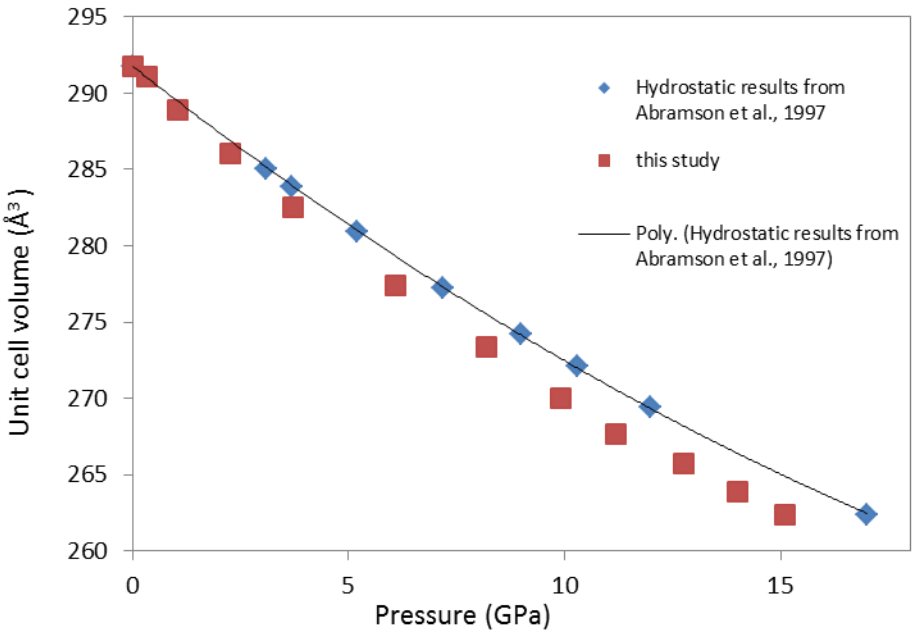

Figure 3. 6 Unit cell volume change as the function of pressure from this study and previous hydrostatic studies. The disagreement indicates the sample experienced differential stress during compression.

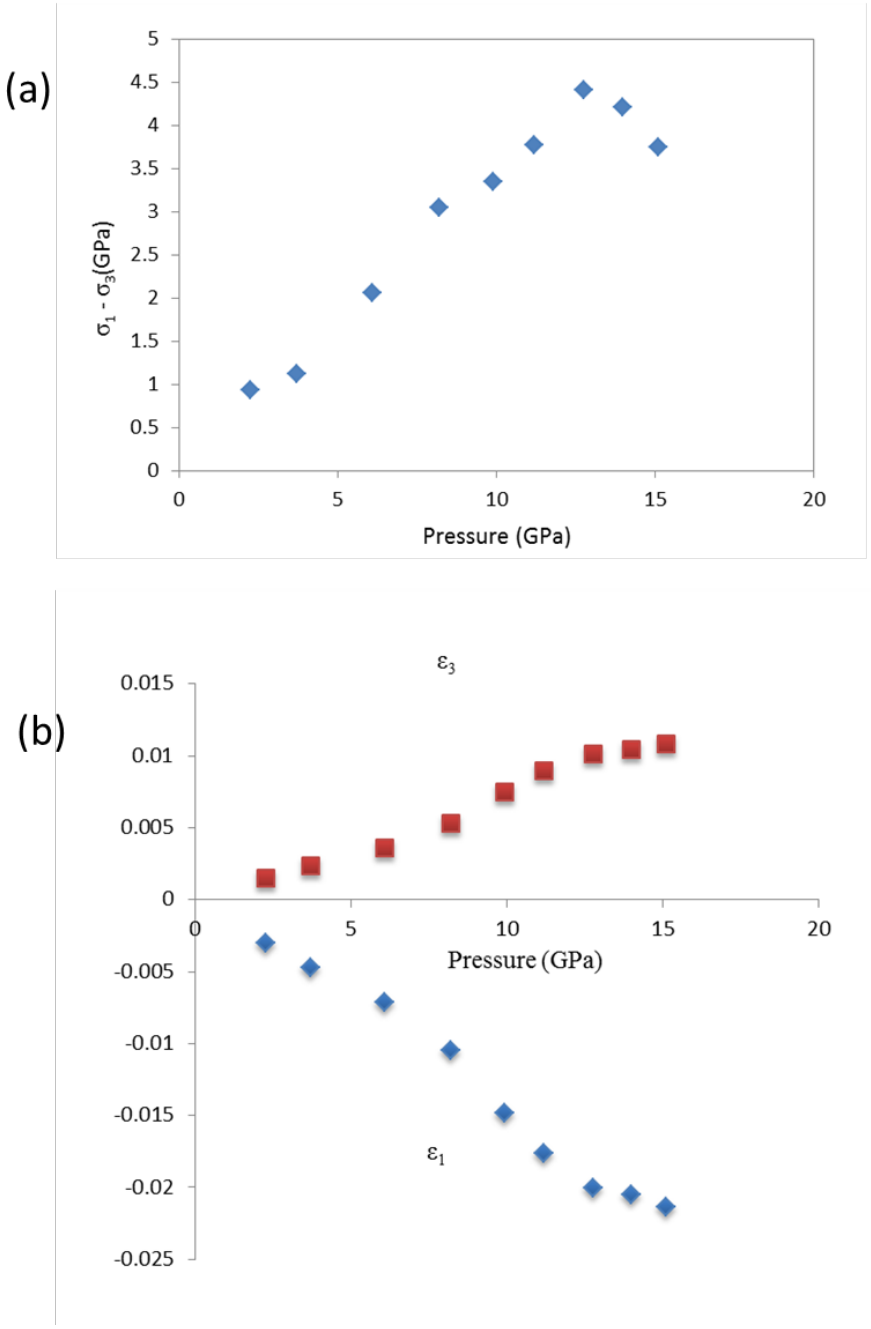

Figure 3. 7 (a): Differential stress of the sample as the function of pressure; (b): Deviatoric strain as the function of pressure.

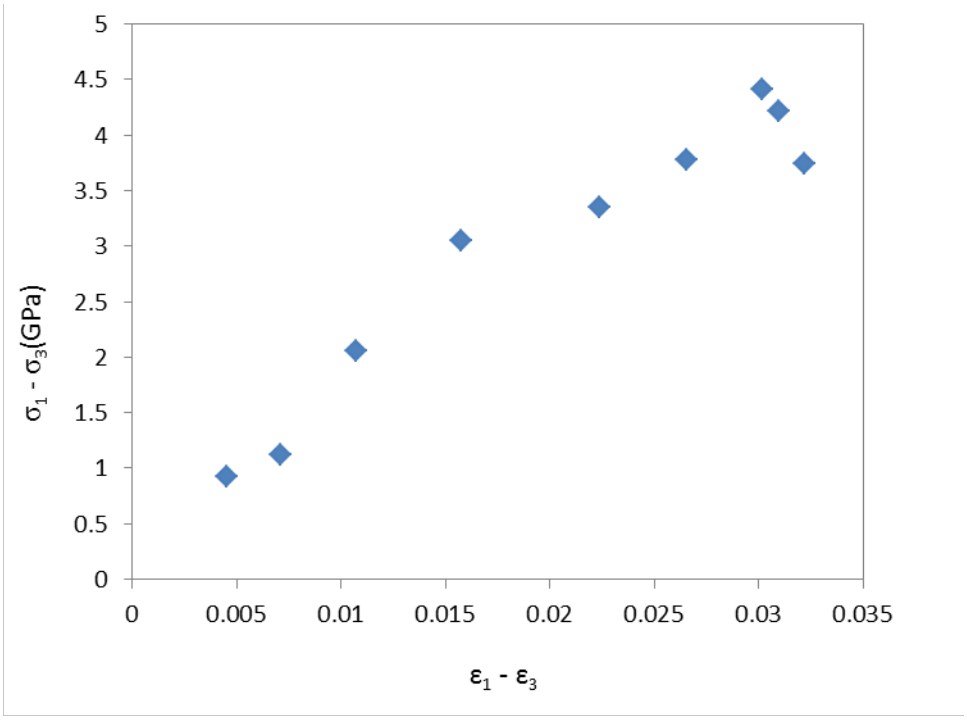

Figure 3. 8 Differential stress as the function of differential strain for the olivine specimen.

Reference

Abramson, E.H., Brown, J.M., Slutsky, L.J. and Zaug, J., 1997. The elastic constants of San Carlos olivine to 17 GPa. Journal of Geophysical Research: Solid Earth, 102(B6), pp.12253-12263.

Anderson, O.L., Isaak, D.G. and Yamamoto, S., 1989. Anharmonicity and the equation of state for gold. Journal of Applied Physics, 65(4), pp.1534-1543.

Angel, R.J., Mosenfelder, J.L. and Shaw, C.S.J., 2001. Anomalous compression and equation of state of coesite. Physics of the Earth and Planetary Interiors, 124(1), pp.71-79.

Bass, J.D., Sinogeikin, S.V. and Li, B., 2008. Elastic properties of minerals: A key for understanding the composition and temperature of Earth's interior. Elements, 4(3), pp.165-170.

Bassett, W.A., 2009. Diamond anvil cell, 50th birthday. High Pressure Research, 29(2), pp.163-186.

Bridgman, P. W., 1948. The Compression of 39 Substances to 100,000 kg/cm2, Proceedings of the American Academy of Arts and Sciences, 76, 55-70.

Chen, T., Gwanmesia, G.D., Wang, X., Zou, Y., Liebermann, R.C., Michaut, C. and Li, B., 2015. Anomalous elastic properties of coesite at high pressure and implications for the upper mantle X-discontinuity. Earth and Planetary Science Letters, 412, pp.42-51.

Decker, D.L., 1965. Equation of state of NaCl and its use as a pressure gauge in high‐pressure research. Journal of applied physics, 36(1), pp.157-161.

Decker, D.L., Bassett, W.A., Merrill, L., Hall, H.T. and Barnett, J.D., 1972. High‐Pressure Calibration: A Critical Review. Journal of Physical and Chemical Reference Data, 1(3), pp.773-836.

Decker, D.L., 1971. High-pressure equation of state for NaCl, KCl, and CsCl. Journal of Applied Physics, 42(8), pp.3239-3244.

Dey, S., Roy, N. and Dutta, A., 1984. P and S waves in a medium under initial stresses and under gravity. Indian Journal of Pure Applied Mathematics, 15(7), pp.795-808.

Dorfman, S.M., Prakapenka, V.B., Meng, Y. and Duffy, T.S., 2012. Intercomparison of pressure standards (Au, Pt, Mo, MgO, NaCl and Ne) to 2.5 Mbar. Journal of Geophysical Research: Solid Earth, 117(B8).

Dorogokupets, P.I. and Oganov, A.R., 2007. Ruby, metals, and MgO as alternative pressure scales: A semiempirical description of shock-wave, ultrasonic, x-ray, and thermochemical data at high temperatures and pressures. Physical Review B, 75(2), p.024115.

Fei, Y., Ricolleau, A., Frank, M., Mibe, K., Shen, G. and Prakapenka, V., 2007. Toward an internally consistent pressure scale. Proceedings of the National Academy of Sciences, 104(22), pp.9182-9186.

Gasparik, T., 1989. Transformation of enstatite-diopside-jadeite pyroxenes to garnet. Contributions to Mineralogy and Petrology, 102(4), pp.389-405.

Gieske, J.H. and Barsch, G.R., 1968. Pressure dependence of the elastic constants of single crystalline aluminum oxide. physica status solidi (b), 29(1), pp.121-131.

Gwanmesia, G.D., Li, B. and Liebermann, R.C., 1993. Hot pressing of polycrystals of high-pressure phases of mantle minerals in multi-anvil apparatus. In Experimental Techniques in Mineral and Rock Physics (pp. 467-484). Birkhäuser Basel.

Hemley, R.J. and Ashcroft, N.W., 1998. The revealing role of pressure in the condensed matter sciences.

Hirose, K., Sata, N., Komabayashi, T. and Ohishi, Y., 2008. Simultaneous volume measurements of Au and MgO to 140GPa and thermal equation of state of Au based on the MgO pressure scale. Physics of the Earth and Planetary Interiors, 167(3), pp.149-154.

Irifune, T., Higo, Y., Inoue, T., Kono, Y., Ohfuji, H. and Funakoshi, K., 2008. Sound velocities of majorite garnet and the composition of the mantle transition region. Nature, 451(7180), pp.814-817.

Irifune, T., Nishiyama, N., Kuroda, K., Inoue, T., Isshiki, M., Utsumi, W., Funakoshi, K.I., Urakawa, S., Uchida, T., Katsura, T. and Ohtaka, O., 1998. The postspinel phase boundary in Mg_2SiO_4 determined by in situ X-ray diffraction. Science, 279(5357), pp.1698-1700.

Jackson, I., and Rigden, S. M.,1998. In the Earth's Mantle: Composition, Structure, and Evolution," ed. Jackson I (Cambridge U. Press, Cambridge, UK), 405–460.

Jamieson, J.C., Fritz, J.N. and Manghnani, M.H., 1982. Pressure measurement at high temperature in X-ray diffraction studies: gold as a primary standard. High-pressure research in Geophysics, 12, pp.27-48.

Kung, J., Li, B., Uchida, T., Wang, Y., Neuville, D. and Liebermann, R.C., 2004. In situ measurements of sound velocities and densities across the orthopyroxene→ high-pressure clinopyroxene transition in $MgSiO_3$ at high pressure. Physics of the Earth and Planetary Interiors, 147(1), pp.27-44.

Li, B., 1996. Ultrasonic measurements of the elastic wave velocities of olivine and beta polymorphs of Mg_2SiO_4 at mantle transition zone P and T and geophysical implications, Ph.D. thesis, Stony Brook University.

Li, B. and Liebermann, R.C., 2007. Indoor seismology by probing the Earth's interior by using sound velocity measurements at high pressures and temperatures. Proceedings of the National Academy of Sciences, 104(22), pp.9145-9150.

Li, B. and Liebermann, R.C., 2014. Study of the Earth's interior using measurements of sound velocities in minerals by ultrasonic interferometry. Physics of the Earth and Planetary Interiors, 233, pp.135-153.

Li, B., Chen, K., Kung, J., Liebermann, R.C. and Weidner, D.J., 2002. Sound velocity measurement using transfer function method. Journal of Physics: Condensed Matter, 14(44), p.11337.

Li, B., Jackson, I., Gasparik, T. and Liebermann, R.C., 1996. Elastic wave velocity measurement in multi-anvil apparatus to 10 GPa using ultrasonic interferometry. Physics of the Earth and Planetary Interiors, 98(1), pp.79-91.

Li, B., Kung, J. and Liebermann, R.C., 2004. Modern techniques in measuring elasticity of Earth materials at high pressure and high temperature using ultrasonic interferometry in conjunction with synchrotron X-radiation in multi-anvil apparatus. Physics of the Earth and Planetary Interiors, 143, pp.559-574.

Li, B., Kung, J., Liu, W. and Liebermann, R.C., 2014. Phase transition and elasticity of enstatite under pressure from experiments and first-principles studies. Physics of the Earth and Planetary Interiors, 228, pp.63-74.

Li, B., Kung, J., Uchida, T. and Wang, Y., 2005. Pressure calibration to 20GPa by simultaneous use of ultrasonic and x-ray techniques. Journal of applied physics, 98(1), p.013521.

Liebermann, R. C., 2000. Elasticity of Mantle Minerals (Experimental Studies), in Earth's Deep Interior: Mineral Physics and Tomography From the Atomic to the Global Scale (eds S.-I. Karato, A. Forte, R. Liebermann, G. Masters and L. Stixrude), American Geophysical Union, Washington, D. C., 181-199. doi: 10.1029/GM117p0181

Liebermann, R. C., 2011. Multi-anvil, high-pressure apparatus: A half century of development and progress," High Pressure Research, 31, 493-532.

Moriarty, J.A., Belak, J.F., Rudd, R.E., Söderlind, P., Streitz, F.H. and Yang, L.H., 2002. Quantum-based atomistic simulation of materials properties in transition metals. Journal of Physics: Condensed Matter, 14(11), p.2825.

Matityahu, S., Emuna, M., Yahel, E., Makov, G. and Greenberg, Y., 2015. Novel experimental design for high pressure-high temperature electrical resistance measurements in a "Paris-Edinburgh" large volume press. Review of Scientific Instruments, 86(4), p.043902.

Matsui, M., 2009. Temperature–pressure–volume equation of state of the B1 phase of sodium chloride. Physics of the Earth and Planetary Interiors, 174(1), pp.93-97.

Mazaki, H., Lee, D.I. and Shimizu, S., 1973. Pressure distribution in a multianvil high-pressure device. Journal of Physics E: Scientific Instruments, 6(11), p.1072.

McDonough, W.F. and Sun, S.S., 1995. The composition of the Earth. Chemical geology, 120(3), pp.223-253.

McMillan, P. F., 2010. High-pressure synthesis of materials. NATO Science for Peace and Security Series B: Physics and Biophysics, 373-383.

McMillan, P.F., 2002. New materials from high-pressure experiments. Nature materials, 1(1), pp.19-25.

Mueller, H.J., Schilling, F.R., Lauterjung, J. and Lathe, C., 2003. A standard-free pressure calibration using simultaneous XRD and elastic property measurements in a multi-anvil device. European journal of mineralogy, 15(5), pp.865-873.

Papadakis, E., 1976. Ultrasonic velocity and attenuation: measurement methods with scientific and industrial applications. (Mason W P & Thurston R N, eds.) Physical acoustics: principles and methods, New York: Academic Press., 12. p. 277-374.

Ruoff, A.L., Lincoln, R.C. and Chen, Y.C., 1973. A new method of absolute high pressure determination. Journal of Physics D: Applied Physics, 6(10), p.1295.

Sinelnikov, Y.D., Chen, G. and Liebermann, R.C., 2004. Dual mode ultrasonic interferometry in multi-anvil high pressure apparatus using single-crystal olivine as the pressure standard. High Pressure Research, 24(1), pp.183-191.

Smyth, J.R., and McCormick, T.C., 1995. Crystallographic data for minerals. Editor: Ahrens, T.J., Mineral Physics and Crystallography: A Handbook of Physical Constants, AGU Reference Shelf 2, (AGU, Washington, DC) p2.

Speziale, S., Zha, C.S., Duffy, T.S., Hemley, R.J. and Mao, H.K., 2001. Quasi-hydrostatic compression of magnesium oxide to 52 GPa: Implications for the pressure-volume-temperature equation of state. Journal of Geophysical Research: Solid Earth, 106(B1), pp.515-528.

Syassen, K., 2008. Ruby under pressure. High Pressure Research, 28, 75-126.

Tsuchiva, T., 2003. First-principles prediction of the PVT equation of state of gold and the 660-km discontinuity in Earth's mantle. Journal of geophysical research, 108(B10), pp.ECV1-1.

Utsumi, W., Weidner, D.J. and Liebermann, R.C., 1998. Volume measurement of MgO at high pressures and high temperatures. Properties of Earth and Planetary Materials at High Pressure and Temperature, pp.327-333.

Wang, X., and Li, B., Acoustoelasticity and yield strength of Al_2O_3 under high pressure. in preparation.

Wang, X., Chen, T., Qi, X., Zou, Y., Liebermann, R.C., Li, B., 2014. Constraints on mantle composition of western North American from direct P and S wave velocities of mantle peridodite to 10 GPa. Abstract and poster for 2014 AGU (American Geophysical Union) Fall Meeting.

Wang, Z., Liu, Y., Bi, Y., Song, W. and Xie, H., 2012. Hydrostatic pressure and temperature calibration based on phase diagram of bismuth. High Pressure Research, 32(2), pp.167-175.

Wu, Z., Wentzcovictch, R., Umemoto, K., Li, B., Hirose, K., 2008. PVT relations in MgO: an ultra-high P-T scale for planetary science applications. Journal of Geophysical Research, 113, B06204.

Yamaoka, H., Zekko, Y., Jarrige, I., Lin, J.F., Hiraoka, N., Ishii, H., Tsuei, K.D. and Mizuki, J.I., 2012. Ruby pressure scale in a low-temperature diamond anvil cell. Journal of Applied Physics, 112(12), p.124503.

Zha, C.S., Duffy, T.S., Downs, R.T., Mao, H.K. and Hemley, R.J., 1998. Brillouin scattering and X-ray diffraction of San Carlos olivine: direct pressure determination to 32 GPa. Earth and Planetary Science Letters, 159(1), pp.25-33.

Zha, C.S., Mao, H.K. and Hemley, R.J., 2000. Elasticity of MgO and a primary pressure scale to 55 GPa. Proceedings of the National Academy of Sciences, 97(25), pp.13494-13499.

Chapter 4 Elastic wave velocities of peridotite KLB-1 at mantle pressures and implications for mantle velocity modeling

4.1 Introduction

To date, the composition of the Earth's upper mantle still remains controversial due to the lack of direct sampling of materials from all locations. Several models, such as pyrolite (Ringwood, 1975; see also Weidner, 1985; Ita and Stixrude, 1992; Jackson and Rigden, 1998; Li and Liebermann, 2007) and piclogite (e.g. Anderson and Bass, 1984; Bass and Anderson, 1984; Duffy and Anderson, 1989) have been proposed based on evidence from geochemical, petrological and seismic studies. The major difference between these two compositional models is that the former is olivine-rich (~ 60 %, Mg/Si ~ 1.2-1.3) while the latter is dominated by garnet and pyroxenes (Mg/Si ~ 1). More recently, a mechanical mixture of dis-equilibrated basalt and harzburgite has been proposed as a viable alternative compositional model (Xu et al., 2008; Ritsema et al., 2009).

One of the most commonly used geophysical approaches to distinguish and constrain the composition of the Earth's mantle is to compare calculated velocity and density profiles for mantle mineralogical models with those observed in global seismic studies, such as PREM (Dziewonski and Anderson, 1981) and AK135 (Kennett et al., 1995). In the last two decades, sound velocities have been measured for many Earth minerals at pressure and temperature conditions relevant to the Earth's upper mantle. While these studies provide indispensable data for characterizing individual phases and formulating possible systematics for the effect of

composition and mineralogy on the elasticity of mantle minerals, discrepancies in the existing elasticity data from different studies/techniques suggest that the extant data may not be sufficient when modeling a system as complex as the Earth's mantle, considering that compositional variations associated with chemical interactions of co-existing phases and element partitioning occur continuously at mantle depths (e.g., Irifune et al., 2008; Xu et al., 2008). Before this study, sound velocities of multiphase aggregate of possible mantle composition, the mostly relevant data to compare with seismic data, have only been available from acoustic studies up to 1GPa 1300^{o}C (e.g., Christensen, 1979; Kern, 1982; Sato et al., 1989).

KLB-1 peridotite is a spinel lherzolite xenolith from the Kilbourne Hole, New Mexico. Since the chemical composition of KLB-1 closely matches that of pyrolite (Table 2.1), many authors have conducted research on its melting temperature at high pressures as well as the compositions of the melts and the residual phases upon partial melting to investigate the petrogenesis of mid-ocean ridge basalts (MORB) and the evolution of the continental lithosphere (e.g., Takahashi, 1986; Zhang and Herzberg, 1994). When equilibrated at various pressures along the geotherm, KLB-1 produces a synthetic "rock" whose mineralogy closely resembles that of pyrolitic mantle; thus, acoustic velocities measurement on these synthetic rocks can yield elasticity data that account for the physical (pressure, temperature) and chemical conditions (phase fractions, elemental partitioning among co-existing phases, and the effect of minor and trace elements on elasticity) at relevant mantle depths. In this chapter, I will report results of ultrasonic P and S velocities of KLB-1 as a function of pressure to 10 GPa at room temperature, followed by comparisons with seismic velocities for the same composition calculated using theoretical averaging models to obtain insights into mantle compositions modeling (e.g., the Voigt-Reuss-Hill VRH or Hashin-Shtrikman HS methods).

4.2 Experimental methods and sample description

Polycrystalline aggregate specimens were hot-pressed at ~ 3 GPa, 1200 °C (K973) and 1400 °C (K657) for 1 hour using a 14/8 cell assembly in a 1000-ton uniaxial split-cylinder apparatus (Li et al., 1996a). The recovered specimens are cylindrical in shape, with ~ 2.5 mm diameter. Density measurement on specimen K973 using the Archimedes' method yielded a bulk density of 3.357(18) g/cm^3; it was prepared for acoustic measurements by polishing with 1-μm diamond paste to yield a final length of 1.82(1) mm. Scanning electron microscope (SEM) analysis reveals that the specimens are well-sintered, of average grain size ~ 10 micron, and free of visible micro-cracks (see details in Chapter 2).

The chemical compositions of the constituent mineral phases were obtained by averaging 4-5 electron microprobe analyses of specimen K973 (see Table 2.3). The olivine (Ol) has a Mg # [Mg / (Mg+Fe)] of 89.7, which is similar to that observed for fertile xenoliths (e.g. Lee 2003). Only trace amounts of Ca, Al, and Mn are detected in olivine grains. The compositions of orthopyroxene (Mg#~89.8, $En_{87}Fs_{10}Wo_2Jd_1$) and clinopyroxene (Mg#~89.2, $En_{44}Fs_5Wo_{48}Jd_3$), in the current KLB-1 aggregate show a good agreement with those reported by Chai et al. (1997) and Collins and Brown (1998) for natural Kilbourne Hole orthopyroxenes (KBH Opx) and clinopyroxenes (KBH Cpx). Lastly, the garnet (Gt) identified in the aggregate can be described by a solid solution of pyrope (Py), almandine (Alm), grossular (Grs) and uvarovite(Uv), $Py_{74}Alm_{12}Grs_{10}Uv_3$; the negligible variation in composition from grain to grain (<1%) suggests that the hot-pressed specimen has reached thermodynamic equilibrium. Spinel was not found in SEM and powder X-ray diffraction analyses, but a few scattered grains were identified during microprobe analyses.

The EPMA analyses yield the phase fractions of Ol ~ 61.6 wt%, Opx ~ 19.0 wt%, Cpx ~ 13.0 wt%, Gt ~ 6.4 wt% for K973 as shown in Table 2.3. The current run product is consistent with that recovered from 2.6 GPa and 1410 ^{o}C by Walter (1998) (Run # 26.01)) using peridotite KR4003 from West Kettle River, British Columbia, taking into account that the difference of Na_2O and Cr_2O_3 in compositions may result in the spinel to garnet transition at different pressures (e.g., O'Neill, 1981; Webb and Wood, 1986; Klemme, 2004).

Acoustic measurements were conducted in a 1000-ton uniaxial split-cylinder apparatus (USCA-1000) using ultrasonic interferometry (Li et al. 1996a, 1998). A dual mode $LiNbO_3$ transducer (50 MHz for P wave and 30 MHz for S wave) mounted on the back of the WC anvil was used as both transmitter and receiver of the acoustic signals. Alumina was used as buffer rod to transmit acoustic pulses into the sample. The transfer function method (Li et al., 2002) was used to acquire the acoustic response in the entire frequency range (25-70 MHz) followed by a pulse echo overlap (PEO, see Papadakis, 1976) analysis at monochromatic frequencies to obtain the travel times. The P and S wave travel times measured using the current method have a precision better than 0.2 % (Li et al., 2002). The alumina buffer rod also served as an in-situ pressure marker as discussed in Chapter 3, whose travel time as a function of pressure was constructed based on similar experiments conducted at synchrotron X-ray beamline, in which the pressure (at the center of the cell assembly) was determined by X-ray diffraction of NaCl (Decker, 1965) while the travel time of the Al_2O_3 buffer rod was measured simultaneously (Li and Liebermann, 2014, Wang et al., 2015). The Decker NaCl pressure scale has a reported uncertainty less than ~ 3 % within the current pressure range (Decker, 1965); the pressure determined in this study is thus estimated to have a maximum uncertainty ~ 0.3 GPa. After the high-pressure acoustic experiment, the sample length was measured to be 1.81(1) mm, which

agrees with its initial length within ~0.5%, (see Table 4.1), which leads to an error of 0.5% in velocity when combined with the error from travel time (0.2%). The specimen (K973) was then ground into fine powder, and X-ray diffraction data were collected using a Scintag powder diffractometer with a Cu target. Rietveld refinement yielded a density of 3.344(3) g/cm^3, 3.295(3) g/cm^3, 3.325(3) g/cm^3, and 3.674(5) g/cm^3 for olivine, orthopyroxene, clinopyroxene, and garnet, respectively; this results in a theoretical density of 3.353(4) g/cm^3 for K973 which is indistinguishable from the measured bulk density [3.357(18) g/cm^3], suggesting a maximum porosity of 0.5 % in the specimen.

4.3 Results and discussion

As shown in Figure 1 (a) and (b) (see also Table 4.1), both V_p and V_s of K973 increase monotonically as a function of pressure; measurements at pressures < 2 GPa are often affected by the gradual improvement of the mechanical coupling between the buffer rod and the specimen which are separated by a thin (~ 2 μm) gold foil (see Li et al., 1996a, 1998; Jackson et al., 1981) and thus not included for analysis and discussion. Figure.1 (a) and (b) also include the V_p and V_s for another specimen K657 which was hot pressed at ~ 3 GPa and 1400 ºC. The 200 ºC temperature difference only resulted in a difference of ~ 2 to 3 wt% in garnet and orthopyroxene content in the modal compositions (see Table 4.2) which will be expected to cause a difference of < 0.1 % in V_P and V_S based on VRH calculations. Note that the measured velocities of these two specimens indeed show excellent agreement for both V_P and V_S, which demonstrates that our experimental results on their relative comparison are robust and reliable. More importantly, it also suggests that in a well-mixed and equilibrated upper mantle with a uniform bulk composition, lateral variations in seismic velocities are largely due to temperature variations (or lattice preferred orientations) rather than compositional variations induced by thermal anomalies.

These data are especially important for the investigation of composition, density and seismic velocities of fertile and depleted peridotites to obtain insights into the dynamics and evolution of the upper mantle (e.g., Lee, 2003; Jordan, 1979; Afonso et al., 2010).

The P and S wave velocities for the individual mineral phases of KLB-1 were calculated using the third-order Eulerian finite strain equations (Davies and Dziewonski, 1975) and the elasticity data in Table 4.3, and the results are compared with those of KLB-1 in Figure 4.1(a) and Figure 4.1(b). We note that the elasticity data in Table 4.3 are our best choices based on literature studies on compositions identical or close to those identified in the current KLB-1 specimens (see Table 4.4). Acoustic data for phases with compositions close to those identified in the current KLB-1 are available for olivine (Liu et al., 2005; Zha et al., 1998; Abramson et al., 1997; Darling et al., 2004) and orthopyroxene (Chai et al., 1997) which were all obtained at pressures comparable to the current study. In addition, the bulk modulus and its pressure derivative from hydrostatic compression on a natural Opx (Specimen N2, Hugh-Jones and Angel, 1997) with compositions similar to the current Opx are highly consistent with the acoustic data. For Kilbourne Hole clinopyroxene, bulk and shear moduli at ambient conditions were reported in a study by Collins and Brown (1998), but no high pressure studies can be found in the literature. Since the composition of the current clinopyroxene is very diopsidic, the pressure derivatives from recent high-pressure acoustic studies on diopside (Li and Neuville, 2010; Sang et al., 2014) are thus considered to be good representative values. These approximations for Cpx are also supported by comparing the bulk modulus and its pressure derivative with those from X-ray diffraction studies by Comodi et al. (1995) and Bindi et al. (2006) on specimens with similar composition to the current study, especially with respect to the of aluminum content. Among all acoustic studies on garnets in literature, we failed to find any

direct measurement on Py73Alm13Grs11Uv3. An estimation using the properties of the end-members resulted in a wide range of 170.0-177.5 GPa and 90.4-93.9 GPa for the bulk and shear moduli, respectively, this is primarily due to the spread of the literature values for the elasticity of the endmembers; instead, the bulk and shear moduli were obtained based on the average of the results from Babuska et al., (1978), Sumino and Anderson (1982), Suzuki and Anderson (1983) and Lu et al. (2013) whose composition are close to the current one in KLB-1, while the pressure derivatives are taken from Lu et al. (2013) (see Table 4.4).

It can be seen that the velocities of KLB-1 follow closely the trend of its constituent phases. Between 2-10 GPa, P and S wave velocities of KLB-1 have an average pressure dependence of ~ 0.078 km/s GPa^{-1} and 0.020 km/s GPa^{-1}, respectively, which falls within those for clinopyroxene (0.085 km/s GPa^{-1}, 0.029 km/s GPa^{-1}), orthopyroxene (0.10 km/s GPa^{-1}, 0.020 km/s GPa^{-1}), garnet (0.060 km/s GPa^{-1}, 0.017 km/s GPa^{-1}) and olivine (0.080 km/s GPa^{-1}, 0.028 km/s GPa^{-1}). Note that the KLB-1 Opx exhibits higher shear wave velocities than KLB-1 olivine at pressures up to ~9 GPa, while for P waves, Opx has lower velocities than olivine below 6 GPa but higher after ~6 GPa (see also Chai et al., 1997). These observations are in sharp contrast to the comparison of their magnesium end members (e.g., Flesch et al., 1998), emphasizing the importance of including the effects of minor elements in modeling mantle compositions.

The largest velocity difference is observed between garnet and clinopyroxene, reaching about 9% and 6% for P and S waves, respectively; these comparisons at mantle temperatures may vary, depending on the similarities of the temperature dependence of the bulk and shear moduli between these phases (see Table 1 in Li and Liebermann, 2014 for latest compilation). Estimations based on pyrope (Gwanmesia et al., 2006) and diopside (Li and Neuville, 2010)

yield a difference of ~10% for both P and S wave velocities at 1473 K at upper mantle pressures. Thus, variations in bulk chemical compositions in a dis-equilibrated upper mantle can also contribute to the lateral seismic heterogeneities in addition to those caused by thermal anomalies (see also Xu and Wiens, 1997; Lebedev and van der Hilst, 2008).

The characteristics of V_P/V_S can also be a diagnostic for compositional or thermal anomalies in the mantle (e.g., Afonso et al., 2010; Lee, 2003). The V_P/V_S ratio of KLB-1 from the two experiments shows very good agreement within mutual uncertainties and exhibits a monotonic increase from 1.74 to 1.82 within 2-10 GPa (Figure 4.1(c)). Although garnet has the highest V_P/V_S value among all co-existing phases in the entire pressure range, the fast increase of V_P/V_S of KLB-1 is mostly attributable to contributions from orthopyroxene (Figure 4.1(c)). Thus, a decrease (increase) in garnet or an increase(decrease) in orthopyroxene content is effective in causing low (high) V_P/V_S anomalies at shallow upper mantle depths (Afonso et al., 2010).

4.4 Implications for mantle velocity modeling

Among many theoretical methods for modeling properties of aggregates, the commonly used approaches for seismic properties of the mineralogical aggregates of mantle minerals are the Hashin-Shtrikman (HS) (Hashin and Shtrikman, 1962a, 1962b, 1963) and/or the Voigt-Reuss-Hill (VRH) (Hill, 1952) methods based on the volume proportions and elasticity of each constituent phase (e.g., Ita and Stixrude, 1992; Jackson and Rigden, 1998; Li and Liebermann, 2007). With the modal composition of KLB-1 from EPMA analyses and the elasticity data for constituent phases, a direct comparison can be made between the measured velocities and those calculated using these theoretical averaging approaches to obtain insights into current mantle velocity modeling.

The VRH and HS bounds calculated using the data in Table 4.3 are compared with the directly measured velocities in Figure 4.2 (a) (see also Table 4.1 and Table 4.5). According to Watt and O'Connell 1980, the polycrystalline end members are almost fully dense (99.8~99.9%) while the aggregates have relatively larger porosity (98.0~99.6% of theoretical value, see table II of Watt and O'Connell, 1980), and the effects of anisotropy and porosity must be taken into account due to the importance in comparison with calculated velocities. Thus, we corrected the effect of porosity (~0.5%) following the approach of MacKenzie (1950) by assuming spherical pores. The velocity anisotropy information for our KLB-1 specimens is not directly available; however, based on studies on an very anisotropic mineral stishovite (up to ~60% variation in S wave velocity along different crystallographic directions) hot-pressed using the same cell assembly, the velocities measured in three orthogonal directions are essentially identical within measurement uncertainties (e.g., Li et al., 1996b). Thus, the anisotropy in the current KLB-1 is assumed to be within the current experimental uncertainties.

Since the difference in the bulk and shear moduli among all major constituent phases are within ~10% (garnet not considered due to its low content), the lower (Reuss, HS^-) and the upper (Voigt, HS^+) bounds as well as the HS average nearly coincide with the VRH average, thus only VRH is shown in Figure 4.2 (a) and used for discussion hereafter. To obtain the upper and lower limits of the predicted values associated with VRH due to uncertainties in the elasticity data for all constituent phases (e.g., Watt and O'Connell, 1980), two additional calculations were performed by using the highest and lowest values, respectively, for the bulk and shear moduli of each phase within their uncertainties; in the current case, the range of Voigt and Reuss values calculated from the reported single crystal elastic constants for each phase are considered as their respective uncertainties (Table 4.3). VRH calculations using all-Voigt (i.e., VRH-upper) and all-

Reuss (i.e., VRH-lower) values yielded an error band of ~±0.8% for both P and S wave velocities (see blue and yellow lines in Figure 4.2 (a)); this calculated range is comparable to that estimated using the reported uncertainties for the bulk and shear moduli in the individual phases considered in this study (e.g., 1.9-2.2% for the bulk and shear moduli for San Carlos olivine, see Table 3 of Zha et al., 1998). Following Watt and O'Connell (1980), the values in the entire range predicted by the theoretical averaging schemes are viewed as equally valid when comparing with experimental data.

As shown in Figure 4.2 (a), the P and S wave velocities of KLB-1 after porosity correction are ~1.0% lower than the average VRH values in the pressure range of 2-6 GPa; these differences gradually increase to 1.4% (P wave) and 1.9% (S wave) at 9.2 GPa. The increased deviation above 6 GPa could be related to the negligible velocity increase with pressure within 6-10 GPa (average $\partial V_S/\partial P \sim 0$ km/s GPa^{-1}) in the KLB-1 pyroxene (see Figure 8 in Kung et al., 2005; Figure 7 in Zhang et al., 2013], which is not adequately accounted for by the third order finite strain equations. On the other hand, a close examination indicates that, except for S wave at pressure above 6 GPa, the velocities of KLB-1 can be found in good agreement with the lower limit of the VRH within experimental uncertainties. Similar observations were obtained in previous studies on two-phase composites, such as KCl+NaCl (Watt and O'Connell, 1980), Al_2O_3+NiAl (Upadhyay et al., 2012), and forsterite+enstatite mixtures (Ji and Wang, 1999); i.e., that the direct experimental data often fall in the vicinity of the lower limit of VRH (Ji and Wang, 1999) or HS (Watt and O'Connell, 1980). In particular, the ultrasonic measurements to 3 GPa on hot-pressed forsterite-enstatite mixtures with 60% forsterite (Ji and Wang, 1999) bear a strong resemblance to the current study on KLB-1 (~62% olivine). As shown in Ji and Wang (1999), the P and S wave velocities at 2 GPa agree within 0.3(±0.1) % with the lower limit of

VRH calculated using the bulk and shear moduli of forsterite and enstatite within their measurement errors, together with an agreement (~1.5%) with the mean value of the VRH, all of which are consistent with the current observations. It is worth noting that if the comparison with VRH for the 60% forsterite mixture is carried out using the same approach undertaken for KLB-1 in this study [i.e., using literature (porosity free) data for the bulk and shear moduli in VRH and applying a correction for the measured porosity (0.9%) to the experimental data] exactly the same conclusions can be drawn as those discussed above.

The densities derived from the current velocity measurements are indistinguishable (within ~0.3%, Figure 4.2 (b)) from the values based on the volumetric fractions of each mineral; unlike VRH velocities, this calculation requires no approximation or assumptions about the aggregate. Similarly, the V_P/V_S values are only different from the VRH value (lower, upper and mean VRH values are indistinguishable) by less than 0.3% at pressures 2-6 GPa and 0.4-0.45% from 6 to 9.2 GPa (Figure 4.2 (c)). The bulk sound velocities ($V_\varphi^2 = V_P^2 - 4V_S^2/3$) calculated from the porosity-corrected KLB-1 velocities show an agreement of <0.1% with the lower limit of the VRH (except for the first and last pressure points ~0.3%) and ~0.7% with the mean VRH value (Figure 4.2 (d)).

In summary, these results demonstrate that precise and reliable P and S velocities and densities of multiphase aggregates of complex mantle compositions can be obtained by direct measurements, offering a unique opportunity for improved studies of the mantle. In addition, the comparisons of the experimental results in Figure 4.2 are analogous to the inverse of geophysical modeling of mantle composition which involves comparison of VRH calculated properties with seismic data; thus, inferences from above comparisons have direct implications for the investigation of mantle composition. Firstly, it is important to include the effect of minor

elements on the elasticity of mantle phases, such as in Opx, Cpx, and Gt (see also Chai et al., 1997; Kono et al., 2007; Irifune et al., 2008); ignoring the effect of aluminum on the elasticity of Opx and Cpx alone lowers the VRH velocities in Figure 4.2 (a) by ~1.1% and leads to different inferences about the comparisons discussed above. Secondly, when modeling mantle composition using VRH calculated velocities based on literature elasticity data for mantle phases, candidate compositions whose density and velocities reproducing seismic data within the limits given by experimental uncertainties should be considered equally valid. For velocity models of mantle compositions calculated at mantle temperatures that are reported to have typical uncertainties of 2-3% (e.g., Irifune et al., 2008; Ita and Stixrude, 1992; Cammarano et al., 2003) due to uncertainties in the elasticity data, the observations in Figure 4.2 (a) do not seem to invalidate the comparisons and/or conclusions made in these previous studies, and have no effect on the modeled velocity contrasts across mantle discontinuities.

Lastly, we note that the P and S wave velocities based on VRH calculations for the KLB-1 composition and those of pyrolite are almost identical due to the similarity in their mineralogy (see Table 2.1), with a difference less than 0.3% . Thus, the current data in Figure 4. 2 (a) can be directly applied to comparisons between pyrolite and seismic data in previous studies, provided that comparable elasticity data are used in VRH calculations (as cautioned above). A test using the elasticity data compiled in Cammarano et al. (2003) or Li and Liebermann (2007) indicated that the resultant VRH velocities for pyrolite are ~1.0% lower than those obtained using the data in Table 4.3 and nearly coincide with the experimental data of KLB-1 (see Figure 4.3), presumably due to the incomplete correction for the effect of aluminum on Opx and Cpx as discussed above. While this does not seem to significantly affect the comparisons with seismic models (see Figure 5 of Li and Liebermann, 2007), it does imply that the velocities for an

aggregate with pyrolitic composition of KLB-1 are in close agreement with seismic data at the depths of the Earth's upper mantle.

Table 4. 1 Elastic properties of KLB-1 at room temperature[1]

P(GPa)	*t_p(μs)*	*t_s(μs)*	*l(mm)*	*ρ(g/cm^3)*	*V_P (km/s)*	*V_s (km/s)*
(a)	**Specimen K657**					
0	0.334	0.557	1.21	3.347	7.25	4.36
0.89	0.306	0.51	1.207	3.368	7.89	4.75
1.26	0.301	0.505	1.206	3.377	8.02	4.79
1.83	0.297	0.503	1.205	3.387	8.13	4.80
3.52	0.281	0.500	1.197	3.455	8.51	4.81
5.07	0.277	0.497	1.194	3.485	8.62	4.83
6.47	0.273	0.492	1.190	3.515	8.73	4.86
7.72	0.269	0.487	1.188	3.540	8.82	4.90
8.83	0.267	0.484	1.185	3.560	8.89	4.91
9.79	0.264	0.482	1.183	3.580	8.97	4.92
(b)	**Specimen K973**					
0	0.457[2]	0.785[2]	1.82	3.357	7.95	4.64
1.29	0.444	0.771	1.819	3.393	8.14	4.70
1.57	0.439	0.763	1.812	3.400	8.23	4.75
1.96	0.435	0.759	1.810	3.411	8.30	4.77
2.56	0.430	0.753	1.808	3.426	8.38	4.80
3.28	0.426	0.75	1.804	3.445	8.45	4.81
3.90	0.422	0.746	1.802	3.460	8.51	4.83
5.09	0.417	0.741	1.797	3.488	8.60	4.85
6.41	0.411	0.735	1.792	3.518	8.70	4.87
7.41	0.407	0.731	1.788	3.541	8.77	4.89
7.86	0.405	0.73	1.786	3.551	8.79	4.89
8.43	0.403	0.728	1.784	3.564	8.82	4.90
9.21	0.401	0.725	1.781	3.581	8.86	4.91

[1]The travel time has a standard deviation less than 0.2ns and 0.4ns for P and S wave, respectively. The overall uncertainty propagated into the calculated velocity is better than 0.5% while the modulus is about 1%, the pressure has a uncertainty of ~3%.
Velocities under 1.83 GPa for K657 and under 1.96 GPa for K973 are not shown in figures and not discussed in the manuscript.
[2] Bench top signals of K973 were not obtained. Zero pressure t_p t_s are from linear fitting.

Table 4. 2 Composition of KLB-1 sample and cell parameters of constituent phases*

K973	**Ol**	**Cpx**	**Opx**	**Gt**	**Sp**	**Bulk composition** *(Herzburg et al., 1990)*
SiO_2	40.45	51.88	54.35	42.19	0.14	44.3
Al_2O_3	0.06	7.71	5.40	23.51	62.09	3.54
FeO	10.11	3.29	6.53	6.63	10.07	8.59
MgO	49.02	15.19	32.26	21.05	20.61	39.5
CaO	0.13	19.22	0.85	5.19	0.05	3.03
Na_2O	0.03	1.73	0.16	0.02	0.00	0.3
TiO_2	0.02	0.55	0.14	0.28	0.14	0.12
Cr_2O_3	0.02	0.33	0.17	0.91	6.80	NA
MnO	0.15	0.10	0.13	0.22	0.09	0.14

Modal Composition (wt %)

K973[1]	**62.5**	**12.9**	**17.8**	**6.8**	**0**[**]	**(3 GPa, 1200 °C)**
K973[2]	**60.7**	**13.1**	**20.3**	**5.9**	**0**[**]	**(3 GPa, 1200 °C)**
K973[3]	**61.6**	**13.0**	**19.0**	**6.4**	**0**	
K657	**62.6**	**13.3**	**14.8**	**9.2**	**0**	**(3 GPa, 1400 °C)**
KLB-1 *(Herzberg et al. , 1990)*	62	14	22	0	2	(0 GPa, 25 °C)
KLB-1 *(Davis et al., 2009)*	60	14	23	0	2	(0 GPa, 25 °C)
Pyrolite *(Ringwood, 1975)*	57	12	17	14		(0 GPa, 25 °C)

*The chemical formulas and lattice parameters of each mineral of K973 are as following:

Ol: $(Mg_{1.8}Fe_{0.2})SiO_4$; a = 4.763 Å, b = 10.227 Å, c = 5.994 Å, ρ = 3.344 g/cm^3.

Cpx: $(Mg_{0.82}Fe_{0.1}Ca_{0.74}Na_{0.12}Al_{0.2}Ti_{0.01})(Al_{0.12}Si_{1.88})O_6$; a = 9.691 Å, b = 8.845 Å, c = 5.272 Å, β = 107.41º, ρ = 3.325 g/cm^3.

Opx: $(Mg_{1.66}Fe_{0.19}Ca_{0.03}Al_{0.12})(Al_{0.1}Si_{1.89})O_6$; a = 18.242 Å, b = 8.804 Å, c =5.195 Å, ρ = 3.295 g/cm^3.

Gt: $(Mg_{2.22}Fe_{0.29}Ca_{0.4}Mn_{0.03}Cr_{0.06}Ti_{0.01})(Al_{1.9}Fe^{3+}_{0.1})(Si_{2.98}Al_{0.04})O_{12}$; a = 11.530 Å, ρ = 3.674 g/cm^3.

Sp: $(Mg_{0.8}Fe_{0.2})(Al_{1.86}Cr_{0.14})O_4$

**The percentage of spinel is based on estimation and fixed in mass balance calculation.

K973[1]: modes were calculated based on the bulk composition of KLB-1 from Herzberg et al., (1990).

K973[2]: modes were calculated based on the bulk composition of KLB-1 from Davis et al., (2009).

K973[3]: Average of K973[1] and K973[2].

Table 4. 3 Elasticity of aggregate KLB-1 (K973) and its constituent minerals*

	Ks_0 (GPa)	Ks_0'	G_0 (GPa)	G_0'	Remarks
KLB-1	123	5.1	75	1.3	*This study*
VRH	127	5.0	77	1.5	*This study*
Ol	129.2	4.6	77.5	1.6	
	(131, 127)		(78.3, 75.7)		*Based on single crystal data from Zha et al. (1998)*
Cpx	117.2	4.85	72.2	1.65	
	(122, 112.4)		(74.7, 69.8)		*Based on single crystal data from Collins and Brown (1998)*
Opx	115.5	6.7	78.1	1.44	
	(116.3, 112.4)		(78.6, 77.3)		*Based on single crystal data from Chai et al. (1997)*
Gt	170.5	4.4	92.3	1.2	

*: The values for the constituent minerals (first entry for each mineral) are best approximations for the composition identified in the current KLB-1 specimen; these values are used to calculate the red lines in Figure 4. 2. Data in parenthesis for each mineral are Voigt and Reuss limits calculated based on single crystal data, respectively; these values are used to calculate the blue (Voigt) and yellow (Reuss) lines in Figure 4.2.

Table 4. 4 Elasticity of constituent minerals of KLB-1

Mineral	Ks_0 (GPa)	Ks_0'	G_0 (GPa)	G_0'	References
San Carlos Olivine	130.3	4.6	77.4	1.6	*[1]*
San Carlos Olivine	131.1(130)	3.8(4.7)	79.4(77)	1.0(1.9)	*[2]*
San Carlos Olivine	129.4	4.35	78.3	1.45	*[3]*
San Carlos Olivine	127.2	4.8	77.4	1.63	*[4]*
KBH Cpx	117.2		72.2		*[5]*
Diopside	114.6	4.8	72.7	1.7	*[6]*
Diopside	116.4	4.9	73	1.6	*[7]*
Natural Cpx	116-117	4.0*			*[8]*
Synthetic Cpx	(117.2)	4.2			*[9]*
KBH Opx	115.5	6.6	78.1	1.44	*[10]*
Natural Opx	(115.5)	6.7			*[11]*
Py68Alm24Gr5Sp1	168.2	4.4	92.1	1.2	*[12]*
Py73Alm16Gr5Uv5An1	170.0		92.6		*[13]*
Py73Alm16Spe6Grs5	171.3		92.6		*[14]*
Py70Alm16Spe9Grs5	170.8		92.0		*[15]*
Py73Alm16An4Uv6	171.2		92.6		*[16]*
Py73Alm14Spe5Grs8	171.6		92.2		*[17]*

1: Liu et al., (2005); Fo90Fa10, Pmax=8GPa
2: Zha et al. (1998); Fo90; Pmax= 32 GPa; results in parenthesis are 3rd order finite strain fit to those below 10 GPa and were used to obtain the average elastic properties in Table 4.3.
3: Abramson et al., (1997); Fo90; Pmax =12 GPa
4: Darling et al. (2004); Fo90; P max=10.6 GPa
5: Collins and Brown (1998); KBH Cpx; P = 0 GPa
6: Sang and Bass. (2014); Diopside; P max = 14 GPa
7: Li and Neuville (2010); Diopside; P max 8GPa
8: Comodi et al. (1995); K' is set to be 4.0;X-ray; P max ~ 5 GPa; cpx composition similar to this study;
9: Bindi et al. (2006), Reanalyzed by setting K=117.2GPa; X-ray, synthetic sample, Pmax =9 GPa
10: Chai et al. (1997); Reanalyzed using 3rd order finite strain; KBH opx; P max=12 GPa
11: Hugh-Jones and Angel (1997); Reanalyzed by setting K=115.5GPa; V_0=833.12 $Å^3$ (834.33 $Å^3$of KLB-1 Opx) Pmax =11 GPa
12: Lu et al. (2013); Pmax=20 GPa
13: Babuska et al. (1978); P = 0 GPa
14: Sumino and Anderson (1982); P = 0 GPa
15: Sumino and Anderson (1982); P = 0 GPa
16: Suzuki and Anderson (1983); P = 0 GPa
17: Sumino and Anderson (1982); P = 0 GPa

Table 4. 5 P and S wave velocities derived from VRH

P(GPa)	*V_P-VRH (km/s)*	*V_S-VRH (km/s)*	*V_P-upper* (km/s)*	*V_S-upper* (km/s)*	*V_P-lower** (km/s)*	*V_S-lower** (km/s)*
0	8.29	4.80	8.35	4.84	8.22	4.77
1.29	8.41	4.84	8.47	4.88	8.34	4.80
1.57	8.43	4.85	8.50	4.89	8.37	4.81
1.96	8.47	4.86	8.53	4.90	8.40	4.82
2.56	8.52	4.88	8.58	4.91	8.46	4.84
3.28	8.58	4.90	8.65	4.93	8.52	4.86
3.90	8.64	4.91	8.70	4.95	8.57	4.87
5.09	8.73	4.94	8.79	4.98	8.67	4.90
6.41	8.84	4.98	8.90	5.01	8.77	4.94
7.41	8.91	5.00	8.97	5.04	8.85	4.96
7.86	8.95	5.01	9.01	5.05	8.88	4.97
8.43	8.99	5.02	9.05	5.06	8.92	4.99
9.21	9.04	5.04	9.10	5.08	8.98	5.00

* V_P-upper and V_S-upper are the upper limits calculated by VRH using Voigt values of K and G of constituent phases.

** V_P-lower and V_S-lower are the lower limits calculated by VRH using Reuss values of K and G of constituent phases.

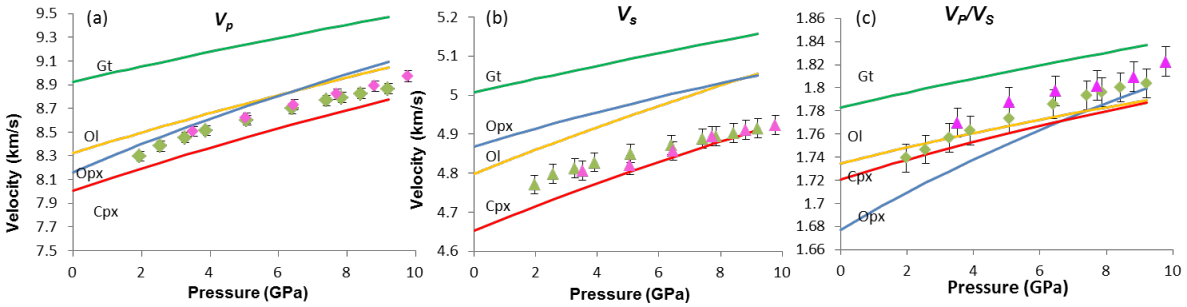

Figure 4. 1 (a) V_p and (b) *Vs* for synthetic KLB-1 specimens and their comparisons with individual minerals using elastic properties from Table 4.3. Errors are ~0.5%. (c) Pressure dependence of V_P/V_S ratio of KLB-1 specimens and individual minerals. Errors are ~0.7%. Green diamonds: K973, pink triangles: K657.

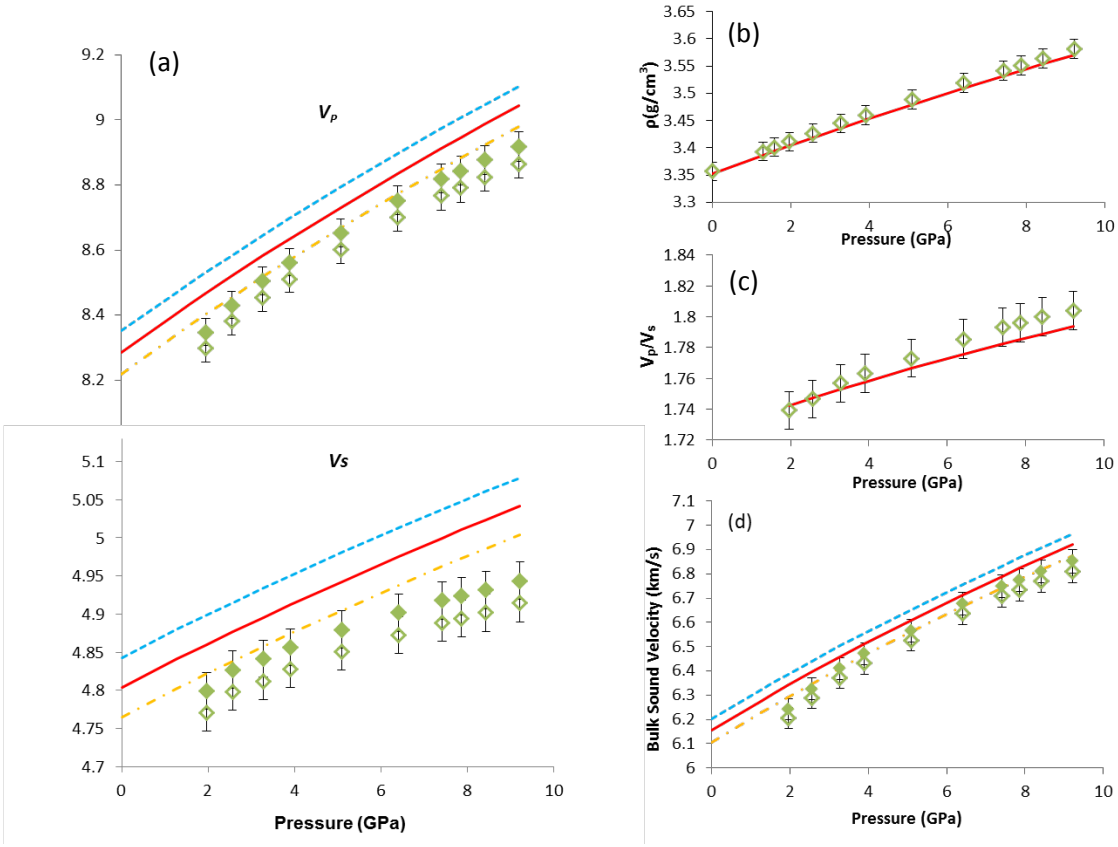

Figure 4. 2 Comparisons of experimentally observed velocities [(a): V_P and V_S, (d) V_φ], densities [(b)] and V_p/V_s [(c)] for KLB-1 (K973) with VRH average based on the fractions and elasticity of individual minerals; note that the two averaging methods (VRH and HS) are indistinguishable in this study. Green empty symbols: measured values of KLB-1 (K973). Green solid symbols: velocities of KLB-1 (K973) after 0.5% porosity correction. The red solid lines are our best estimates according to the individual mineral data with compositions closest to the KLB-1 specimen. Blue and yellow dashed lines are the upper and lower limit calculated by VRH using Voigt and Reuss values of all minerals, respectively. The legend in (a) is also applicable to (b) (c) (d).

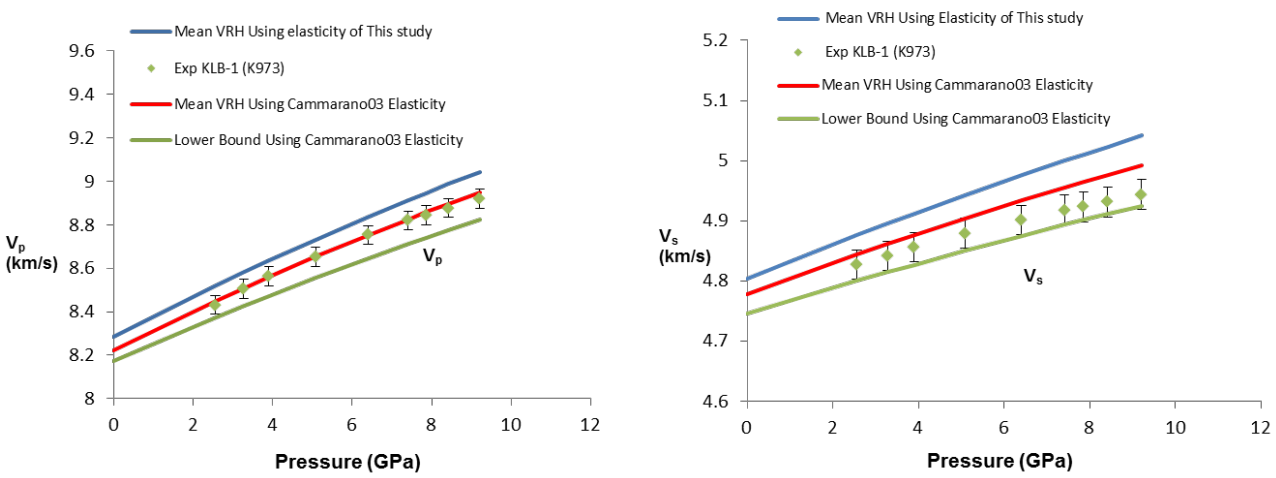

Figure 4. 3 Comparisons of V_p and V_s for K973 with calculations using the mineral elasticity data compiled in Cammarano et al., (2003) and in Table 4.3 of this study.

Reference

Abramson, E.H., Brown, J.M., Slutsky, L.J. and Zaug, J., 1997. The elastic constants of San Carlos olivine to 17 GPa. Journal of Geophysical Research: Solid Earth, 102(B6), pp.12253-12263.

Afonso, J.C., Ranalli, G., Fernàndez, M., Griffin, W.L., O'Reilly, S.Y. and Faul, U., 2010. On the Vp/Vs–Mg# correlation in mantle peridotites: Implications for the identification of thermal and compositional anomalies in the upper mantle. Earth and Planetary Science Letters, 289(3), pp.606-618.

Anderson, D.L. and Bass, J.D., 1984. Mineralogy and composition of the upper mantle. Geophysical Research Letters, 11(7), pp.637-640.

Babuška, V., Fiala, J., Kumazawa, M., Ohno, I. and Sumino, Y., 1978. Elastic properties of garnet solid-solution series. Physics of the Earth and Planetary Interiors, 16(2), pp.157-176.

Bass, J.D. and Anderson, D.L., 1984. Composition of the upper mantle: Geophysical tests of two petrological models. Geophysical Research Letters, 11(3), pp.229-232.

Bindi, L., Downs, R.T., Harlow, G.E., Safonov, O.G., Litvin, Y.A., Perchuk, L.L., Uchida, H. and Menchetti, S., 2006. Compressibility of synthetic potassium-rich clinopyroxene: In-situ high-pressure single-crystal X-ray study. American Mineralogist, 91(5-6), pp.802-808.

Cammarano, F., Goes, S., Vacher, P. and Giardini, D., 2003. Inferring upper-mantle temperatures from seismic velocities. Physics of the Earth and Planetary Interiors, 138(3), pp.197-222.

Chai, M., Brown, J.M. and Slutsky, L.J., 1997. The elastic constants of an aluminous orthopyroxene to 12.5 GPa. Journal of Geophysical Research: Solid Earth, 102(B7), pp.14779-14785.

Christensen, N.I., 1979. Compressional wave velocities in rocks at high temperatures and pressures, critical thermal gradients, and crustal low-velocity zones. Journal of Geophysical Research: Solid Earth, 84(B12), pp.6849-6857.

Collins, M.D. and Brown, J.M., 1998. Elasticity of an upper mantle clinopyroxene. Physics and chemistry of minerals, 26(1), pp.7-13.

Comodi, P., Princivalle, F., Tirone, M. and Zanazzi, P.F., 1995. Comparative compressibility of clinopyroxenes from mantle nodules. European Journal of Mineralogy-Ohne Beihefte, 7(1), pp.141-150.

Darling, K.L., Gwanmesia, G.D., Kung, J., Li, B. and Liebermann, R.C., 2004. Ultrasonic measurements of the sound velocities in polycrystalline San Carlos olivine in multi-anvil, high-pressure apparatus. Physics of the Earth and Planetary Interiors, 143, pp.19-31.

Davies, G.F. and Dziewonski, A.M., 1975. Homogeneity and constitution of the Earth's lower mantle and outer core. Physics of the Earth and Planetary Interiors, 10(4), pp.336-343.

Davis, F.A., Tangeman, J.A., Tenner, T.J. and Hirschmann, M.M., 2009. The composition of KLB-1 peridotite. American Mineralogist, 94(1), pp.176-180.

Decker, D.L., 1965. Equation of state of NaCl and its use as a pressure gauge in high-pressure research. Journal of applied physics, 36(1), pp.157-161.

Duffy, T.S. and Anderson, D.L., 1989. Seismic velocities in mantle minerals and the mineralogy of the upper mantle. Journal of Geophysical Research: Solid Earth, 94(B2), pp.1895-1912.

Duffy, T.S., Zha, C.S., Downs, R.T., Mao, H.K. and Hemley, R.J., 1995. Elasticity of forsterite to 16 GPa and the composition of the upper mantle. Nature, 378(6553), pp.170-173.

Dziewonski, A.M. and Anderson, D.L., 1981. Preliminary reference Earth model. Physics of the earth and planetary interiors, 25(4), pp.297-356.

Flesch, L.M., Li, B. and Liebermann, R.C., 1998. Sound velocities of polycrystalline $MgSiO_3$-orthopyroxene to 10 GPa at room temperature. American Mineralogist, 83(5), pp.444-450.

Gwanmesia, G.D., Wang, L., Heady, A. and Liebermann, R.C., 2014. Elasticity and sound velocities of polycrystalline grossular garnet ($Ca_3Al_2Si_3O_{12}$) at simultaneous high pressures and high temperatures. Physics of the Earth and Planetary Interiors, 228, pp.80-87.

Gwanmesia, G.D., Zhang, J., Darling, K., Kung, J., Li, B., Wang, L., Neuville, D. and Liebermann, R.C., 2006. Elasticity of polycrystalline pyrope ($Mg_3Al_2Si_3O_{12}$) to 9 GPa and 1000 ºC. Physics of the Earth and Planetary Interiors, 155(3), pp.179-190.

Hashin, Z. and Shtrikman, S., 1962a. A variational approach to the theory of the effective magnetic permeability of multiphase materials. Journal of applied Physics, 33(10), pp.3125-3131.

Hashin, Z. and Shtrikman, S., 1962b. On some variational principles in anisotropic and nonhomogeneous elasticity. Journal of the Mechanics and Physics of Solids, 10(4), pp.335-342.

Hashin, Z. and Shtrikman, S., 1963. A variational approach to the theory of the elastic behaviour of multiphase materials. Journal of the Mechanics and Physics of Solids, 11(2), pp.127-140.

Herzberg, C., Gasparik, T. and Sawamoto, H., 1990. Origin of mantle peridotite: constraints from melting experiments to 16.5 GPa. Journal of Geophysical Research: Solid Earth, 95(B10), pp.15779-15803.

Hill, R., 1952. The elastic behaviour of a crystalline aggregate. Proceedings of the Physical Society. Section A, 65(5), p.349.

Hugh-Jones, D.A. and Angel, R.J., 1997. Effect of Ca^{2+} and Fe^{2+} on the equation of state of $MgSiO_3$ orthopyroxene. Journal of Geophysical Research: Solid Earth, 102(B6), pp.12333-12340.

Irifune, T., Higo, Y., Inoue, T., Kono, Y., Ohfuji, H. and Funakoshi, K., 2008. Sound velocities of majorite garnet and the composition of the mantle transition region. Nature, 451(7180), pp.814-817.

Ita, J. and Stixrude, L., 1992. Petrology, elasticity, and composition of the mantle transition zone. Journal of Geophysical Research: Solid Earth, 97(B5), pp.6849-6866.

Jackson, I., and Rigden, S. M., 1998. In the Earth's Mantle: Composition, Structure, and Evolution, ed. Jackson I (Cambridge U. Press, Cambridge, UK), 405–460.

Jackson, I., Niesler, H. and Weidner, D.J., 1981. Explicit correction of ultrasonically determined elastic wave velocities for transducer-bond phase shifts. Journal of Geophysical Research: Solid Earth, 86(B5), pp.3736-3748.

Ji, S. and Wang, Z., 1999. Elastic properties of forsterite–enstatite compositesup to 3.0 GPa. Journal of Geodynamics, 28(2), pp.147-174.

Jiang, F., Speziale, S. and Duffy, T.S., 2004. Single-crystal elasticity of grossular-and almandine-rich garnets to 11 GPa by Brillouin scattering. Journal of Geophysical Research: Solid Earth, 109(B10).

Jordan, T.H., 1979. Mineralogies, densities and seismic velocities of garnet lherzolites and their geophysical implications. The Mantle Sample: Inclusion in Kimberlites and Other Volcanics, pp.1-14.

Kennett, B.L.N., Engdahl, E.R. and Buland, R., 1995. Constraints on seismic velocities in the Earth from traveltimes. Geophysical Journal International, 122(1), pp.108-124.

Kern, H., 1982. Elastic-wave velocity in crustal and mantle rocks at high pressure and temperature: The role of the high-low quartz transition and of dehydration reactions. Physics of the Earth and Planetary Interiors, 29(1), pp.12-23.

Klemme, S., 2004. The influence of Cr on the garnet–spinel transition in the Earth's mantle: experiments in the system MgO-Cr_2O_3-SiO_2 and thermodynamic modelling. Lithos, 77(1), pp.639-646.

Kono, Y., Higo, Y., Ohfuji, H., Inoue, T. and Irifune, T., 2007. Elastic wave velocities of garnetite with a MORB composition up to 14 GPa. Geophysical Research Letters, 34(14).

Kung, J., Li, B., Uchida, T. and Wang, Y., 2005. In-situ elasticity measurement for the unquenchable high-pressure clinopyroxene phase: Implication for the upper mantle. Geophysical research letters, 32(1).

Kung, J., Li, B., Uchida, T., Wang, Y., Neuville, D. and Liebermann, R.C., 2004. In situ measurements of sound velocities and densities across the orthopyroxene→ high-pressure clinopyroxene transition in $MgSiO_3$ at high pressure. Physics of the Earth and Planetary Interiors, 147(1), pp.27-44.

Lebedev, S. and Van Der Hilst, R.D., 2008. Global upper-mantle tomography with the automated multimode inversion of surface and S-wave forms. Geophysical Journal International, 173(2), pp.505-518.

Lee, C.T.A., 2003. Compositional variation of density and seismic velocities in natural peridotites at STP conditions: Implications for seismic imaging of compositional heterogeneities in the upper mantle. Journal of Geophysical Research: Solid Earth, 108(B9).

Li, B. and Liebermann, R.C., 2007. Indoor seismology by probing the Earth's interior by using sound velocity measurements at high pressures and temperatures. Proceedings of the National Academy of Sciences, 104(22), pp.9145-9150.

Li, B. and Liebermann, R.C., 2014. Study of the Earth's interior using measurements of sound velocities in minerals by ultrasonic interferometry. Physics of the Earth and Planetary Interiors, 233, pp.135-153.

Li, B. and Neuville, D.R., 2010. Elasticity of diopside to 8GPa and 1073K and implications for the upper mantle. Physics of the Earth and Planetary interiors, 183(3), pp.398-403.

Li, B., Chen, G., Gwanmesia, G.D. and Liebermann, R.C., 1998. Sound velocity measurements at mantle transition zone conditions of pressure and temperature using ultrasonic interferometry in a multianvil apparatus, in Properties of Earth & Planetary Materials at High Pressure & Temperature, edited by M. H. Manghnani, Y. Syono and T. Yagi, 41-61.

Li, B., Chen, K., Kung, J., Liebermann, R.C. and Weidner, D.J., 2002. Sound velocity measurement using transfer function method. Journal of Physics: Condensed Matter, 14(44), p.11337.

Li, B., Jackson, I., Gasparik, T. and Liebermann, R.C., 1996 a. Elastic wave velocity measurement in multi-anvil apparatus to 10 GPa using ultrasonic interferometry. Physics of the Earth and Planetary Interiors, 98(1), pp.79-91.

Li, B., Rigden, S.M. and Liebermann, R.C., 1996 b. Elasticity of stishovite at high pressure. Physics of the Earth and Planetary Interiors, 96(2), pp.113-127.

Liu, Q., Liu, W., Whitaker, M.L., Wang, L. and Li, B., 2008. Compressional and shear wave velocities of Fe_2SiO_4 spinel at high pressure and high temperature. High Pressure Research, 28(3), pp.405-413.

Liu, W., Kung, J. and Li, B., 2005. Elasticity of San Carlos olivine to 8 GPa and 1073 K. Geophysical Research Letters, 32(16).

Lu, C., Mao, Z., Lin, J.F., Zhuravlev, K.K., Tkachev, S.N. and Prakapenka, V.B., 2013. Elasticity of single-crystal iron-bearing pyrope up to 20 GPa and 750 K. Earth and Planetary Science Letters, 361, pp.134-142.

Mackenzie, J.K., 1950. The elastic constants of a solid containing spherical holes. Proceedings of the Physical Society. Section B, 63(1), p.2.

O'Neill, H.S.C., 1981. The transition between spinel lherzolite and garnet lherzolite, and its use as a geobarometer. Contributions to Mineralogy and Petrology, 77(2), pp.185-194.

Papadakis, E.P., 1976. Ultrasonic velocity and attenuation: Measurement methods with scientific and industrial applications. Physical acoustics, 12, pp.277-374.

Ringwood, A. E., 1975. Composition and petrology of the earth's mantle, McGraw-Hill, New York, pp. 618.

Ritsema, J., Xu, W., Stixrude, L. and Lithgow-Bertelloni, C., 2009. Estimates of the transition zone temperature in a mechanically mixed upper mantle. Earth and Planetary Science Letters, 277(1), pp.244-252.

Sang, L. and Bass, J.D., 2014. Single-crystal elasticity of diopside to 14 GPa by Brillouin scattering. Physics of the Earth and Planetary Interiors, 228, pp.75-79.

Sato, H., Sacks, I.S., Murase, T., Muncill, G. and Fukuyama, H., 1989. Qp-melting temperature relation in peridotite at high pressure and temperature: Attenuation mechanism and implications for the mechanical properties of the upper mantle. Journal of Geophysical Research: Solid Earth, 94(B8), pp.10647-10661.

Sinogeikin, S.V. and Bass, J.D., 2000. Single-crystal elasticity of pyrope and MgO to 20 GPa by Brillouin scattering in the diamond cell. Physics of the Earth and Planetary Interiors, 120(1), pp.43-62.

Sumino, Y. and Anderson, O.L., 1982. Elastic constants of minerals. In R.S. Carmichael, Ed., Handbook of Physical Properties of Rocks, Vol. 3, p. 39–138.CRC Press, Boca Raton, Florida.

Suzuki, I., and Anderson O. L., 1983. Elasticity and thermal expansion of a natural garnet up to 1000 K. Journal of Physics of the Earth, 31(2), pp.125-138.

Takahashi, E., 1986. Melting of a dry peridotite KLB-1 up to 14 GPa: Implications on the origin of peridotitic upper mantle. Journal of Geophysical Research: Solid Earth, 91(B9), pp.9367-9382.

Upadhyay, A., Beniwal, R.S. and Singh, R., 2012. Elastic properties of Al_2O_3–NiAl: a modified version of Hashin–Shtrikman bounds. Continuum Mechanics and Thermodynamics, 24(3), pp.257-266.

Walter, M.J., 1998. Melting of garnet peridotite and the origin of komatiite and depleted lithosphere. Journal of Petrology, 39(1), pp.29-60.

Wang, X., Chen, T., Qi, X., Zou, Y., Kung, J., Yu, T., Wang, Y., Liebermann, R.C. and Li, B., 2015. Acoustic travel time gauges for in-situ determination of pressure and temperature in multi-anvil apparatus. Journal of Applied Physics, 118(6), p.065901.

Watt, J.P. and O'Connell, R.J., 1980. An experimental investigation of the Hashin-Shtrikman bounds on two-phase aggregate elastic properties. Physics of the Earth and Planetary Interiors, 21(4), pp.359-370.

Webb, S.A.C. and Wood, B.J., 1986. Spinel-pyroxene-garnet relationships and their dependence on Cr/Al ratio. Contributions to Mineralogy and Petrology, 92(4), pp.471-480.

Weidner, D.J., 1985. A mineral physics test of a pyrolite mantle.Geophysical Research Letters, 12(7), pp.417-420.

Xu, W., Lithgow-Bertelloni, C., Stixrude, L. and Ritsema, J., 2008. The effect of bulk composition and temperature on mantle seismic structure. Earth and Planetary Science Letters, 275(1), pp.70-79.

Xu, Y. and Wiens, D.A., 1997. Upper mantle structure of the southwest Pacific from regional waveform inversion. Journal of Geophysical Research: Solid Earth, 102(B12), pp.27439-27451.

Zha, C.S., Duffy, T.S., Mao, H.K., Downs, R.T., Hemley, R.J. and Weidner, D.J., 1997. Single-crystal elasticity of β-Mg 2 SiO 4 to the pressure of the 410 km seismic discontinuity in the Earth's mantle. Earth and Planetary Science Letters, 147(1), pp.E9-E15.

Zhang, D., Jackson, J.M., Chen, B., Sturhahn, W., Zhao, J., Yan, J. and Caracas, R., 2013. Elasticity and lattice dynamics of enstatite at high pressure. Journal of Geophysical Research: Solid Earth, 118(8), pp.4071-4082.

Zhang, J. and Herzberg, C., 1994. Melting experiments on anhydrous peridotite KLB-1 from 5.0 to 22.5 GPa. Journal of Geophysical Research: Solid Earth, 99(B9), pp.17729-17742.

Zou, Y., Gréaux, S., Irifune, T., Whitaker, M.L., Shinmei, T. and Higo, Y., 2012. Thermal equation of state of $Mg_3Al_2Si_3O_{12}$ pyrope garnet up to 19 GPa and 1,700 K. Physics and Chemistry of Minerals, 39(7), pp.589-598.

Chapter 5 Mantle composition and temperature of western North America revealed from direct P and S wave velocities of KLB-1 peridotite to the conditions of the transition zone

5.1 Introduction

The composition and thermal structure of the Earth's mantle have been studied extensively by seismology, geochemistry, petrology and mineral physics, but they still remain controversial. The challenge lies in that, without samples from these depths for direct laboratory analyses, only indirect constraints can be obtained by examining models based on evidence from geochemical and petrological studies on surface/crustal rocks (e.g., Anderson, 1989; McDonough and Sun, 1995) or by comparing global and/or regional seismic observations with the elastic properties of constituent minerals and their high-pressure phases (Goes and Van der Lee, 2002; Kuskov and Kronrod, 2006). Some research shows that pyrolite model (~57vol% olivine, 29vol% pyroxenes, 14vol% garnet; see Ringwood, 1975) along ~1300(±100) ^{o}C adiabatic geotherm yields seismic velocities more consistent with typical seismological models than those of piclogite in the whole mantle (e.g., Ita and Stixrude, 1992; Jackson and Rigden, 1998; Li and Liebermann, 2007). However, there are also studies arguing that the seismic velocity jumps at 410 km can be better reproduced with a piclogitic composition (< 40% olivine), thereby calling for a layered mantle with a piclogitic transition zone (e.g., Bass and Anderson, 1984). More recent mineral physics studies show that there is not a single compositional model that can reproduce all the featured velocity discontinuities and gradients in global seismological models at mantle depths (e.g., Irifune et al., 2008; Xu et. al., 2008),

prompting more investigations on regional variations of composition and/or temperature in various tectonic settings in connection with 3D tomographic studies (Masters et al., 2000; Grand et al., 1997, Romanowicz, 1995) and/or 1D regional velocity models (Nolet et al., 1994; Van der Lee and Nolet, 1997).

Chemical interactions are known to occur among co-existing mantle phases (e.g., Fumagalli and Klemme, 2015; Zhang and Herzberg, 1994 and references therein) and partitioning of minor and trace elements can play important roles in affecting the velocities of aggregates (e.g., Weidner and Wang, 1998; Chai and Brown, 1997; Walter, 1998). Construction of velocity-depth profiles for the aggregate of mantle composition necessitates accurate thermodynamic and elasticity data for all minerals and phases in equilibrium at depths (e.g., Ita and Stixrude, 1992). The extant laboratory sound velocity measurements, however, are predominantly limited to single mineral phases of simple compositions; data on natural mineral samples are still scarce and of limited coverage in composition (see reviews by Li and Liebermann, 2014; Bass, 1995). This incompleteness as well as the inconsistency of the current elastic properties of mantle minerals and phases may have undermined previous comparisons between seismic data and mineral physics modeling, which is believed to be partially, if not entirely, responsible for the standing controversies.

In this study, we overcome this challenge by performing in-situ X-ray and ultrasonic velocity measurements on a series of polycrystalline aggregates of peridotite KLB-1 hot-pressed at 5-15 GPa 1200-1400°C under the mantle pressures and temperatures to depths of the transition zone (which begins at 410 km); with this approach, phase transitions and chemical interactions among all phases at various depths are fully included in a self-consistent fashion. The starting material KLB-1 peridotite (e.g., Herzberg et al., 1990), as described in Chapter 2, is a spinel

lherzolite xenolith from the Kilbourne Hole crater in New Mexico, which is under the region of Rio Grande Rift. It is a natural fertile lherzolite [Mg/(Mg+Fe) ~89.1] and is considered to be representive of the upper part of the Earth's mantle with composition close to pyrolite (e.g., Takahashi, 1986; Zhang and Herzberg, 1994; Davies, 2009; Walter, 1998). From seismic studies, the detailed velocity structure of the upper mantle and transition zone for the tectonic western North American has been obtained by regional seismic studies [e.g., TNA (Grand and Helmberger 1984), TNA2 (Yang et al., 2014), GCA (Walck 1984), etc.]. By comparing the directly measured velocities on these "synthetic" rocks under the pressure and temperature conditions of mantle depths with the most relevant seismic models for the same region, we derive unique constraints on the composition and thermal structure of western North America.

5.2 Experimental methods

Polycrystalline aggregate specimens of KLB-1 were hot-pressed at ~ 5 GPa (K998), 6GPa (K986), 8GPa (K1000 K1001 K1032) 1200 °C for 1 hour using a 14/8 cell assembly in a 1000-ton uniaxial split-cylinder apparatus (USCA-1000; Li et al., 1996) and 15 GPa 1200 °C (S4255) for 11 hour using a 14/8 cell assembly in a 2000-ton uniaxial split-cylinder apparatus (USSA-2000; Gwanmesia and Liebermann, 1992; Gwanmesia et al., 1993 and Liebermann and Wang, 1992) at Stony Brook University. SEM analysis reveals that the specimens are well sintered, of average grain size ~ 10 micron, and free of visible micro-cracks. The chemical compositions of the equilibrated mineral phases were determined by electron microprobe analyses at Rutgers University. The mineral modal compositions are obtained by mass balance calculations and Rietveld refinement from powder X-ray diffraction as discussed in Chapter 2 (see summary in Table 5.1). In-situ X-ray diffraction and ultrasonic velocity measurements were performed under the pressures and temperatures to the transition zone in a 1000-ton uniaxial

split-cylinder apparatus at beamline 13-ID-D in Argonne National Laboratory operated by GSECARS. See the setup, cell assembly, data collection and data processing methods in Chapter 2 and previous studies (e.g., Li et al., 2004; Li et al., 2005; Li and Liebermann, 2014). KLB-1 specimens are compressed and heated to condition close to those where they were hot pressed before collecting the travel time and sample length data. If the conditions between the hot-pressing and ultrasonic experiments are not the same, the run was extended for another 1 hour to maintain equilibrium at the new target pressure. The peak experimental conditions for each specimen are shown in Table 5.1. The P and S wave velocities at each condition are summarized in Table 5.2.

5.3 Results and discussion

5.3.1 Temperature under western North America revealed from velocity measurements

Two regional seismological models are used as references to represent the average mantle velocities under tectonic western North America: The Tectonic North America model (TNA2; Yang et al., 2014) for S wave velocity and the Gulf California America (GCA; Walck 1984) for P wave velocity. Figure 5.1 shows the comparison of P and S wave velocities from global models, regional models and experimental results of this study. The velocities of AK135 and PREM global models are obviously higher than those of the regional models and the experimental results for both P and S waves (except for P wave at ~220 km and ~410 km). Previous P and S wave tomography studies (e.g., Porritt et al., 2014; Wilson et al., 2005; Gao et al., 2004) show that the P and S wave velocities of Rio Grande Rift area are lower than global velocities, which is consistent with the velocities from the regional seismological models (TNA/TNA2, GCA). At upper mantle depths, S wave velocities of KLB-1 peridodite match best

with TNA2 model along ~1450°C adiabat based on the experimental results with no correction for anelasticity/attenuation. If we assume the Q_{Shear} (quality factor) is in the range of 100-200 in the upper mantle (e.g., Karato et al., 2015) then the change of seismic velocity ($\delta V/V$) due to anelasticity is no more than ~1% as estimated by $\delta V/V \approx Q^{-1}$ (e.g. Karato et al., 2015; Liu et al., 1976). Thus, if the velocities are corrected by taking the attenuation into account, the velocity decrease of ~1% is equivalent to ~100-150 ºC change in temperature, resulting in a mantle potential temperature of 1300~1350 ºC. It is worth noting that even though the temperature is obtained by comparing the S wave velocities of KLB-1 with TNA2 model, the P wave velocities corrected to this potential temperature match very well and nearly coincide with the GCA model (Figure 5.1), not only the absolute velocities, but also the characteristic features of the low (100-250 km) and high velocity gradients (250-400 km) (see below for more discussions). This agreement appears to provide strong validation to the composition and the derived mantle temperature.

Figure 5.2 shows a comparison of upper mantle temperature profiles of western North America based on (a) xenolith thermobarometric results (for the Rio Grande Rift and Colorado Platuea), (b) inversion of seismic velocities of western North America (western North America average and Rio Grande Rift) and (c) the mantle adiabat from this study. The mantle temperature under this region follows the mantle adiabat with a potential temperature of 1300 °C after 150 km as inferred from infinitesimal strain approximation for the calculation of seismic velocities by Goes and Van der Lee (2002). The mantle adiabat from our results after the correction of inelasticity (blue region of Figure 5.2) is consistent with that of western North America average (dark grey dashed line) and Rio Grande Rift (light grey dashed line) by Goes and Van der Lee (2002) (Figure 5.2). At the shallower depths, the thermal structure of

continental thermal boundary layers can be constrained by mantle xenoliths as the high ascent speed preserved the equilibrium state of the constitute minerals in the deep Earth (Boyd 1987; Rudnick et al., 1988; Lee et al., 2011). The temperature of peridotites from the Rio Grande Rift calculated using geothermometers (e.g. Brey and Köhler, 1990) is 1000-1100 ºC at 1-2 GPa (Baldridge 1979; Smith 2000; Porreca et al., 2006), which is higher than that under Colorado Plateau (Smith and Barron, 1991; Riter and Smith, 1996; Smith, 2000) as shown in Figure 5.2. The heat flow data also show the crustal temperature of the Rio Grande Rift is above that of its neighboring areas (Reiter et al., 1978). The high surface heat flux indicates a very thin thermal boundary layer (Lee et al., 2011), which is consistent with the rift process that results in the thermal boundary layer under Rio Grande Rift thinning to an average thickness of 30-35 km (e.g., Baldridge et al., 1984; Olsen, et al., 1987; Wilson et al., 2005); this is thinner by 10–15 km than the Colorado Plateau and the Great Plains (Perry et al., 1987).

The continental lithosphere and upper mantle near Rio Grande Rift have been investigated by many previous studies including geochemistry, isotope, geophysics and tectonics (Wilson et al., 2005, Olsen et al., 1987; Gao et al., 2004; Slack et al., 1996; Baldridge et al., 1984; Kil and Wendlandt, 2004). The seismic structure of this region is characterized by low P and S wave velocities beneath the Rio Grande Rift, which has been attributed to the hot mantle and high crustal temperatures and possibly the presence of partial melting (e.g., Baldridge et al., 1984; Wilson et al., 2005). However, Gao et al. (2004) argues that tomographic imaging studies show no indication of low seismic anomalies in the mantle beneath the Rio Grande Rift associated with upwelling mantle below 150 km depth. This is consistent with the interpretation by Olsen et al. (1987) that there is no major heat source associated with this region and no deep mantle upwelling beneath the rift and the thinning has been accomplished with little addition of

heat to the system during rift process. Melting and hydration from previous processes, if present, has been mechanically removed to the east by the convection flow indicated by the Great Plains down-welling (Gao et al., 2004). Note that the temperature from our study is far below the melting curve of anhydrous KLB-1 (Zhang and Herzberg, 1994). In addition, the slope of a linear relationship between the S and P wave travel time residuals is ~3.0 (Slack et al, 1996) which is not large enough to require the existence of partial melting (Ritzwoller et al., 1988).

5.3.2 Velocity jump at 410 km

If the velocities across the 410 km (13.5 GPa) seismic discontinuity are compared with those produced by the phase transformation from olivine to its high-pressure polymorph wadsleyite, it is possible to constrain the fraction of olivine in the mantle mineralogy. However, as mentioned above the results from previous attempts to do this are very discrepant, ranging from 27 to 61 wt% (e.g., Duffy and Anderson, 1989, Duffy et. al, 1995; Li and Liebermann, 2007; Cammarano and Romanowicz, 2007; Irifune et al., 2008). Based on the current data shown in Fig. 5.1, the directly measured P and S wave velocities of KLB-1 peridodite at ~13 GPa show excellent agreement with those of regional seismic models GCA and TNA2. At this pressure, in-situ X-ray diffraction during the current measurement indicated that no back transformation from wadsletiye to olivine structure was observed.

Direct acoustic measurements on KLB-1 before the 410 km discontinuity, however, could not be obtained due to technical difficulties; instead, the velocities before phase transition are derived from the data at ~13 GPa by replacing wadsleyite with olivine in the aggregate using VRH calculations based on the elasticity of San Carlos olivine and wadsleyite from previous studies (Liu et al., 2005; Zha et al., 1998; Abramson et al., 1997; Darling et al., 2004; Núñez-

Valdez et al., 2011; Liu et al., 2009; Li and liebermann 2000, 2007; Mayama et al., 2004) since the uncertainties in VRH calculations have no effect on the modeled velocity jump for the mantle discontinuities as discussed in Chapter 4 (page 93). As shown in Irifune et al. (1998) and Nunez-Valdez et al. (2013), the effect of iron on the discontinuities across the olivine-wadsleyite transition cannot be neglected. From the microprobe analyses, the Mg# of our specimen equilibrated at 13 GPa is 90. Thus, only the elasiticity data of olivine and wadsleyite with Mg# of ~90 are taken into account when calculating the velocities before the 410 km discontinuity. The olivine data are from San Carlos olivine from Wang et al., 2015a (average of Liu et al., 2005; Zha et al., 1998; Abramson et al., 1997; and Darling et al., 2004). The wadsleyite elasticity data used in the calculation are from the average of the values listed in Table 5.3. The density of wadsleyite (3.605 g/cm^3) is from the refinement of the powder X-ray diffraction of a specimen hot pressed at the same condition as S4255. A ~80ºC temperature difference before and after the 410 km is also taken into account in the calculation of the velocity jumps. The temperature dependence of K and G of olivine and wadsleyite are taken from Li and Liebermann (2007). Thermal expansion data for the calculation of the densities of olivine and wadsleyite at high temperatures are from Fei (1995). The densities of olivine and wadsleyite at the experimental pressures around the 410 km are calculated from the "high-temperature Birch Murnaghan equation of state" by using K_0, and ρ_0 at high temperatures (e.g. Wang et al., 1996; Uchida et al., 2001). Then the bulk and shear moduli are calculated by finite strain equation of state discussed in Chapter 2. Thus the velocity jumps can be obtained from VRH calculations by substitute the elasticities of wadsleyite with those of olivine in the aggregate. Water content can effectively decrease the velocity jump of 410 km as shown in Mao et al., (2008). However, the water

content in olivine of the KLB-1 sample is less than 20 ppm (Schaffer et al., 2013) and the effect of such a small amount of water on the velocity jumps is negligible.

The resultant values (red dots in Figure 5.1) are found to be in good agreement with the seismic models as well as the projected values based on the experimental data between 3 and 10 GPa. Based on powder X-ray diffraction data for a sample hot-pressed at the same P-T condition as those for S4255, the volume fraction of modal olivine is determined to be ~70% by a full-profile Rietveld refinement (see Table 5.1). We infer that the velocity jumps for KLB-1 peridotite are ~6.6 % for P wave and ~7.0 % for S wave at the 410 km discontinuity (the velocity jump for P wave may range from 7.3% and 5.1% and S wave from 7.9% to 6.1% by using different elasticity data of wadsleyite from different studies listed in Table 5.3). These results are consistent with the regional TNA/TNA2 and GCA models as well as recent mineral physics calculations on pyrolite model by Li and Liebermann (2007) and Irifune et al (2008), but are much larger than the globally averaged values in PREM and AK135. In addition, according to Gao et al., (2006) the velocity jumps beneath the southeastern Mexico across 410 km are 6.2% and 7.3 % for P and S waves, respectively, which is also consistent with the current experimental data on KLB-1. These observations appear to suggest that lateral heterogeneity in the deeper upper mantle and the transition zone in the western North American is small, which is consistent with that indicated by tomographic studies (e.g., Masters, et al., 2000) as well as the lack of a localized thermal anomaly as inferred by the negligible topography of the 410 km discontinuity in this region (Wilson et al., 2005).

5.3.3 Lehmann discontinuity under Rio Grande Rift

A closer examination of the velocity data in Figure 5.1 seems to suggest a noticeable discontinuity at the pressure of 7.5-7.8 GPa (230-240 km) with velocity jumps of 1.7% and 1.6% for P and S waves, respectively. Note that the slopes of P and S wave velocities as the function of pressure change significantly before and after this pressure, which is consistent with the gradients in TNA2 and GCA; note that no velocity discontinuities are observed in these regional models. This pressure range is near the 220 km discontinuity in the PREM model and the characteristic velocity features observed here are consistent with those for the Lehmann discontinuity (Lehmann, 1961). This discontinuity has been observed by SS precursors under both continents and oceans (e.g., Deuss and Woodhouse, 2002) and various causes have been suggested. These include the bottom of the asthenospheric low-velocity zone, a phase transition in pyroxenes, the coesite-stishovite transition, or a shear-induced anisotropic boundary (Wilson et al., 2005; Leven, 1981; Mendelssohn and Price, 1997; Revenaugh and Jordan, 1991; Karato, 1992). For the regional seismic structure relevant to the current KLB-1 peridodite, an upper mantle discontinuity was observed from receiver functions by Wilson et al. (2005) at ~250 km depth from Rio Grande Rift to Colorado Pleateau, which is in good agreement with the current observations in Figure 5.1.

As shown in Figure 2.6, the KLB-1 specimens hot pressed within 3-8 GPa show negligible changes in chemical and mineralogical compositions (see also Wang et al., 2015a). Orthopyroxene in KLB-1 completely dissolves into garnet at ~8 GPa (Table 5.1) after which all the phases become more Mg-rich with increasing pressure, which is consistent with the trend observed by Irifune et al., (1998) on synthetic pyrolite. Thus, the origin of the Lehmann discontinuity may be attributed in part to mineralogical and chemical compositional changes at

~230-250 km and could possibly be a global feature for an upper mantle with pyrolitic composition.

5.4 Conclusion

The mantle temperature under Rio Grande Rift revealed from the comparison between the velocities of KLB-1 specimens and TNA2 shear velocity model is along 1450 ºC adiabat or along 1300-1350 ºC adiabat with the correction for anelasticity effect. The velocity jump at 410 km is 6.6% for P wave and 7.0% for S wave with a volume fraction of 70% for olivine. A Lehmann discontinuity is observed at the pressure of 7.5-7.8 GPa (230-240 km) with velocity jumps of ~1.5% and changes in the velocity-depth slope for both P and S waves, which may be caused by mineralogical and compositional changes before and after this pressure range. Our results also suggest that the temperatures in the mantle of this region are below the solidus and the observed velocity reductions do not require the presence of partial melt beneath this region.

Table 5. 1* Modes for mineral compositions of KLB-1 specimens at varies pressures and conditions for in-situ acoustic measurements. For transition of orthopyroxene to garnet above 8 GPa, see also Irifune et al., (1998).

Pressure (GPa)	Experimental conditions	Ol (wt%)	Cpx (wt%)	Opx (wt%)	Gt (wt%)
3 (K973)	3 GPa RT	62(56)	13(13)	18(24)	7(7)
5(K998)	5GPa 1200 °C	63	13	17	7
6(K986)	6GPa 1005 °C	64	13	16	7
8(K1000 K1001)	8 GPa 1100 °C	63	13	16	8
10 (K1032**)	10 GPa 1160 °C	70	17	0	13
13 (S4255***)	13 GPa 1026 °C	71(71)	13(10)	0(0)	16(19)

*Values in the parenthesis are from Rietveld refinement of data from powder X-ray diffraction.

**Sample K1032 was re-equilibrated at ~10 GPa for 1 hour during ultrasonic measurement. The composition in the table was measured after experiment.

***Sample S4255 was re-equilibrated at ~13 GPa for 1 hour during ultrasonic measurement. The composition in the table was measured after experiment.

Table 5. 2 Summary of velocities of KLB-1 specimens at high pressures and temperatures before and after the temperature correction.

P (GPa)	Results after T correction*		Orignial results before T correction		
	Vp (km/s)	Vs (km/s)	T (ºC)	Vp (km/s)	Vs (km/s)
5.01	7.99	4.34	1200	8.14	4.44
5.93	8.09	4.37	1005	8.34	4.62
7.53	7.98	4.36	1100	8.19	4.51
7.82	8.10	4.44	1000	8.36	4.62
8.24	8.15	4.43	860	8.48	4.66
9.80	8.51	4.58	1162	8.70	4.72
9.82	8.49	4.57	1162	8.67	4.71
10.50	8.51	4.59	1020	8.77	4.77
10.57	8.45	4.56	1020	8.71	4.74
10.60	8.44	4.55	1020	8.70	4.73
10.70	8.47	4.56	1020	8.73	4.75
12.65	9.34	5.07	1026	9.55	5.24
13.00	9.30	5.05	1026	9.55	5.24
13.10	9.37	5.08	1000	9.59	5.26
13.65	9.36	5.07	907	9.62	5.28

Velocities before 410 km from VRH calculations		
P(GPa)	Vp (km/s)	Vs (km/s)
12.65	8.75	4.73
13.00	8.71	4.71
13.10	8.79	4.75
13.65	8.78	4.74

***** Temperature for each pressure is along 1450ºC or 1325ºC after Q correction.

Table 5. 3 Elasticities of wadsleyite used in calculation of the velocities at 13 GPa before 410 km

	mg#	K	G
Núñez-Valdez et al., 2011	87.5	180.4	106
Liu et al., 2009	87	171.3	108.7
	87	175.4	108
Li and Liebermann, 2000	88	172	106
Li and Liebermann, 2007	90	173	108
Mayama et al., 2004	91	165.7	105.43

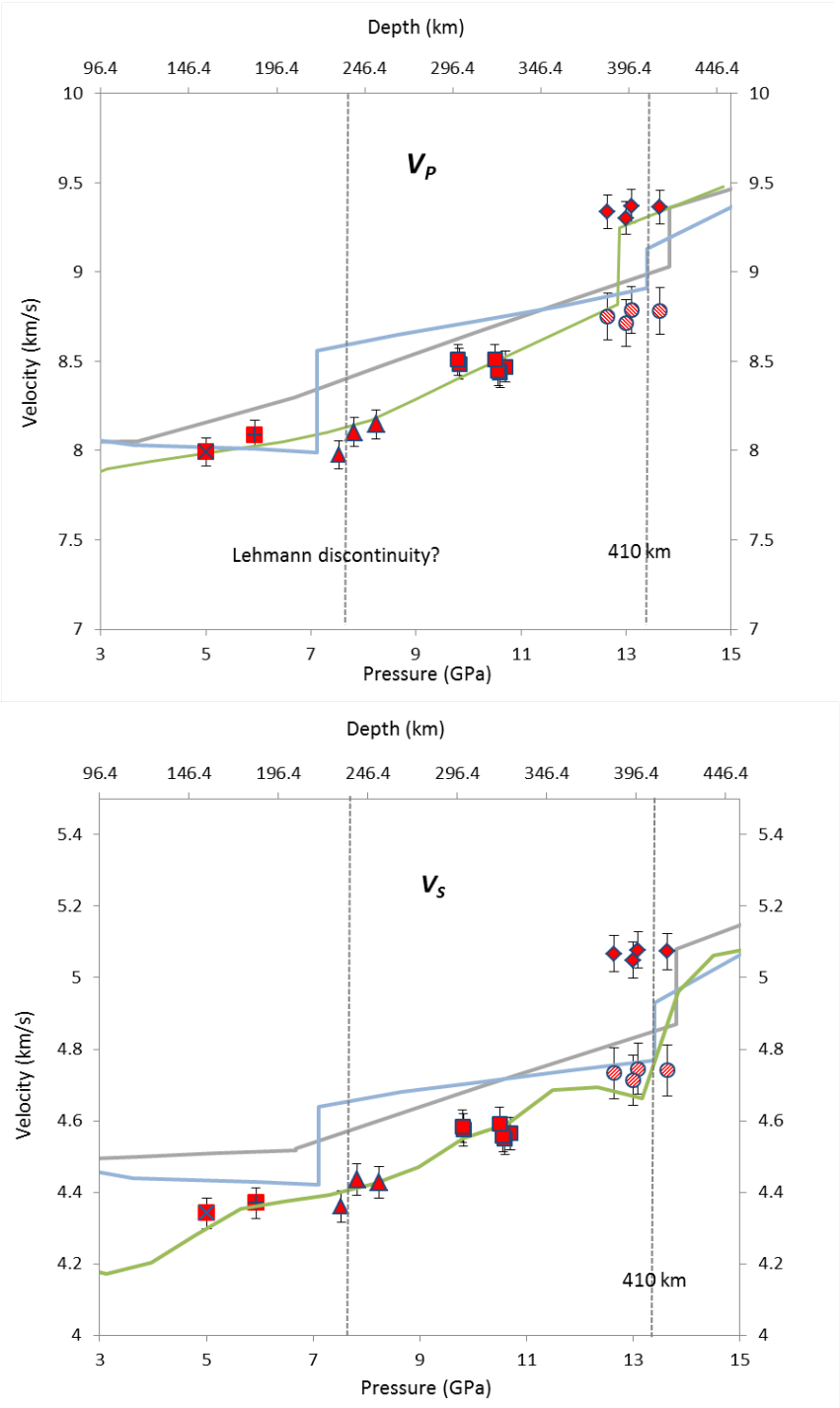

Figure 5. 1 Comparison of Vp and Vs at mantle conditions between KLB-1 and seismic models. Red symbols: KLB-1 along 1450 ºC adiabat without Q correction; KLB-1 along 1325 ºC adiabat with Q correction. Same red symbols are from the same specimen from one run by collecting data at a small range of variations in pressure and temperature. Grey line: AK135; Blue line: PREM; Green Line in Vp: GCA; Green line in Vs: TNA2. Grey shadows show the slope change of the velocities before and after the possible Lehmann discontinuity.

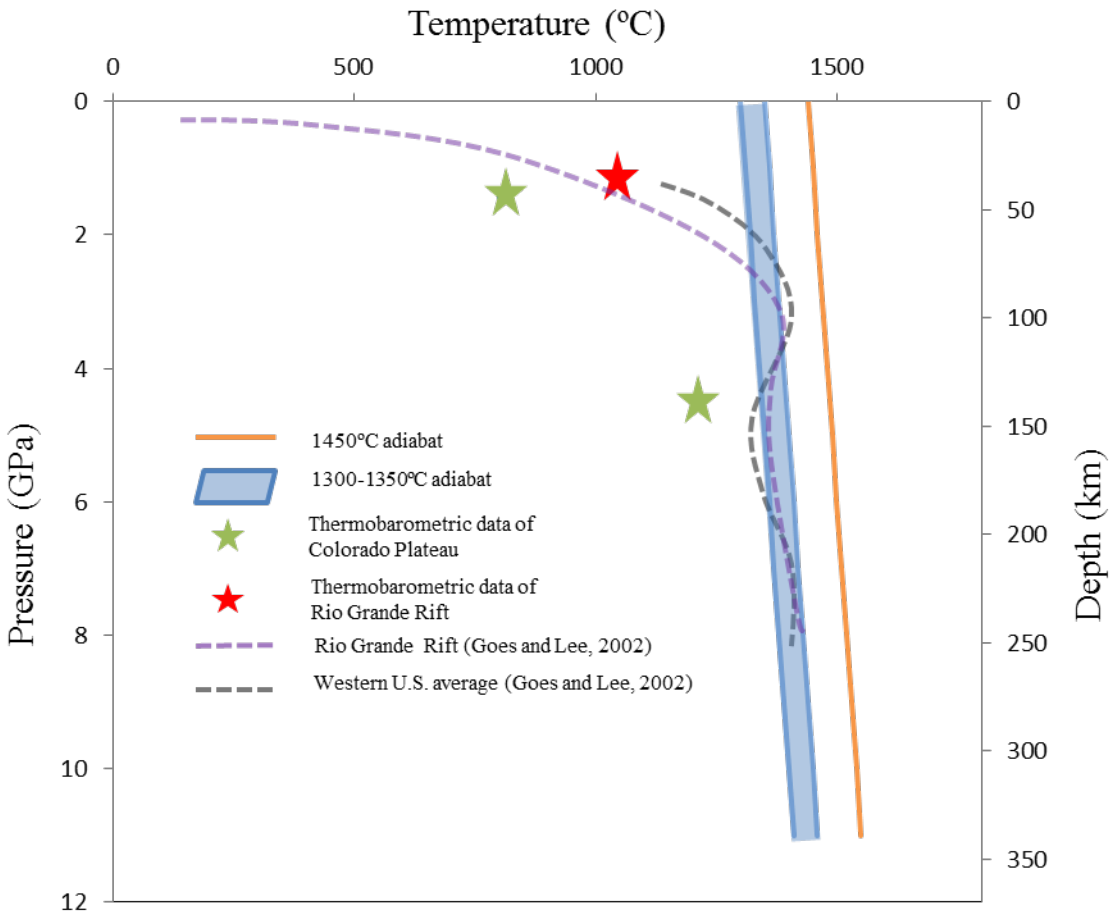

Figure 5. 2 The comparison of upper mantle temperature profile of western North America among xenolith thermobarometric results (red star: Rio Grande Rift; green star: Colorado Platuea), temperature from inversion of seismic velocities of western North America (grey dash line: western North America average; purple dash line: Rio Grande Rift) and mantle adiabat from this study (blue region: temperature after Q correction; orange line: temperature without Q correction).

Reference

Abramson, E. H., J. M. Brown, L. J. Slutsky, and Zaug, J., 1997. The elastic constants of San Carlos olivine to 17 GPa, J. Geophys. Res., 102, 12253– 12264.

Anderson, D.L. 1989. Theory of the Earth. Blackwell Scientific Publications.

Baldridge, W. S., K. H. Olsen, and Callender, J. F., 1984. Rio Grande rift: problems and perspectives. In Rio Grande Rift: Northern New Mexico. New Mexico Geological Society 35th Field Conference Guidebook (pp. 1-12).

Bass, J.D., 1995. Elasticity of minerals, glasses, and melts. Mineral physics & crystallography: a handbook of physical constants, pp.45-63.

Bass, J.D., and Anderson, D.L., 1984. Composition of the upper mantle: geophysical tests of two petrological models, Geophys. Res. Lett., 11, 237-240.

Boyd F.R., 1987. High- and low-temperature garnet peridotite xenoliths and their possible relation to the lithosphere-asthenosphere boundary beneath southern Africa. Mantle Xenoliths, ed.PHNixon, pp. 403–412. New York: Wiley

Brey, G.P., and Köhler, T., 1990. Geothermobarometry in four-phase lherzolites II. New thermobarometers, and practical assessment of existing thermobarometers. Journal of Petrology, 31:1353–1378.

Cammarano, F. and Romanowicz, B., 2007. Insights into the nature of the transition zone from physically constrained inversion of long-period seismic data, PNAS, 104, 9139–9144.

Chai, M., J. M. Brown, and Slutsky, L. J., 1997. The elastic constants of an aluminous orthopyroxene to 12.5 GPa, J. Geophys. Res., 102(B7), 14779–14785, doi:10.1029/97JB00893.

Darling, K. L., G. D. Gwanmesia, J. Kung, B. Li, and Liebermann R. C., 2004. Ultrasonic measurements of the sound velocities in polycrystalline San Carlos olivine in multi-anvil, high-pressure apparatus, Physics of the Earth Planetary Interiors, 143– 144, 19– 31.

Davis, F.A., J.A. Tangeman, T.J. Tenner, and Hirschmann, M.M., 2009. The composition of KLB-1 peridotite, Am. Mineral. 94, 176–180.

Deuss, A. and Woodhouse, J.H., 2002. A systematic search for mantle discontinuities using SS-precursors. Geophysical Research Letters, 29(8).

Duffy, T. S., and Anderson D. L., 1989. Seismic velocities in mantle minerals and the mineralogy of the upper mantle, Journal of Geophysical Research: Solid Earth, 94(B2), 1895–1912, doi:10.1029/JB094iB02p01895.

Duffy, T. S., C. S. Zha, R. T. Downs, H. K. Mao, and Hemley, R. J., 1995. Elasticity of forsterite to 16 GPa and the composition of the upper mantle, Nature, 378, 170-173.

Fei, Y., 1995. Thermal expansion. In: Ahrens, T.J. (Ed.), Mineral Physics, Crystallography: A Handbook of Physical Constants, vol. 2. AGU Reference Shelf, pp. 283–291.

Fumagalli, P. and Klemme, S., 2015. Mineralogy of the Earth: Phase Transitions and Mineralogy of the Upper Mantle, Treatise on Geophysics, 2nd Edition, pp. 7-31, Elsevier, Oxford.

Gao, W., Grand, S.P., Baldridge, W.S., Wilson, D., West, M., Ni, J.F. and Aster, R., 2004. Upper mantle convection beneath the central Rio Grande rift imaged by P and S wave tomography. Journal of Geophysical Research: Solid Earth, 109(B3).

Gao, W., Matzel, E. and Grand, S.P., 2006. Upper mantle seismic structure beneath eastern Mexico determined from P and S waveform inversion and its implications. Journal of Geophysical Research: Solid Earth, 111(B8).

Goes, S. and van der Lee, S., 2002. Thermal structure of the North American uppermost mantle inferred from seismic tomography. Journal of Geophysical Research: Solid Earth, 107(B3).

Grand, S., van der Hilst, R.D. and Widiyantoro, S., 1997. Global seismic tomography: a snapshot of convection in the Earth, GSA Today, 7(4), 1–7.

Grand, S.P. and Helmberger, D.V.,1984. Upper mantle shear structure of North America. Geophysical Journal International, 76(2), pp.399-438.

Gwanmesia, G. D., and Liebermann, R. C., 1992. Polycrystals of high-pressure phases of mantle minerals: Hot-pressing and characterization of physical properties. In High Pressure Research: Application to Earth and Planetary Sciences (eds. Syono, Y. and Manghnani, M.) (Terra Scientific Publishing Co., and American Geophysical Union, Tokyo and Washington, D.C.) pp. 117-135.

Gwanmesia, G.D., Li, B. and Liebermann, R.C., 1993. Hot-pressing of polycrystals of high pressure phases of mantle minerals in multi-anvil apparatus, PAGEOPH, Schreiber Volume, (eds. R.C. Liebermann and C. H. Sondergeld) pp. 467-484.

Herzberg, C., T. Gasparik, and Sawamoto, H., 1990. Origin of mantle peridotite: Constraints from melting experiments to 16.5 GPa, J. Geophys. Res., 95, 15779–15803.

Irifune, T., Y. Higo , T. Inoue, Y. Kono, H. Ohfuji, andFunakoshi, K., 2008. Sound velocities of majorite garnet and the composition of the mantle transition region, Nature, 451 (7180), 814–817.

Ita, J., and Stixrude, L., 1992. Petrology, elasticity and composition of the transition zone, J. Geophys. Res., 97, 6849-6866.

Jackson, I., and Rigden, S. M., 1998. In the Earth's Mantle: Composition, Structure, and Evolution, ed. Jackson I (Cambridge U. Press, Cambridge, UK), pp 405–460.

Karato, S.I. 1992. On the Lehmann discontinuity. Geophysical Research Letters, 19(22), pp.2255-2258.

Karato, S.I., Olugboji, T. and Park, J., 2015. Mechanisms and geologic significance of the mid-lithosphere discontinuity in the continents. Nature Geoscience, 8(7), pp.509-514.

Kil, Y. and Wendlandt, R.F., 2004. Pressure and temperature evolution of upper mantle under the Rio Grande Rift. Contributions to Mineralogy and Petrology, 148(3), pp.265-280.

Kuskov, O.L. and Kronrod, V.A., 2006. Determining the temperature of the Earth's continental upper mantle from geochemical and seismic data. Geochemistry International, 44(3), pp.232-248.

Lee, C.T.A., Luffi, P. and Chin, E.J., 2011. Building and destroying continental mantle. Annual Review of Earth and Planetary Sciences, 39, pp.59-90.

Lehmann, I., 1961. S and the structure of the upper mantle. Geophysical Journal International, 4(Supplement 1), pp.124-138.

Leven, J.H., Jackson, I. and Ringwood, A.E., 1981. Upper mantle seismic anisotropy and lithospheric decoupling. Nature, 289, pp.234-239.

Li, B. and Liebermann, R.C., 2014. Study of the Earth's interior using measurements of sound velocities in minerals by ultrasonic interferometry, Phys. Earth Planet. Interiors, 233(2014) 135-153.

Li, B., and Liebermann, R. C., 2000. Sound velocities of wadsleyite β–$(Mg_{0.88},Fe_{0.12})_2SiO_4$ to 10 GPa, American Mineralogist, 85, 292–295.

Li, B., and Liebermann, R.C., 2007. Indoor seismology by probing the Earth's interior by using sound velocity measurements at high pressures and temperatures, Proc. National Acad. Sci., 104, 9145-9150.

Li, B., I. Jackson, T. Gasparik and Liebermann, R.C., 1996. Elastic wave velocity measurement in multi-anvil apparatus to 10 GPa using ultrasonic interferometry, Phys. Earth Planet. Interiors, 98, 79-91.

Li, B., K. Chen, J. Kung, R.C. Liebermann, and Weidner, D.J., 2002. Ultrasonic velocity measurement using transfer function method, J. of Physics: Condensed Matter, 14, 11337-11342.

Li, B., Kung, J. and Liebermann, R.C., 2004. Modern techniques in measuring elasticity of Earth materials at high pressure and high temperature using ultrasonic interferometry in conjunction with synchrotron X-radiation in multi-anvil apparatus. Physics of the Earth and Planetary Interiors, 143, pp.559-574.

Li, B., Kung, J., Uchida, T. and Wang, Y., 2005. Pressure calibration to 20GPa by simultaneous use of ultrasonic and x-ray techniques. Journal of applied physics, 98(1), p.013521.

Liebermann, R. C., and Wang, Y., 1992. Characterization of sample environment in a uniaxial split-sphere apparatus. In High Pressure Research: Application to Earth and Planetary Sciences (eds. Syono, Y., and Manghnani, M.) (Terra Scientific Publishing Co., and American Geophysical Union, Tokyo and Washington, D.C.) pp. 19-31.

Liu, H.P., Anderson, D.L. and Kanamori, H., 1976. Velocity dispersion due to anelasticity; implications for seismology and mantle composition. Geophysical Journal International, 47(1), pp.41-58.

Liu, W., J. Kung, and Li, B., 2005. Elasticity of San Carlos olivine to 8 GPa and 1073K, Geophysical Research Letters, 32 (16), L16301, doi:10.1029/2005GL023453.

Liu, W., Kung, J., Li, B., Nishiyama, N. and Wang, Y., 2009. Elasticity of $(Mg_{0.87}Fe_{0.13})_2SiO_4$ wadsleyite to 12GPa and 1073K. Physics of the Earth and Planetary Interiors, 174(1), pp.98-104.

Mao, Z., Jacobsen, S.D., Jiang, F., Smyth, J.R., Holl, C.M. and Duffy, T.S., 2008. Elasticity of hydrous wadsleyite to 12 GPa: implications for Earth's transition zone. Geophysical Research Letters, 35(21).

Masters G, Laske G, Bolton H, and Dziewonski, A.M., 2000. The relative behavior of shear velocity, bulk sound speed, and compressional velocity in the mantle: implications for chemical and thermal structure. In Earth's Deep Interior: Mineral Physics and Tomography from the Atomic to the Global Scale, ed. S Karato, AM Forte, RC Liebermann, G Masters, L Stixrude, 117:63–87. Washington, DC: Am. Geophys. Union

Mayama, N., Suzuki, I., Saito, T., Ohno, I., Katsura, T. and Yoneda, A., 2004. Temperature dependence of elastic moduli of β- $(Mg, Fe)_2SiO_4$. Geophysical research letters, 31(4).

McDonough, W. F. and Sun, S. S., 1995. The composition of the Earth.Chemical geology, 120(3), 223-253.

Mendelssohn, M.J. and Price, G.D., 1997. Computer modelling of a pressure induced phase change in clinoenstatite pyroxenes. Physics and chemistry of minerals, 25(1), pp.55-62.

Nolet, G., S. P. Grand, and Kennett, B. L. N., 1994. Seismic heterogeneity in the upper mantle. Journal of Geophysical Research: Solid Earth 99, no. B12: 23753-23766.

Núñez-Valdez, M., da Silveira, P. and Wentzcovitch, R.M., 2011. Influence of iron on the elastic properties of wadsleyite and ringwoodite. Journal of Geophysical Research: Solid Earth, 116(B12).

Olsen, K.H., Baldridge, W.S. and , Callender, J.F., 1987. Rio Grande rift: an overview. Tectonophysics, 143(1), pp.119-139.

Perry, F.V., Baldridge, W.S. and DePaolo D.J., 1987. Role of asthenosphere and lithosphere in the genesis of late Cenozoic basaltic rocks from the Rio Grande rift and adjacent regions of the southwestern United States. Journal of Geophysical Research: Solid Earth, 92(B9), pp.9193-9213.

Porritt, R.W., Allen, R.M. and Pollitz F.F., 2014. Seismic imaging east of the Rocky Mountains with USArray. Earth and Planetary Science Letters, 402, pp.16-25.

Reiter, M., Shearer, C. and Edwards, C.L., 1978. Geothermal anomalies along the Rio Grande rift in New Mexico. Geology, 6: 85--88.

Revenaugh, J. and Jordan T.H., 1991. Mantle layering from ScS reverberations: 1. Waveform inversion of zeroth-order reverberations. Journal of Geophysical Research: Solid Earth, 96(B12), pp.19749-19762.

Ringwood, A. E., 1975. Composition and petrology of the earth's mantle, McGraw-Hill, New York, pp. 618.

Riter, J.C.A. and Smith D., 1996. Xenolith constraints on the thermal history of the mantle below the Colorado Plateau. Geology, 24(3), pp.267-270.

Ritzwoller, M., Masters, G. and Gilbert, F., 1988. Constraining aspherical structure with low degree interaction coefficients: Application to uncoupled multiplets. Journal of Geophysical Research: Solid Earth, 93(B6), pp.6369-6396.

Romanowicz, B., 1995. A global tomographic model of shear attenuation in the upper mantle, J. geophys. Res., 100, 12 375–12 394.

Rudnick R.L., McDonough W.F. and O'Connell, R.J., 1998. Thermal structure, thickness and composition of continental lithosphere. Chem. Geol. 145:395–411.

Schaffer, L.A., Peslier, A.H. and Brandon, A.D., 2013. Water contents of the mantle beneath the Rio Grande Rift: FTIR analysis of Kilbourne Hole peridotite xenoliths. In AGU Fall Meeting Abstracts (Vol. 1, p. 2724).

Slack, P.D., Davis, P.M., Baldridge, W.S., Olsen, K.H., Glahn, A., Achauer, U. and Spence, W., 1996. The upper mantle structure of the central Rio Grande rift region from teleseismic P and S wave travel time delays and attenuation. Journal of Geophysical Research: Solid Earth, 101(B7), pp.16003-16023.

Smith, D., 2000. Insights into the evolution of the uppermost continental mantle from xenolith localities on and near the Colorado Plateau and regional comparisons: Journal of Geophysical Research, v. 105, no. B7, p. 16,769–16,781.

Smith, D., and Barron, B.R., 1991. Pyroxene-garnet equilibration during cooling in the mantle: The American Mineralogist, v. 76, no. 11–12, p. 1950–1963.

Takahashi, E., 1986. Melting study of a dry peridotite KLB-1 up to 14 GPa: implications on the origin of peridotitic upper mantle, Journal of Geophysical Research: Solid Earth, 91, 9367-9382.

Uchida, T., Wang, Y., Rivers, M.L. and Sutton, S.R., 2001. Stability field and thermal equation of state of ε-iron determined by synchrotron X-ray diffraction in a multianvil apparatus. Journal of Geophysical Research: Solid Earth, 106(B10), pp.21799-21810.

Van der Lee, S., and Nolet, G., 1997. Upper mantle S velocity structure of North America. Journal of Geophysical Research: Solid Earth, 102(B10), pp.22815-22838.

Walck, M.C., 1984. The P-wave upper mantle structure beneath an active spreading centre: the Gulf of California. Geophysical Journal International,76(3), pp.697-723.

Walter, M.J.,1998. Melting of garnet peridotite and the origin of komatiite and depleted lithosphere, Journal of Petrology, 39: 29-60.

Wang, X., Chen, T., Qi, X., Zou, Y., Kung, J., Yu, T., Wang, Y., Liebermann, R.C. and Li, B., 2015 b. Acoustic travel time gauges for in-situ determination of pressure and temperature in multi-anvil apparatus. Journal of Applied Physics, 118(6), p.065901.

Wang, X., Chen, T., Zou, Y., Liebermann, R.C. and Li, B., 2015 a. Elastic wave velocities of peridotite KLB-1 at mantle pressures and implications for mantle velocity modeling. Geophysical Research Letters, 42(9), pp.3289-3297.

Wang, Y., Grand, S. P., and Tang, Y., 2014. Shear velocity structure and mineralogy of the transition zone beneath the East Pacific Rise. Earth and Planetary Science Letters, 402, 313-323.

Wang, Y., Weidner, D.J. and Guyot, F., 1996. Thermal equation of state of CaSiO3 perovskite. Journal of Geophysical Research: Solid Earth, 101(B1), pp.661-672.

Weidner, D.J. and Wang, Y., 1998. Chemical- and Clapeyron- induced buoyancy at the 660 km discontinuity. Journal of Geophysical Research: Solid Earth, 103(B4), pp.7431-7441.

Wilson, D., Aster, R., Ni, J., Grand, S., West, M., Gao, W., Baldridge, W.S. and Semken, S., 2005. Imaging the seismic structure of the crust and upper mantle beneath the Great Plains, Rio Grande Rift, and Colorado Plateau using receiver functions. Journal of Geophysical Research: Solid Earth, 110(B5).

Xu, W., C. Lithgow-Bertelloni, L. Stixrude, and Ritsema, J., 2008. The effect of bulk composition and temperature on mantle seismic structure, Earth Planet. Sci. Lett., 275, 70–79.

Zha, C. S., T. S. Duffy, R. T. Downs, H. K. Mao, and Hemley, R. J., 1998. Brillouin scattering and X-ray diffraction of San Carlos olivine: Direct pressure determination to 32 GPa, Earth and Planetary Science Letters, 159, 25-34.

Zhang, J., and Herzberg, C., 1994. Melting experiments on an anhydrous peridotite KLB-1 from 5.0 to 22.5 GPa, Journal of Geophysical Research: Solid Earth, 99, 17729-17742.

Bibliography

Abramson, E. H., J. M. Brown, L. J. Slutsky, and Zaug, J., 1997. The elastic constants of San Carlos olivine to 17 GPa, J. Geophys. Res., 102, 12253– 12264.

Abramson, E.H., Brown, J.M. and Slutsky, L.J., 1999. Applications of impulsive stimulated scattering in the earth and planetary sciences. Annual review of physical chemistry, 50(1), pp.279-313.

Afonso, J.C., Ranalli, G., Fernàndez, M., Griffin, W.L., O'Reilly, S.Y. and Faul, U., 2010. On the Vp/Vs–Mg# correlation in mantle peridotites: Implications for the identification of thermal and compositional anomalies in the upper mantle. Earth and Planetary Science Letters, 289(3), pp.606-618.

Akaogi M, Ito E, Navrotsky A. 1989. Olivine-modified spinel-spinel transitions in the system Mg2SiO4- Fe2SiO4: calorimetric measurements, thermochemical calculation, and geophysical application. J. Geophys. Res. 94:15671–85.

Akimoto, S.I. and Fujisawa, H., 1968. Olivine-spinel solid solution equilibria in the system Mg2SiO4 - Fe2SiO4. Journal of Geophysical Research, 73(4), pp.1467-1479.

Akimoto, S.I., Fujisawa, H. and Katsura, T., 1965. The olivine-spinel transition in Fe2SiO4 and Ni2SiO4. Journal of Geophysical Research, 70(8), pp.1969-1977.

Anderson, D.L. 1989. Theory of the Earth. Blackwell Scientific Publications.

Anderson, D.L. and Bass, J.D., 1984. Mineralogy and composition of the upper mantle. Geophysical Research Letters, 11(7), pp.637-640.

Anderson, O.L. and Isaak, D.G., 1995. Elastic constants of mantle minerals at high temperature. Mineral Physics & Crystallography: A Handbook of Physical Constants, pp.64-97.

Anderson, O.L., Isaak, D.G. and Yamamoto, S., 1989. Anharmonicity and the equation of state for gold. Journal of Applied Physics, 65(4), pp.1534-1543.

Anderson, O.L., Schreiber, E., Liebermann, R.C. and Soga, N., 1968. Some elastic constant data on minerals relevant to geophysics. Reviews of Geophysics, 6(4), pp.491-524.

Angel, R.J. and Jackson, J.M., 2002. Elasticity and equation of state of orthoenstatite, $MgSiO_3$. American Mineralogist, 87(4), pp.558-561.

Angel, R.J., Mosenfelder, J.L. and Shaw, C.S.J., 2001. Anomalous compression and equation of state of coesite. Physics of the Earth and Planetary Interiors, 124(1), pp.71-79.

Babuška, V., Fiala, J., Kumazawa, M., Ohno, I. and Sumino, Y., 1978. Elastic properties of garnet solid-solution series. Physics of the Earth and Planetary Interiors, 16(2), pp.157-176.

Baldridge, W. S., K. H. Olsen, and Callender, J. F., 1984. Rio Grande rift: problems and perspectives. In Rio Grande Rift: Northern New Mexico. New Mexico Geological Society 35th Field Conference Guidebook (pp. 1-12).

Bass, J.D. and Anderson, D.L., 1984. Composition of the upper mantle: Geophysical tests of two petrological models. Geophysical Research Letters, 11(3), pp.229-232.

Bass, J.D. and Parise, J.B., 2008. Deep Earth and recent developments in mineral physics. Elements, 4(3), pp.157-163.

Bass, J.D., 1995. Elasticity of minerals, glasses, and melts. Mineral physics & crystallography: a handbook of physical constants, pp.45-63.

Bass, J.D., Sinogeikin, S.V. and Li, B., 2008. Elastic properties of minerals: A key for understanding the composition and temperature of Earth's interior. Elements, 4(3), pp.165-170.

Bassett, W.A., 2009. Diamond anvil cell, 50th birthday. High Pressure Research, 29(2), pp.163-186.

Bindi, L., Downs, R.T., Harlow, G.E., Safonov, O.G., Litvin, Y.A., Perchuk, L.L., Uchida, H. and Menchetti, S., 2006. Compressibility of synthetic potassium-rich clinopyroxene: In-situ high-pressure single-crystal X-ray study. American Mineralogist, 91(5-6), pp.802-808.

Birch, F., 1952. Elasticity and constitution of the Earth's interior. Journal of Geophysical Research, 57(2), pp.227-286.

Birch, F., 1960. The velocity of compressional waves in rocks to 10 kilobars: 1. Journal of Geophysical Research, 65(4), pp.1083-1102.

Birch, F., 1961. The velocity of compressional waves in rocks to 10 kilobars: 2. Journal of Geophysical Research, 66(7), pp.2199-2224.

Boyd F.R., 1987. High- and low-temperature garnet peridotite xenoliths and their possible relation to the lithosphere-asthenosphere boundary beneath southern Africa. Mantle Xenoliths, ed.PHNixon, pp. 403–412. New York: Wiley

Brey, G.P. and Köhler, T., 1990. Geothermobarometry in four-phase lherzolites II. New thermobarometers, and practical assessment of existing thermobarometers. Journal of Petrology, 31(6), pp.1353-1378.

Bridgman, P. W., 1948. The Compression of 39 Substances to 100,000 kg/cm2, Proceedings of the American Academy of Arts and Sciences, 76, 55-70.

Burkel, E., 2000. Phonon spectroscopy by inelastic x-ray scattering. Reports on Progress in Physics, 63(2), p.171.

Cammarano, F. and Romanowicz, B., 2007. Insights into the nature of the transition zone from physically constrained inversion of long-period seismic data, PNAS, 104, 9139–9144.

Cammarano, F., Goes, S., Vacher, P. and Giardini, D., 2003. Inferring upper-mantle temperatures from seismic velocities. Physics of the Earth and Planetary Interiors, 138(3), pp.197-222.

Chai, M., Brown, J.M. and Slutsky, L.J., 1997. The elastic constants of an aluminous orthopyroxene to 12.5 GPa. Journal of Geophysical Research: Solid Earth, 102(B7), pp.14779-14785.

Chantel, J., Frost, D.J., McCammon, C.A., Jing, Z. and Wang, Y., 2012. Acoustic velocities of pure and iron-bearing magnesium silicate perovskite measured to 25 GPa and 1200 K. Geophysical Research Letters, 39(19).

Chen, G., Cooke, J.A., Gwanmesia, G.D. and Liebermann, R.C., 1999. Elastic wave velocities of Mg3Al2Si3O12-pyrope garnet to 10 GPa. American Mineralogist, 84(3), pp.384-388.

Chen, G., Liebermann, R.C. and Weidner, D.J., 1998. Elasticity of single-crystal MgO to 8 gigapascals and 1600 kelvin. Science, 280(5371), pp.1913-1916.

Chen, T., Gwanmesia, G.D., Wang, X., Zou, Y., Liebermann, R.C., Michaut, C. and Li, B., 2015. Anomalous elastic properties of coesite at high pressure and implications for the upper mantle X-discontinuity. Earth and Planetary Science Letters, 412, pp.42-51.

Christensen, N.I., 1979. Compressional wave velocities in rocks at high temperatures and pressures, critical thermal gradients, and crustal low-velocity zones. Journal of Geophysical Research: Solid Earth, 84(B12), pp.6849-6857.

Collins, M.D. and Brown, J.M., 1998. Elasticity of an upper mantle clinopyroxene. Physics and chemistry of minerals, 26(1), pp.7-13.

Comodi, P., Princivalle, F., Tirone, M. and Zanazzi, P.F., 1995. Comparative compressibility of clinopyroxenes from mantle nodules. European Journal of Mineralogy-Ohne Beihefte, 7(1), pp.141-150.

Conrad, P.G., Zha, C.S., Mao, H.K. and Hemley, R.J., 1999. The high-pressure, single-crystal elasticity of pyrope, grossular, and andradite. American Mineralogist, 84(3), pp.374-383.

Cook, R.K., 1957. Variation of elastic constants and static strains with hydrostatic pressure: a method for calculation from ultrasonic measurements. The Journal of the Acoustical Society of America, 29(4), pp.445-449.

Darling, K.L., Gwanmesia, G.D., Kung, J., Li, B. and Liebermann, R.C., 2004. Ultrasonic measurements of the sound velocities in polycrystalline San Carlos olivine in multi-anvil, high-pressure apparatus. Physics of the Earth and Planetary Interiors, 143, pp.19-31.

Davies, G.F. and Dziewonski, A.M., 1975. Homogeneity and constitution of the Earth's lower mantle and outer core. Physics of the Earth and Planetary Interiors, 10(4), pp.336-343.

Davis, F.A., J.A. Tangeman, T.J. Tenner, and Hirschmann, M.M., 2009. The composition of KLB-1 peridotite, Am. Mineral. 94, 176–180.

Decker, D.L., 1965. Equation of state of NaCl and its use as a pressure gauge in high‐pressure research. Journal of applied physics, 36(1), pp.157-161.

Decker, D.L., 1971. High-pressure equation of state for NaCl, KCl, and CsCl. Journal of Applied Physics, 42(8), pp.3239-3244.

Decker, D.L., Bassett, W.A., Merrill, L., Hall, H.T. and Barnett, J.D., 1972. High-Pressure Calibration: A Critical Review. Journal of Physical and Chemical Reference Data, 1(3), pp.773-836.

Deuss, A. and Woodhouse, J.H., 2002. A systematic search for mantle discontinuities using SS-precursors. Geophysical Research Letters, 29(8).

Dey, S., Roy, N. and Dutta, A., 1984. P and S waves in a medium under initial stresses and under gravity. Indian Journal of Pure Applied Mathematics, 15(7), pp.795-808.

Dorfman, S.M., Prakapenka, V.B., Meng, Y. and Duffy, T.S., 2012. Intercomparison of pressure standards (Au, Pt, Mo, MgO, NaCl and Ne) to 2.5 Mbar. Journal of Geophysical Research: Solid Earth, 117(B8).

Dorogokupets, P.I. and Oganov, A.R., 2007. Ruby, metals, and MgO as alternative pressure scales: A semiempirical description of shock-wave, ultrasonic, x-ray, and thermochemical data at high temperatures and pressures. Physical Review B, 75(2), p.024115.

Duffy, T. S., C. S. Zha, R. T. Downs, H. K. Mao, and Hemley, R. J., 1995. Elasticity of forsterite to 16 GPa and the composition of the upper mantle, Nature, 378, 170-173.

Duffy, T.S. and Anderson, D.L., 1989. Seismic velocities in mantle minerals and the mineralogy of the upper mantle. Journal of Geophysical Research: Solid Earth, 94(B2), pp.1895-1912.

Duffy, T.S., Zha, C.S., Downs, R.T., Mao, H.K. and Hemley, R.J., 1995. Elasticity of forsterite to 16 GPa and the composition of the upper mantle. Nature, 378(6553), pp.170-173.

Dziewonski, A.M. and Anderson, D.L., 1981. Preliminary reference Earth model. Physics of the earth and planetary interiors, 25(4), pp.297-356.

Fei, Y., 1995. Thermal expansion. In: Ahrens, T.J. (Ed.), Mineral Physics, Crystallography: A Handbook of Physical Constants, vol. 2. AGU Reference Shelf, pp. 283–291.

Fei, Y., Ricolleau, A., Frank, M., Mibe, K., Shen, G. and Prakapenka, V., 2007. Toward an internally consistent pressure scale. Proceedings of the National Academy of Sciences, 104(22), pp.9182-9186.

Flesch, L.M., Li, B. and Liebermann, R.C., 1998. Sound velocities of polycrystalline $MgSiO_3$-orthopyroxene to 10 GPa at room temperature. American Mineralogist, 83(5), pp.444-450.

Fumagalli, P. and Klemme, S., 2015. Mineralogy of the Earth: Phase Transitions and Mineralogy of the Upper Mantle, Treatise on Geophysics, 2nd Edition, pp. 7-31, Elsevier, Oxford.

Gao, W., Grand, S.P., Baldridge, W.S., Wilson, D., West, M., Ni, J.F. and Aster, R., 2004. Upper mantle convection beneath the central Rio Grande rift imaged by P and S wave tomography. Journal of Geophysical Research: Solid Earth, 109(B3).

Gao, W., Matzel, E. and Grand, S.P., 2006. Upper mantle seismic structure beneath eastern Mexico determined from P and S waveform inversion and its implications. Journal of Geophysical Research: Solid Earth, 111(B8).

Gasparik, T., 1989. Transformation of enstatite-diopside-jadeite pyroxenes to garnet. Contributions to Mineralogy and Petrology, 102(4), pp.389-405.

Gasparik, T., 1992. Enstatite-jadeite join and its role in the Earth's mantle. Contributions to Mineralogy and Petrology, 111(3), pp.283-298.

Gieske, J.H. and Barsch, G.R., 1968. Pressure dependence of the elastic constants of single crystalline aluminum oxide. physica status solidi (b), 29(1), pp.121-131.

Goes, S. and van der Lee, S., 2002. Thermal structure of the North American uppermost mantle inferred from seismic tomography. Journal of Geophysical Research: Solid Earth, 107(B3).

Grand, S., van der Hilst, R.D. and Widiyantoro, S., 1997. Global seismic tomography: a snapshot of convection in the Earth, GSA Today, 7(4), 1–7.

Grand, S.P. and Helmberger, D.V.,1984. Upper mantle shear structure of North America. Geophysical Journal International, 76(2), pp.399-438.

Grand, S.P., van der Hilst, R.D. and Widiyantoro, S., 1997. High resolution global tomography: a snapshot of convection in the Earth. Geological Society of America Today, 7(4).

Gwanmesia, G. D., and Liebermann, R. C., 1992. Polycrystals of high-pressure phases of mantle minerals: Hot-pressing and characterization of physical properties. In High Pressure Research: Application to Earth and Planetary Sciences (eds. Syono, Y. and Manghnani, M.) (Terra Scientific Publishing Co., and American Geophysical Union, Tokyo and Washington, D.C. 1992) pp. 117-135.

Gwanmesia, G.D., Li, B. and Liebermann, R.C., 1993. Hot-pressing of polycrystals of high pressure phases of mantle minerals in multi-anvil apparatus, PAGEOPH, Schreiber Volume, editors: R.C. Liebermann and C. H. Sondergeld, pp. 467-484.

Gwanmesia, G.D., Wang, L., Heady, A. and Liebermann, R.C., 2014. Elasticity and sound velocities of polycrystalline grossular garnet ($Ca_3Al_2Si_3O_{12}$) at simultaneous high pressures and high temperatures. Physics of the Earth and Planetary Interiors, 228, pp.80-87.

Gwanmesia, G.D., Wang, L., Triplett, R. and Liebermann, R.C., 2009. Pressure and temperature dependence of the elasticity of pyrope–majorite ($Py_{60}Mj_{40}$ and $Py_{50}Mj_{50}$) garnets solid solution measured by ultrasonic interferometry technique. Physics of the Earth and Planetary Interiors, 174(1), pp.105-112.

Gwanmesia, G.D., Zhang, J., Darling, K., Kung, J., Li, B., Wang, L., Neuville, D. and Liebermann, R.C., 2006. Elasticity of polycrystalline pyrope ($Mg_3Al_2Si_3O_{12}$) to 9 GPa and 1000 C. Physics of the Earth and Planetary Interiors, 155(3), pp.179-190.

Hashin, Z. and Shtrikman, S., 1962a. A variational approach to the theory of the effective magnetic permeability of multiphase materials. Journal of applied Physics, 33(10), pp.3125-3131.

Hashin, Z. and Shtrikman, S., 1962b. On some variational principles in anisotropic and nonhomogeneous elasticity. Journal of the Mechanics and Physics of Solids, 10(4), pp.335-342.

Hashin, Z. and Shtrikman, S., 1963. A variational approach to the theory of the elastic behaviour of multiphase materials. Journal of the Mechanics and Physics of Solids, 11(2), pp.127-140.

Hemley, R.J. and Ashcroft, N.W., 1998. The revealing role of pressure in the condensed matter sciences.

Herzberg, C., Gasparik, T. and Sawamoto, H., 1990. Origin of mantle peridotite: constraints from melting experiments to 16.5 GPa. Journal of Geophysical Research: Solid Earth, 95(B10), pp.15779-15803.

Higo, Y., Inoue, T., Irifune, T., Funakoshi, K.I. and Li, B., 2008. Elastic wave velocities of $(Mg_{0.91}Fe_{0.09})_2SiO_4$ ringwoodite under P–T conditions of the mantle transition region. Physics of the Earth and Planetary Interiors, 166(3), pp.167-174.

Hill, R., 1952. The elastic behaviour of a crystalline aggregate. Proceedings of the Physical Society. Section A, 65(5), p.349.

Hirose, K., Sata, N., Komabayashi, T. and Ohishi, Y., 2008. Simultaneous volume measurements of Au and MgO to 140GPa and thermal equation of state of Au based on the MgO pressure scale. Physics of the Earth and Planetary Interiors, 167(3), pp.149-154.

Hughes, D.S. and Jones, H.J., 1950. Variation of elastic moduli of igneous rocks with pressure and temperature. Geological Society of America Bulletin, 61(8), pp.843-856.

Hugh-Jones, D.A. and Angel, R.J., 1997. Effect of Ca^{2+} and Fe^{2+} on the equation of state of MgSiO3 orthopyroxene. Journal of Geophysical Research: Solid Earth, 102(B6), pp.12333-12340.

Irifune, T. and Isshiki, M., 1998. Iron partitioning in a pyrolite mantle and the nature of the 410-km seismic discontinuity. Nature, 392(6677), pp.702-705.

Irifune, T. and Ringwood, A.E., 1987. Phase transformations in a harzburgite composition to 26 GPa: implications for dynamical behaviour of the subducting slab. Earth and Planetary Science Letters, 86(2), pp.365-376.

Irifune, T. and Ringwood, A.E., 1993. Phase transformations in subducted oceanic crust and buoyancy relationships at depths of 600–800 km in the mantle. Earth and Planetary Science Letters, 117(1-2), pp.101-110.

Irifune, T., 1987. An experimental investigation of the pyroxene-garnet transformation in a pyrolite composition and its bearing on the constitution of the mantle. Physics of the Earth and Planetary Interiors, 45(4), pp.324-336.

Irifune, T., Higo, Y., Inoue, T., Kono, Y., Ohfuji, H. and Funakoshi, K., 2008. Sound velocities of majorite garnet and the composition of the mantle transition region. Nature, 451(7180), pp.814-817.

Irifune, T., Nishiyama, N., Kuroda, K., Inoue, T., Isshiki, M., Utsumi, W., Funakoshi, K.I., Urakawa, S., Uchida, T., Katsura, T. and Ohtaka, O., 1998. The postspinel phase boundary in Mg2SiO4 determined by in situ X-ray diffraction. Science, 279(5357), pp.1698-1700.

Ita, J. and Stixrude, L., 1992. Petrology, elasticity, and composition of the mantle transition zone. Journal of Geophysical Research: Solid Earth, 97(B5), pp.6849-6866.

Ito, E. and Yamada, H., 1982. Stability relations of silicate spinels, ilmenites, and perovskites. High-pressure research in geophysics, pp.405-419.

Jackson, I. and Niesler, H., 1982. The elasticity of periclase to 3 GPa and some geophysical implications. High pressure research in geophysics, 12, pp.93-113.

Jackson, I., and Rigden, S. M., 1998. In the Earth's Mantle: Composition, Structure, and Evolution, ed. Jackson I (Cambridge U. Press, Cambridge, UK), 405–460.

Jackson, I., Niesler, H. and Weidner, D.J., 1981. Explicit correction of ultrasonically determined elastic wave velocities for transducer-bond phase shifts. Journal of Geophysical Research: Solid Earth, 86(B5), pp.3736-3748.

Jacobsen, S.J., Reichmann, H.J., Kantor A., Spetzler, H.A., 2005. A gigahertz ultrasonic interferometry for the diamond anvil cell and high-presure elasticity of some iron-oxide materials. In: Advances in High-Pressure Technology for Geophysical Applications, Chen, J. Wang, Y. Duffy, T.S. Shen, G. Dobrzhinetskaya, L.F. Elsevier, pp. 25–48

Jamieson, J.C., Fritz, J.N. and Manghnani, M.H., 1982. Pressure measurement at high temperature in X-ray diffraction studies: gold as a primary standard. High-pressure research in Geophysics, 12, pp.27-48.

Ji, S. and Wang, Z., 1999. Elastic properties of forsterite–enstatite compositesup to 3.0 GPa. Journal of Geodynamics, 28(2), pp.147-174.

Jiang, F., Speziale, S. and Duffy, T.S., 2004. Single-crystal elasticity of grossular-and almandine-rich garnets to 11 GPa by Brillouin scattering. Journal of Geophysical Research: Solid Earth, 109(B10).

Jordan, T.H., 1979. Mineralogies, densities and seismic velocities of garnet lherzolites and their geophysical implications. The Mantle Sample: Inclusion in Kimberlites and Other Volcanics, pp.1-14.

Karato, S.I. 1992. On the Lehmann discontinuity. Geophysical Research Letters, 19(22), pp.2255-2258.

Karato, S.I., Olugboji, T. and Park, J., 2015. Mechanisms and geologic significance of the mid-lithosphere discontinuity in the continents. Nature Geoscience, 8(7), pp.509-514.

Katahara, K.W., Rai, C.S., Manghnani, M.H. and Balogh, J., 1981. An interferometric technique for measuring velocity and attenuation in molten rocks. Journal of Geophysical Research: Solid Earth, 86(B12), pp.11779-11786.

Katsura, T. and Ito, E., 1989. The system Mg_2SiO_4-Fe_2SiO_4 at high pressures and temperatures: Precise determination of stabilities of olivine, modified spinel, and spinel. Journal of Geophysical Research: Solid Earth, 94(B11), pp.15663-15670.

Kennett, B.L.N., Engdahl, E.R. and Buland, R., 1995. Constraints on seismic velocities in the Earth from traveltimes. Geophysical Journal International, 122(1), pp.108-124.

Kern, H., 1982. Elastic-wave velocity in crustal and mantle rocks at high pressure and temperature: The role of the high-low quartz transition and of dehydration reactions. Physics of the Earth and Planetary Interiors, 29(1), pp.12-23.

Kil, Y. and Wendlandt, R.F., 2004. Pressure and temperature evolution of upper mantle under the Rio Grande Rift. Contributions to Mineralogy and Petrology, 148(3), pp.265-280.

Klemme, S., 2004. The influence of Cr on the garnet–spinel transition in the Earth's mantle: experiments in the system $MgO–Cr_2O_3–SiO_2$ and thermodynamic modelling. Lithos, 77(1), pp.639-646.

Kono, Y., Gréaux, S., Higo, Y., Ohfuji, H. and Irifune, T., 2010. Pressure and temperature dependences of elastic properties of grossular garnet up to 17 GPa and 1 650 K. Journal of Earth Science, 21(5), pp.782-791.

Kono, Y., Higo, Y., Ohfuji, H., Inoue, T. and Irifune, T., 2007. Elastic wave velocities of garnetite with a MORB composition up to 14 GPa. Geophysical Research Letters, 34(14).

Kung, J., Li, B., Uchida, T. and Wang, Y., 2005. In-situ elasticity measurement for the unquenchable high-pressure clinopyroxene phase: Implication for the upper mantle. Geophysical research letters, 32(1).

Kung, J., Li, B., Uchida, T., Wang, Y., Neuville, D. and Liebermann, R.C., 2004. In situ measurements of sound velocities and densities across the orthopyroxene→ high-pressure clinopyroxene transition in $MgSiO_3$ at high pressure. Physics of the Earth and Planetary Interiors, 147(1), pp.27-44.

Kung, J., Li, B., Weidner, D.J., Zhang, J. and Liebermann, R.C., 2002. Elasticity of $(Mg_{0.83}, Fe_{0.17})O$ ferropericlase at high pressure: ultrasonic measurements in conjunction with X-radiation techniques. Earth and Planetary Science Letters, 203(1), pp.557-566.

Kuskov, O.L. and Kronrod, V.A., 2006. Determining the temperature of the Earth's continental upper mantle from geochemical and seismic data. Geochemistry International, 44(3), pp.232-248.

Lebedev, S. and Van Der Hilst, R.D., 2008. Global upper-mantle tomography with the automated multimode inversion of surface and S-wave forms. Geophysical Journal International, 173(2), pp.505-518.

Lee, C.T.A., 2003. Compositional variation of density and seismic velocities in natural peridotites at STP conditions: Implications for seismic imaging of compositional heterogeneities in the upper mantle. Journal of Geophysical Research: Solid Earth, 108(B9).

Lee, C.T.A., Luffi, P. and Chin, E.J., 2011. Building and destroying continental mantle. Annual Review of Earth and Planetary Sciences, 39, pp.59-90.

Lehmann, I., 1961. S and the structure of the upper mantle. Geophysical Journal International, 4(Supplement 1), pp.124-138.

Leinenweber, K.D., Tyburczy, J.A., Sharp, T.G., Soignard, E., Diedrich, T., Petuskey, W.B., Wang, Y. and Mosenfelder, J.L., 2012. Cell assemblies for reproducible multi-anvil experiments (the COMPRES assemblies). American Mineralogist, 97(2-3), pp.353-368.

Leven, J.H., Jackson, I. and Ringwood, A.E., 1981. Upper mantle seismic anisotropy and lithospheric decoupling. Nature, 289, pp.234-239.

Li, B. and Liebermann, R.C., 2000. Sound velocities of wadsleyite b-$(Mg_{0.88}Fe_{0.12})_2SiO_4$ to 10 GPa. American Mineralogist, 85(2-3), pp.292-295.

Li, B. and Liebermann, R.C., 2007. Indoor seismology by probing the Earth's interior by using sound velocity measurements at high pressures and temperatures. Proceedings of the National Academy of Sciences, 104(22), pp.9145-9150.

Li, B. and Liebermann, R.C., 2014. Study of the Earth's interior using measurements of sound velocities in minerals by ultrasonic interferometry. Physics of the Earth and Planetary Interiors, 233, pp.135-153.

Li, B. and Neuville, D.R., 2010. Elasticity of diopside to 8GPa and 1073K and implications for the upper mantle. Physics of the Earth and Planetary interiors, 183(3), pp.398-403.

Li, B. and Zhang, J., 2005. Pressure and temperature dependence of elastic wave velocity of MgSiO 3 perovskite and the composition of the lower mantle. Physics of the Earth and Planetary Interiors, 151(1), pp.143-154.

Li, B., 1996. Ultrasonic measurements of the elastic wave velocities of olivine and beta polymorphs of Mg_2SiO_4 at mantle transition zone P and T and geophysical implications, Ph.D. thesis, Stony Brook University.

Li, B., 2003. Compressional and shear wave velocities of ringwoodite γ-Mg_2SiO_4 to 12 GPa. American Mineralogist, 88(8-9), pp.1312-1317.

Li, B., Chen, G., Gwanmesia, G.D. and Liebermann, R.C., 1998. Sound velocity measurements at mantle transition zone conditions of pressure and temperature using ultrasonic interferometry in a multianvil apparatus, in Properties of Earth & Planetary Materials at High Pressure & Temperature, edited by M. H. Manghnani, Y. Syono and T. Yagi, 41-61.

Li, B., Chen, K., Kung, J., Liebermann, R.C. and Weidner, D.J., 2002. Sound velocity measurement using transfer function method. Journal of Physics: Condensed Matter, 14(44), p.11337.

Li, B., Gwanmesia, G.D. and Liebermann, R.C., 1996. Sound velocities of olivine and beta polymorphs of Mg_2SiO_4 at Earth's transition zone pressures. Geophysical Research Letters, 23(17), pp.2259-2262.

Li, B., Jackson, I., Gasparik, T. and Liebermann, R.C., 1996a. Elastic wave velocity measurement in multi-anvil apparatus to 10 GPa using ultrasonic interferometry. Physics of the Earth and Planetary Interiors, 98(1), pp.79-91.

Li, B., K. Chen, J. Kung, R.C. Liebermann, and Weidner, D.J., 2002. Ultrasonic velocity measurement using transfer function method, J. of Physics: Condensed Matter, 14, 11337-11342.

Li, B., Kung, J. and Liebermann, R.C., 2004. Modern techniques in measuring elasticity of Earth materials at high pressure and high temperature using ultrasonic interferometry in conjunction with synchrotron X-radiation in multi-anvil apparatus. Physics of the Earth and Planetary Interiors, 143, pp.559-574.

Li, B., Kung, J., Liu, W. and Liebermann, R.C., 2014. Phase transition and elasticity of enstatite under pressure from experiments and first-principles studies. Physics of the Earth and Planetary Interiors, 228, pp.63-74.

Li, B., Kung, J., Uchida, T. and Wang, Y., 2005. Pressure calibration to 20GPa by simultaneous use of ultrasonic and X-ray techniques. Journal of applied physics, 98(1), p.013521.

Li, B., Liebermann, R.C. and Weidner, D.J., 1998. Elastic moduli of wadsleyite (β-Mg_2SiO_4) to 7 Gigapascals and 873 Kelvin. Science, 281(5377), pp.675-677.

Li, B., Rigden, S.M. and Liebermann, R.C., 1996 b. Elasticity of stishovite at high pressure. Physics of the Earth and Planetary Interiors, 96(2), pp.113-127.

Li, B., Woody, K. and Kung, J., 2006. Elasticity of MgO to 11 GPa with an independent absolute pressure scale: Implications for pressure calibration. Journal of Geophysical Research: Solid Earth, 111(B11).

Liebermann, R. C., 2000. Elasticity of Mantle Minerals (Experimental Studies), in Earth's Deep Interior: Mineral Physics and Tomography From the Atomic to the Global Scale (eds S.-I. Karato, A. Forte, R. Liebermann, G. Masters and L. Stixrude), American Geophysical Union, Washington, D. C., 181-199. doi: 10.1029/GM117p0181

Liebermann, R. C., 2011. Multi-anvil, high-pressure apparatus: A half century of development and progress," High Pressure Research, 31, 493-532.

Liebermann, R. C., and Wang, Y., 1992. Characterization of sample environment in a uniaxial split-sphere apparatus. In High Pressure Research: Application to Earth and Planetary Sciences (eds. Syono, Y., and Manghnani, M.) (Terra Scientific Publishing Co., and American Geophysical Union, Tokyo and Washington, D.C.) pp. 19-31.

Liebermann, R.C. and Mayson, D.J., 1976. Elastic properties of polycrystalline diopside ($CaMgSi_2O_6$). Physics of the Earth and Planetary Interiors, 11(3), pp.P1-P4.

Liu, H.P., Anderson, D.L. and Kanamori, H., 1976. Velocity dispersion due to anelasticity; implications for seismology and mantle composition. Geophysical Journal International, 47(1), pp.41-58.

Liu, L.G., 1977. The system enstatite-pyrope at high pressures and temperatures and the mineralogy of the earth's mantle. Earth and Planetary Science Letters, 36(1), pp.237-245.

Liu, Q., Liu, W., Whitaker, M.L., Wang, L. and Li, B., 2008. Compressional and shear wave velocities of Fe2SiO4 spinel at high pressure and high temperature. High Pressure Research, 28(3), pp.405-413.

Liu, W., Kung, J. and Li, B., 2005. Elasticity of San Carlos olivine to 8 GPa and 1073 K. Geophysical Research Letters, 32(16).

Liu, W., Kung, J., Li, B., Nishiyama, N. and Wang, Y., 2009. Elasticity of $(Mg_{0.87}Fe_{0.13})_2SiO_4$ wadsleyite to 12GPa and 1073K. Physics of the Earth and Planetary Interiors, 174(1), pp.98-104.

Liu, W., Zeng, Q., Jiang, Q., Wang, L. and Li, B., 2011. Density and elasticity of $Zr_{46}Cu_{37.6}$ $Ag_{8.4}$ Al_8 bulk metallic glass at high pressure. Scripta Materialia, 65(6), pp.497-500.

Lu, C., Mao, Z., Lin, J.F., Zhuravlev, K.K., Tkachev, S.N. and Prakapenka, V.B., 2013. Elasticity of single-crystal iron-bearing pyrope up to 20 GPa and 750 K. Earth and Planetary Science Letters, 361, pp.134-142.

Mackenzie, J.K., 1950. The elastic constants of a solid containing spherical holes. Proceedings of the Physical Society. Section B, 63(1), p.2.

Mao, H.K., Wu, Y., Chen, L.C., Shu, J.F. and Jephcoat, A.P., 1990. Static compression of iron to 300 GPa and $Fe_{0.8}Ni_{0.2}$ alloy to 260 GPa: Implications for composition of the core. Journal of Geophysical Research: Solid Earth, 95(B13), pp.21737-21742.

Mao, Z., Jacobsen, S.D., Frost, D.J., McCammon, C.A., Hauri, E.H. and Duffy, T.S., 2011. Effect of hydration on the single-crystal elasticity of Fe-bearing wadsleyite to 12 GPa. American Mineralogist, 96(10), pp.1606-1612.

Mao, Z., Jacobsen, S.D., Jiang, F., Smyth, J.R., Holl, C.M. and Duffy, T.S., 2008. Elasticity of hydrous wadsleyite to 12 GPa: implications for Earth's transition zone. Geophysical Research Letters, 35(21).

Mao, Z., Lin, J.F., Jacobsen, S.D., Duffy, T.S., Chang, Y.Y., Smyth, J.R., Frost, D.J., Hauri, E.H. and Prakapenka, V.B., 2012. Sound velocities of hydrous ringwoodite to 16GPa and 673K. Earth and Planetary Science Letters, 331, pp.112-119.

Masters G, Laske G, Bolton H, and Dziewonski, A.M., 2000. The relative behavior of shear velocity, bulk sound speed, and compressional velocity in the mantle: implications for chemical and thermal structure. In Earth's Deep Interior: Mineral Physics and Tomography from the

Atomic to the Global Scale, ed. S Karato, AM Forte, RC Liebermann, G Masters, L Stixrude, 117:63–87. Washington, DC: Am. Geophys. Union

Matityahu, S., Emuna, M., Yahel, E., Makov, G. and Greenberg, Y., 2015. Novel experimental design for high pressure-high temperature electrical resistance measurements in a "Paris-Edinburgh" large volume press. Review of Scientific Instruments, 86(4), p.043902.

Matsui, M., 2009. Temperature–pressure–volume equation of state of the B1 phase of sodium chloride. Physics of the Earth and Planetary Interiors, 174(1), pp.93-97.

Mayama, N., Suzuki, I., Saito, T., Ohno, I., Katsura, T. and Yoneda, A., 2004. Temperature dependence of elastic moduli of β- (Mg, Fe) $_2SiO_4$. Geophysical research letters, 31(4).

Mazaki, H., Lee, D.I. and Shimizu, S., 1973. Pressure distribution in a multianvil high-pressure device. Journal of Physics E: Scientific Instruments, 6(11), p.1072.

McDonough, W. F. and Sun, S. S., 1995. The composition of the Earth.Chemical geology, 120(3), 223-253.

McMillan, P. F., 2010. High-pressure synthesis of materials. NATO Science for Peace and Security Series B: Physics and Biophysics, 373-383.

McMillan, P.F., 2002. New materials from high-pressure experiments. Nature materials, 1(1), pp.19-25.

McSkimin, H.J., 1950. Ultrasonic measurement techniques applicable to small solid specimens. The Journal of the Acoustical Society of America, 22(4), pp.413-418.

McSkimin, H.J., 1961. Pulse superposition method for measuring ultrasonic wave velocities in solids. The Journal of the acoustical society of America, 33(1), pp.12-16.

Mendelssohn, M.J. and Price, G.D., 1997. Computer modelling of a pressure induced phase change in clinoenstatite pyroxenes. Physics and chemistry of minerals, 25(1), pp.55-62.

Meng, Y., Shen, G. and Mao, H.K., 2006. Double-sided laser heating system at HPCAT for in situ x-ray diffraction at high pressures and high temperatures. Journal of Physics: Condensed Matter, 18(25), p.S1097.

Moriarty, J.A., Belak, J.F., Rudd, R.E., Söderlind, P., Streitz, F.H. and Yang, L.H., 2002. Quantum-based atomistic simulation of materials properties in transition metals. Journal of Physics: Condensed Matter, 14(11), p.2825.

Morishima, H., Kato, T., Suto, M., Ohtani, E., Urakawa, S., Utsumi, W., Shimomura, O. and Kikegawa, T., 1994. The phase boundary between α-and β-Mg_2SiO_4 determined by in situ X-ray observation. Science, 265(5176), pp.1202-1203.

Mueller, H.J., Schilling, F.R., Lauterjung, J. and Lathe, C., 2003. A standard-free pressure calibration using simultaneous XRD and elastic property measurements in a multi-anvil device. European journal of mineralogy, 15(5), pp.865-873.

Nimis, P. and Taylor, W.R., 2000. Single clinopyroxene thermobarometry for garnet peridotites. Part I. Calibration and testing of a Cr-in-Cpx barometer and an enstatite-in-Cpx thermometer. Contributions to Mineralogy and Petrology, 139(5), pp.541-554.

Nolet, G., Grand, S.P. and Kennett, B.L.N., 1994. Seismic heterogeneity in the upper mantle. Journal of Geophysical Research: Solid Earth, 99(B12), pp.23753-23766.

Núñez-Valdez, M., da Silveira, P. and Wentzcovitch, R.M., 2011. Influence of iron on the elastic properties of wadsleyite and ringwoodite. Journal of Geophysical Research: Solid Earth, 116(B12).

Núñez‐Valdez, M., Wu, Z., Yu, Y.G. and Wentzcovitch, R.M., 2013. Thermal elasticity of (Fex, Mg1− x) 2SiO4 olivine and wadsleyite. Geophysical Research Letters, 40(2), pp.290-294.

Olsen, K.H., Baldridge, W.S. and , Callender, J.F., 1987. Rio Grande rift: an overview. Tectonophysics, 143(1), pp.119-139.

O'Neill, B., Bass, J.D., Smyth, J.R. and Vaughan, M.T., 1989. Elasticity of a grossular-pyrope-almandine garnet. Journal of Geophysical Research: Solid Earth, 94(B12), pp.17819-17824.

O'Neill, H.S.C., 1981. The transition between spinel lherzolite and garnet lherzolite, and its use as a geobarometer. Contributions to Mineralogy and Petrology, 77(2), pp.185-194.

Papadakis, E., 1976. Ultrasonic velocity and attenuation: measurement methods with scientific and industrial applications. (Mason W P & Thurston R N, eds.) Physical acoustics: principles and methods, New York: Academic Press., 12. p. 277-374.

Perkins, D. and Anthony, E.Y., 2011. The evolution of spinel lherzolite xenoliths and the nature of the mantle at Kilbourne Hole, New Mexico. Contributions to Mineralogy and Petrology, 162(6), pp.1139-1157.

Perry, F.V., Baldridge, W.S. and DePaolo D.J., 1987. Role of asthenosphere and lithosphere in the genesis of late Cenozoic basaltic rocks from the Rio Grande rift and adjacent regions of the southwestern United States. Journal of Geophysical Research: Solid Earth, 92(B9), pp.9193-9213.

Poirier, J.P., 2000. Introduction to the Physics of the Earth's Interior. Cambridge University Press.

Porritt, R.W., Allen, R.M. and Pollitz F.F., 2014. Seismic imaging east of the Rocky Mountains with USArray. Earth and Planetary Science Letters, 402, pp.16-25.

Rai, C.S., Manghnani, M.H. and Katahara, K.W., 1981. Ultrasonic studies on a basalt melt. Geophysical Research Letters, 8(12), pp.1215-1218.

Reiter, M., Shearer, C. and Edwards, C.L., 1978. Geothermal anomalies along the Rio Grande rift in New Mexico. Geology, 6: 85--88.

Revenaugh, J. and Jordan T.H., 1991. Mantle layering from ScS reverberations: 1. Waveform inversion of zeroth-order reverberations. Journal of Geophysical Research: Solid Earth, 96(B12), pp.19749-19762.

Rigden, S.M. and Jackson, I., 1991. Elasticity of germanate and silicate spinels at high pressure. Journal of Geophysical Research: Solid Earth, 96(B6), pp.9999-10006.

Rigden, S.M., Gwanmesia, G.D., Jackson, I. and Liebermann, R.C., 1993. Progress in High-Pressure Ultrasonic Interferometry, the Pressure Dependence of Elasticity of Mg_2SiO_4 Polymorphs and Constraints on the Composition of the Transition Zone of the Earth's Mantle. High-pressure research: application to earth and planetary sciences, pp.167-182.

Ringwood, A. E., 1975. Composition and petrology of the earth's mantle, McGraw-Hill, New York, pp. 618.

Riter, J.C.A. and Smith D., 1996. Xenolith constraints on the thermal history of the mantle below the Colorado Plateau. Geology, 24(3), pp.267-270.

Ritsema, J., Xu, W., Stixrude, L. and Lithgow-Bertelloni, C., 2009. Estimates of the transition zone temperature in a mechanically mixed upper mantle. Earth and Planetary Science Letters, 277(1), pp.244-252.

Ritzwoller, M., Masters, G. and Gilbert, F., 1988. Constraining aspherical structure with low□ degree interaction coefficients: Application to uncoupled multiplets. Journal of Geophysical Research: Solid Earth, 93(B6), pp.6369-6396.

Romanowicz, B., 1995. A global tomographic model of shear attenuation in the upper mantle. Journal of Geophysical Research: Solid Earth, 100(B7), pp.12375-12394.

Rudnick R.L., McDonough W.F. and O'Connell, R.J., 1998. Thermal structure, thickness and composition of continental lithosphere. Chem. Geol. 145:395–411.

Ruoff, A.L., Lincoln, R.C. and Chen, Y.C., 1973. A new method of absolute high pressure determination. Journal of Physics D: Applied Physics, 6(10), p.1295.

Sang, L. and Bass, J.D., 2014. Single-crystal elasticity of diopside to 14GPa by Brillouin scattering. Physics of the Earth and Planetary Interiors, 228, pp.75-79.

Sato, H., Sacks, I.S., Murase, T., Muncill, G. and Fukuyama, H., 1989. Qp-melting temperature relation in peridotite at high pressure and temperature: Attenuation mechanism and implications for the mechanical properties of the upper mantle. Journal of Geophysical Research: Solid Earth, 94(B8), pp.10647-10661.

Schaffer, L.A., Peslier, A.H. and Brandon, A.D., 2013. Water contents of the mantle beneath the Rio Grande Rift: FTIR analysis of Kilbourne Hole peridotite xenoliths. In AGU Fall Meeting Abstracts (Vol. 1, p. 2724).

Sinelnikov, Y.D., Chen, G. and Liebermann, R.C., 2004. Dual mode ultrasonic interferometry in multi-anvil high pressure apparatus using single-crystal olivine as the pressure standard. High Pressure Research, 24(1), pp.183-191.

Sinogeikin, S.V. and Bass, J.D., 2000. Single-crystal elasticity of pyrope and MgO to 20 GPa by Brillouin scattering in the diamond cell. Physics of the Earth and Planetary Interiors, 120(1), pp.43-62.

Slack, P.D., Davis, P.M., Baldridge, W.S., Olsen, K.H., Glahn, A., Achauer, U. and Spence, W., 1996. The upper mantle structure of the central Rio Grande rift region from teleseismic P and S wave travel time delays and attenuation. Journal of Geophysical Research: Solid Earth, 101(B7), pp.16003-16023.

Smith, D., 2000. Insights into the evolution of the uppermost continental mantle from xenolith localities on and near the Colorado Plateau and regional comparisons: Journal of Geophysical Research, v. 105, no. B7, p. 16,769–16,781.

Smith, D., and Barron, B.R., 1991. Pyroxene-garnet equilibration during cooling in the mantle: The American Mineralogist, v. 76, no. 11–12, p. 1950–1963.

Smyth, J.R., and McCormick, T.C., 1995. Crystallographic data for minerals. Editor: Ahrens, T.J., Mineral Physics and Crystallography: A Handbook of Physical Constants, AGU Reference Shelf 2, (AGU, Washington, DC) p2.

Sojda, S.M. and Wang, L., 2002, December. Kinetics of the Pyroxene-Garnet Transformation: Preliminary Results. In AGU Fall Meeting Abstracts (Vol. 1, p. 1085).

Speziale, S., Zha, C.S., Duffy, T.S., Hemley, R.J. and Mao, H.K., 2001. Quasi-hydrostatic compression of magnesium oxide to 52 GPa: Implications for the pressure-volume-temperature equation of state. Journal of Geophysical Research: Solid Earth, 106(B1), pp.515-528.

Sumino, Y. and Anderson, O.L., 1982. Elastic constants of minerals. In R.S. Carmichael, Ed., Handbook of Physical Properties of Rocks, Vol. 3, p. 39–138.CRC Press, Boca Raton, Florida.

Suzuki, I., and Anderson O. L., 1983. Elasticity and thermal expansion of a natural garnet up to 1000 K. Journal of Physics of the Earth, 31(2), pp.125-138.

Syassen, K., 2008. Ruby under pressure. High Pressure Research, 28, 75-126.

Takahashi, E., 1986. Melting of a dry peridotite KLB-1 up to 14 GPa: Implications on the origin of peridotitic upper mantle. Journal of Geophysical Research: Solid Earth, 91(B9), pp.9367-9382.

Taylor. S.R. and McLennan. S.M., 1985. The continental crust: Its composition and evolution. Blackwcll. Oxford, pp.312.

Thurston, R.N. and Brugger, K., 1964. Third-order elastic constants and the velocity of small amplitude elastic waves in homogeneously stressed media. Physical Review, 133(6A), p.A1604.

Tsuchiva, T., 2003. First-principles prediction of the PVT equation of state of gold and the 660-km discontinuity in Earth's mantle. Journal of geophysical research, 108(B10), pp.ECV1-1.

Uchida, T., Wang, Y., Rivers, M.L. and Sutton, S.R., 2001. Stability field and thermal equation of state of ε-iron determined by synchrotron X-ray diffraction in a multianvil apparatus. Journal of Geophysical Research: Solid Earth, 106(B10), pp.21799-21810.

Upadhyay, A., Beniwal, R.S. and Singh, R., 2012. Elastic properties of Al_2O_3–NiAl: a modified version of Hashin–Shtrikman bounds. Continuum Mechanics and Thermodynamics, 24(3), pp.257-266.

Utsumi, W., Weidner, D.J. and Liebermann, R.C., 1998. Volume measurement of MgO at high pressures and high temperatures. Properties of Earth and Planetary Materials at High Pressure and Temperature, pp.327-333.

Van der Lee, S., and Nolet, G., 1997. Upper mantle S velocity structure of North America. Journal of Geophysical Research: Solid Earth, 102(B10), pp.22815-22838.

Walck, M.C., 1984. The P-wave upper mantle structure beneath an active spreading centre: the Gulf of California. Geophysical Journal International,76(3), pp.697-723.

Walker, D., Carpenter, M.A. and Hitch, C.M., 1990. Some simplifications to multianvil devices for high pressure experiments. American Mineralogist, 75(9-10), pp.1020-1028.

Walter, M.J., 1998. Melting of garnet peridotite and the origin of komatiite and depleted lithosphere. Journal of Petrology, 39(1), pp.29-60.

Wang, X., and Li, B., Acoustoelasticity and yield strength of Al_2O_3 under high pressure. in preparation.

Wang, X., Chen, T., Qi, X., Zou, Y., Kung, J., Yu, T., Wang, Y., Liebermann, R.C. and Li, B., 2015b. Acoustic travel time gauges for in-situ determination of pressure and temperature in multi-anvil apparatus. Journal of Applied Physics, 118(6), p.065901.

Wang, X., Chen, T., Qi, X., Zou, Y., Liebermann, R.C., Li, B., 2014. Constraints on mantle composition of western North American from direct P and S wave velocities of mantle peridodite to 10 GPa. Abstract and poster for 2014 AGU (American Geophysical Union) Fall Meeting.

Wang, X., Chen, T., Zou, Y., Liebermann, R.C. and Li, B., 2015 a. Elastic wave velocities of peridotite KLB-1 at mantle pressures and implications for mantle velocity modeling. Geophysical Research Letters, 42(9), pp.3289-3297.

Wang, Y., Grand, S. P., and Tang, Y., 2014. Shear velocity structure and mineralogy of the transition zone beneath the East Pacific Rise. Earth and Planetary Science Letters, 402, 313-323.

Wang, Y., Weidner, D.J. and Guyot, F., 1996. Thermal equation of state of $CaSiO_3$ perovskite. Journal of Geophysical Research: Solid Earth, 101(B1), pp.661-672.

Wang, Z. and Ji, S., 2001. Elasticity of six polycrystalline silicate garnets at pressure up to 3.0 GPa. American Mineralogist, 86(10), pp.1209-1218.

Wang, Z., Liu, Y., Bi, Y., Song, W. and Xie, H., 2012. Hydrostatic pressure and temperature calibration based on phase diagram of bismuth. High Pressure Research, 32(2), pp.167-175.

Watt, J.P. and O'Connell, R.J., 1980. An experimental investigation of the Hashin-Shtrikman bounds on two-phase aggregate elastic properties. Physics of the Earth and Planetary Interiors, 21(4), pp.359-370.

Webb, S.A.C. and Wood, B.J., 1986. Spinel-pyroxene-garnet relationships and their dependence on Cr/Al ratio. Contributions to Mineralogy and Petrology, 92(4), pp.471-480.

Weidner, D.J. and Wang, Y., 1998. Chemical- and Clapeyron- induced buoyancy at the 660 km discontinuity. Journal of Geophysical Research: Solid Earth, 103(B4), pp.7431-7441.

Weidner, D.J., 1985. A mineral physics test of a pyrolite mantle. Geophysical Research Letters, 12(7), pp.417-420.

Weidner, D.J., Sawamoto, H., Sasaki, S. and Kumazawa, M., 1984. Single-crystal elastic properties of the spinel phase of Mg_2SiO_4. Journal of Geophysical Research: Solid Earth, 89(B9), pp.7852-7860.

Weidner, D.J., Swyler, K. and Carleton, H.R., 1975. Elasticity of microcrystals. Geophysical Research Letters, 2(5), pp.189-192.

Wen, L. and Anderson, D.L., 1995. The fate of slabs inferred from seismic tomography and 130 million years of subduction. Earth and Planetary Science Letters, 133(1), pp.185-198.

Wen, L. and Anderson, D.L., 1997. Slabs, hotspots, cratons and mantle convection revealed from residual seismic tomography in the upper mantle. Physics of the Earth and Planetary Interiors, 99(1), pp.131-143.

Wilson, D., Aster, R., Ni, J., Grand, S., West, M., Gao, W., Baldridge, W.S. and Semken, S., 2005. Imaging the seismic structure of the crust and upper mantle beneath the Great Plains, Rio Grande Rift, and Colorado Plateau using receiver functions. Journal of Geophysical Research: Solid Earth, 110(B5).

Wu, Z., Wentzcovictch, R., Umemoto, K., Li, B., Hirose, K., 2008. PVT relations in MgO: an ultra-high P-T scale for planetary science applications. Journal of Geophysical Research, 113, B06204.

Xu, W., Lithgow-Bertelloni, C., Stixrude, L. and Ritsema, J., 2008. The effect of bulk composition and temperature on mantle seismic structure. Earth and Planetary Science Letters, 275(1), pp.70-79.

Xu, Y. and Wiens, D.A., 1997. Upper mantle structure of the southwest Pacific from regional waveform inversion. Journal of Geophysical Research: Solid Earth, 102(B12), pp.27439-27451.

Yamaoka, H., Zekko, Y., Jarrige, I., Lin, J.F., Hiraoka, N., Ishii, H., Tsuei, K.D. and Mizuki, J.I., 2012. Ruby pressure scale in a low-temperature diamond anvil cell. Journal of Applied Physics, 112(12), p.124503.

Yoneda, A., 1990. Pressure derivatives of elastic constants of single crystal MgO and $MgAl_2O_4$. Journal of Physics of the Earth, 38(1), pp.19-55.

Yoneda, A., Cooray, T. and Shatskiy, A., 2012. Single-crystal elasticity of stishovite: New experimental data obtained using high-frequency resonant ultrasound spectroscopy and a Gingham check structure model. Physics of the Earth and Planetary Interiors, 190, pp.80-86.

Zha, C.S., Duffy, T.S., Downs, R.T., Mao, H.K. and Hemley, R.J., 1996. Sound velocity and elasticity of single-crystal forsterite to 16 GPa. Journal of Geophysical Research: Solid Earth, 101(B8), pp.17535-17545.

Zha, C.S., Duffy, T.S., Downs, R.T., Mao, H.K. and Hemley, R.J., 1998. Brillouin scattering and X-ray diffraction of San Carlos olivine: direct pressure determination to 32 GPa. Earth and Planetary Science Letters, 159(1), pp.25-33.

Zha, C.S., Duffy, T.S., Mao, H.K., Downs, R.T., Hemley, R.J. and Weidner, D.J., 1997. Single-crystal elasticity of β-Mg_2SiO_4 to the pressure of the 410 km seismic discontinuity in the Earth's mantle. Earth and Planetary Science Letters, 147(1), pp.E9-E15.

Zha, C.S., Mao, H.K. and Hemley, R.J., 2000. Elasticity of MgO and a primary pressure scale to 55 GPa. Proceedings of the National Academy of Sciences, 97(25), pp.13494-13499.

Zhang, D., Jackson, J.M., Chen, B., Sturhahn, W., Zhao, J., Yan, J. and Caracas, R., 2013. Elasticity and lattice dynamics of enstatite at high pressure. Journal of Geophysical Research: Solid Earth, 118(8), pp.4071-4082.

Zhang, J. and Herzberg, C., 1994. Melting experiments on anhydrous peridotite KLB-1 from 5.0 to 22.5 GPa. Journal of Geophysical Research: Solid Earth, 99(B9), pp.17729-17742.

Zou, Y., Gréaux, S., Irifune, T., Whitaker, M.L., Shinmei, T. and Higo, Y., 2012. Thermal equation of state of $Mg_3Al_2Si_3O_{12}$ pyrope garnet up to 19 GPa and 1,700 K. Physics and Chemistry of Minerals, 39(7), pp.589-598.